

People's Democratic Republic of Algeria
وزارة التعليم العالي والبحث العلمي
Ministry of Higher Education and Scientific Research

Ibn Khaldoun University of Tiaret

Vice Rectorate in charge of Postgraduate Higher Education, University Habilitation, Scientific Research, and Postgraduate Higher Education.



جامعة ابن خلدون تيارت

نيسابة مديرية الجامعة المكلفة بالتكوين العالي في الطور الثالث، التأهيل الجامعي، البحث العلمي والتكوين العالي فيما بعد التدرج

Faculty of Material Sciences

Department of Physics

THESIS

To obtain the diploma of

DOCTORATE

Physics Specialty

Specialty: Materials Engineering

Presented by

SAID Kheira

Theme:

First principle study of the interactions between the intrinsic defects of ZnO and the dopants for obtaining p-type ZnO

Publicly defended on 14/12/2022

In front of the jury:

President	H. Belarbi	Prof.	University of Tiaret
Examiner	H. Bouafia	Prof.	University of Tiaret
Examiner	K. Boudia	Prof.	University of Tissemsilt
Examiner	A. Akriche	M.C.A	University of Ouargla
Supervisor	R. Baghdad	Prof.	University of Tiaret

Academic year: 2022/2023

Acknowledgements

Acknowledgements

This work was carried out within the Laboratory of synthesis and catalysis of the University Ibn Khaldoun, Tiaret; under the direction of Mr. Rachid Baghdad professor at the University Ibn Khaldoun, Tiaret. I thank him for having directed my doctoral work and for having constantly enlightened me by knowledge. I would like to express my gratitude to him for their availability and for the trust he shown me by giving me freedom of action in the realization of my research work. I could appreciate during my PhD him great scientific, human and cultural qualities.

I would like to thank:

Mr Habib Belarbi, Professor at the University of Tiaret for having accepted to chair this jury. May he find here the expression of my respectful gratitude.

I would like to thank the following people: H .Bouafia Professor at the University of Tiered, K.Boudia Professor at university of Tissemsilt and A. Akriche, M.C.A at university of Ouargla who took the time to examine and judge this work.

I thank very warmly Dr .SOUADIA ZAHRA of the laboratory Laboratory for Developing New Materials and their Characterization, Department of Physics, Faculty of Science, University of Setif 1, Algeria who helped me in the mastery of the ab-initio tool and the calculation methods using the castep code.

Finally, I would like to thank all the team of the laboratory synthesis and catalysis and all the people who supported and helped me throughout this work.

Dedication

To my dearest father

To my little sister: Nadia

To my mother, my sisters and brothers

For my niece: Ritèdj and nephew: Mohamed Rayen

To my best friends: Khaldia Sediri, Taybi Nassira and

Belhadj Nawel

To all those who are dear to me

Table of Contents

Table of contents

General Introduction	01
Chapter 1: Fundamentals of ZnO	
1.1 Crystal Structure	06
1.2 Physical Properties	08
1.3 Electronic Properties	08
1.4 Optical properties.....	09
1.5 Electrical Properties	11
1.6 p-types Conductivity	11
1.6.1 Historical Background.....	11
1.7 ZnO as a photo-catalyst	12
1.8 ZnO on spin-tronic	13
1.9 Nonmetal Doping of ZnO	14
1.9.1 Carbon doped ZnO	14
1.10 Transition metal Doping in ZnO	15
1.10.1 Silicium doped ZnO	15
1.11 Co-doping of ZnO.....	16
1.12 Intrinsic Defects points	16
1.12.1 Some Experimental and Theoretical Background.....	19
1.12.2 Intrinsic Defects Points and Conductivity Control	21
1.13 Experimental approach and Ab initio approach	21
1.14 Conclusion	22
Bibliography.....	23
Chapter 2: Fundamentals of the Density Functional Theory	
2.1 Some history of science.....	32
2.2 Quantum Many-Body Problem	35
2.3 The Born-Oppenheimer approximation.....	36
2.4 Hartree and Hartree-Fock approximations.....	36
2.5 Density Functional Theory	38
2.6 Equations of Kohn and Sham	39
2.7 Hubbard Correction U.....	43
2.8 Kohn and Hohenberg theorem	44
2.9 The solution of the one-particle Kohn-Sham equations	45
2.10 Bloch's theorem and plane waves	46

2.11 Pseudo-potential-plane wave method	47
2.11.1 Principle	47
2.11.2 The pseudo-potentials types	49
2.12 The PAW formalism	50
2.13 Cambridge Serial Total Energy Package (CASTEP)	51
2.14 Conclusion.....	53
Bibliography.....	54

Chapter 3: Results and Discussion

Carbon and Silicon codoping ZnO

1. Reminder on the calculation method.....	61
1.1 Convergence test	61
2. Results and discussion	64
2.1 Structural Properties	64
2.2 Elastic Properties	70
2.3 Electronic Properties	71
2.3.1 Band Structure	71
2.3.2 Density of state	75
2.3.3 Electron Density distribution analyses.....	77
2.3.4 Mulliken population analysis	78
2.4 Optical Properties	80
2.4.1 Dielectric function	80
2.4.2 The absorption coefficient and reflectivity.....	82
2.4.3 Loss function energy.....	84
2.4.4 Refractive index and extinction coefficient	85
2.4.5 Optical conductivity.....	87

Point defects

2.5 Point defects in C:Si:ZnO.....	89
2.6 Electronic properties	93
2.6.1 Band structure	93
2.6.2 Density of state	93
2.6.3 Optical properties	95
2.6.3.1 Dielectric function	95
2.6.3.2 The absorption coefficient and reflectivity	96
2.6.3.3 Loss function energy	97

2.6.3.4 Refractive index and extinction coefficient	97
2.6.3.5 Optical conductivity	98
Bibliography.....	99
General Conclusion	110

ملخص

List of tables

List of tables

Table	Title	Page
	Chapter2	
Table 1 :	The physical parameters of ZnO	07
Table 2:	Values of static (ϵ_0) and high frequency (ϵ_{∞}) dielectric constants	10
	Chapter3	
Table 1:	The three Kohn-Sham equations	42
	Chapter3	
Table 1:	Cutoff energy, number of k points and other impute values used in our calculation.....	62
Table 2:	The equilibrium lattice parameters, internal parameter and bulk modulus in comparison with other theoretical and experimental works results.....	69
Table 3:	Calculated band gap values in comparison with other theoretical and experimental works results	71
Table 4:	Calculated band gap values in comparison with other theoretical and experimental works results	72
Table 5:	Mulliken atomic and bond populations of C:Si:ZnO	79
Table 6:	Calculated lattice parameters a, c, the volume V, final energy E and bulk modulus B of ZnO-C: Si, (ZnO-C: Si)-O_V, (ZnO-C: Si)- Zn_V, (ZnO-C: Si)- O_i and (ZnO-C: Si)- Zn_i.	92
Table 7:	Band gap of C: Si:ZnO, (C: Si:ZnO)O_V , (C: Si:ZnO) Zn_V, (C: Si:ZnO)O_i and (C: Si:ZnO)Zn_i.	93

List of figures

List of figures

Figure	Title	Page
Chapter 1		
Figure 1 :	The hexagonal unit cell of ZnO (A) and (B) tetrahedral coordination where the green atoms are Zn and the red atoms are O.....	07
Figure 2:	Band Structure of ZnO Wurtzite using LDA method.....	08
Figure 3:	Technologies enabled by high-performance and thin-film transistors over the past 25 years. (Top) Silicon transistors have driven the microprocessors used in computational devices ranging from low-power gadgets to large servers. (Bottom) Various forms of cheaper silicon enabled the display revolution, now being shared by IGZO. (Right) Nano-materials may be the next transistor material for enabling a new generation of technologies	09
Figure 4:	Photoluminescence spectrum of massive n-type ZnO (He-Cd excitation) showing donor-acceptor pairs	10
Figure 5:	The photo-catalytic applications of the ZnO nanostructures in the environment and energy fields. (b) The number of publications of ZnO and doped ZnO as a photocatalys from 1 January 2000 to 22 May 2015 in the Scopus citation database using keywords in title section "photo-cataly" and "Zinc Oxide" or ZnO	13
Figure 6:	A systematic diagram of formation of the Zero ZnO (V^0_o).....	17
Figure7:	A systematic diagram of formation of the One ZnO (V^+_o).....	17
Figure 8:	A systematic diagram of formation of the Two ZnO (V^{+2}_o)	18
Figure 9:	Different native points	19
Figure 10:	Calculated local atomic geometry for (a) the Zn vacancy; (b) the zinc interstitial and (c) Calculated local atomic geometry of the zinc anti-site	21
Chapter 2		
Figure 1:	The different approximations basis	43
Figure 2:	The self consistent calculation scheme of the density functional.....	46
Figure 3:	Representation of the replacement of an exact wave function all electrons and the associated potential by a pseudo wave function and pseudopotential... 	48
Figure 4:	The two types of the pseudo-potentials	49

Figure 5: PDOS for BN. The left window is for 'boron, nitrogen' the right schematic represents the super-cell calculation of a substitutional impurity in a bulk and the last: is the super-cell calculation of a small molecule adsorption on a surface..... 52

Figure 6: Experimental vs. CASTEP calculated lattice parameters..... 52

Figure 7: Dependence of the bulk modulus of the NaCl/KCl solid solution on concentration. Experimental data are from Walker et al. (2004). The solid line shows a polynomial fit to the calculated results 53

Chapter 3

Figure 1: undoped ZnO, C doped ZnO, Si doped ZnO and C:Si doped ZnO (1.a, 1.b, 1.c and 1.d) respectively, on $2 \times 2 \times 1$ super cell..... 63

Figure 2: Fig.2: (a)The parts of periodic table,(b) carbon characterizations and (c) silicon characterizations..... 66

Figure 3: Calculated energy versus volume for pure ZnO (a) ZnO:C (b), ZnO:Si (c) and (d) ZnO:C:Si. 68

Figure 4: Band structures of (a) undoped ZnO and (b) C doped ZnO, (c) Si doped ZnO and (d) C:Si co-doped ZnO. 74

Figure 5: Density of states of (a) undoped ZnO and (b) C doped ZnO, (c) Si doped ZnO and (d) C:Si co-doped ZnO. 76

Figure 6: Charge densities for: (a) undoped ZnO and (b) C doped ZnO, (c) Si doped ZnO and (d) C:Si co-doped ZnO. 78

Figure 7: Dielectric Function of undoped ZnO and ZnO:C, ZnO:Si and ZnO:C:Si (0 eV – 30eV): (a) real parts and (b) imaginary part 81

Figure 8: Simulation light absorption (a) and reflectivity (b) of pure ZnO, ZnO:C, ZnO:Si and ZnO:C:Si. 83

Figure 9: Loss function of undoped ZnO, C-doped, Si-doped and C: Si co-doped ZnO 85

Figure 10: (a) Refractive index n and (b) Extinction Coefficient k of undoped ZnO, C-doped, Sidoped and C: Si co-doped ZnO versus energy. 86

Figure 11: (a) real part and (b) imaginary part of optical conductivity for different systems: undoped ZnO, C-doped, Si-doped and C: Si co-doped ZnO..... 87

Figure 12: Defects model: (a) ZnO-C: Si, (b) (ZnO-C: Si) $^{-}O_V$, (c) (ZnO-C: Si) $^{-}Zn_V$, (d) (ZnO-C: Si) $^{-}O_i$ and (e) (ZnO-C: Si) $^{-}Zn_i$ 91

Figure 13: TDOS and PDOS of (a) C: Si:ZnO, (b) (C: Si:ZnO)_{OV}, (c) (C: Si:ZnO)_{ZnV}, (d) (C: Si:ZnO)_{Oi} and (e) (C: Si:ZnO)_{Zni}. 94

Figure 14: Dielectric Function of of C: Si:ZnO, (C: Si:ZnO)_{OV}, (C: Si:ZnO)_{ZnV}, (C: Si:ZnO)_{Oi} and (C: Si:ZnO)_{Zni} in the range (0 eV – 30 eV): (a) real parts and (b) imaginary part. 95

Figure 15: The absorption coefficient (a) and reflectivity (b) of C: Si:ZnO, (C: Si:ZnO)_{OV}, (C: Si:ZnO)_{ZnV}, (C: Si:ZnO)_{Oi} and (C: Si:ZnO)_{Zni} 96

Figure 16: The loss function of C: Si:ZnO, (C: Si:ZnO)_{OV}, (C: Si:ZnO)_{ZnV}, (C: Si:ZnO)_{Oi} and (C: Si:ZnO)_{Zni} 97

Figure 17: Refractive index (a) and extinction coefficient (b) of C: Si:ZnO, (C: Si:ZnO)_{OV}, (C: Si:ZnO)_{ZnV}, (C: Si:ZnO)_{Oi} and (C: Si:ZnO)_{Zni} 98

Figure 18: Optical conductivity of C: Si:ZnO, (C: Si:ZnO)_{OV}, (C: Si:ZnO)_{ZnV}, (C: Si:ZnO)_{Oi} and (C: Si:ZnO)_{Zni} in the range (0 eV – 30 eV): (a) real parts and (b) imaginary part 99

**List of the most
Commonly used
abbreviations**

$\psi(r_1; r_2; \dots; r_{66})$	The wave function
HFM	Hartree-Fock Method
DFT	Density-Functional Theory
\hat{H}	Hamiltonian operator
E	The total energy of the system
Φ_i	The product of the mono-electronic wave functions
LDA	Local Density Approximation
$\rho(r)$	The density of states
GGA	Generalized Gradient Approximation
LDA+U	Local density with the Hubbard correction
GGA+U	Generalized gradient with the Hubbard correction
$C_{i\alpha}$	The coefficients of the expansion
ϕ_α	The basic functions
$V_{\text{eff}}(\vec{r})$	The potential
CASTEP	Cambridge Serial Total Energy Package
SCF	Self Consistent Field cycle
APW	Augmented Plane Wave
PP	Pseudopotential (Pseudo-potential)
US-PP	Ultra soft pseudopotential
PW	Plane wave
LAPW	Linearized augmented plane wave
ZB	Brillouin zone (Brillouin zone)
EOS	Equation of state
B	Bulk modulus of compressibility
E_{XC}	Exchange-Correlation energy
E_{F}	Fermi energy
E	Young modulus
E_{g}	Energy band gap
DOS	Density of states
TDOS/PDOS	Total/Partial density of states
O _v	Oxygen vacancy
Z _{nv}	Zinc vacancy
O _{i,tet}	Oxygen interstitial tetrahedral
Z _{ni,tet}	Zinc interstitial tetrahedral

General

Introduction

General Introduction

Nanocrystals often show novel physical and chemical properties different from those of the corresponding bulk material. Zinc Oxide powders are extensively used in a variety of applications such as optoelectronics, semiconductors, luminescent devices, pigments and components for cosmetics industries, sunscreens and rubber, etc.

ZnO have diameters less than 100 nanometers. It has a large surface area relative to its size and high catalytic activity. The exact physical and chemical properties of zinc oxide nano-particles depend on the different ways it is synthesized. Some possible ways to produce ZnO nano-particles are laser ablation, hydrothermal methods, electrochemical depositions, sol-gel method, chemical vapor deposition, thermal decomposition, ultrasound, microwave-assisted combustion method, two-step mechano-chemical-thermal synthesis, co-precipitation, and precipitation processes using solution concentration, pH, and washing medium. ZnO is a wide-band gap semiconductor with an energy gap of 3.37 eV at room temperature. [1]

ZnO nanostructures are believed to be one of the most produced materials. They are very used because they effectively absorb ultraviolet light, but to be completely transparent to visible light. [2]

ZnO is a wide-band gap semiconductor of the II-VI semiconductor group. The native doping of the semiconductor due to oxygen vacancies or zinc interstitials is n-type.[3] Other favorable properties include good transparency, high electron mobility, wide band gap, and strong room-temperature luminescence. Those properties make ZnO valuable for a variety of emerging applications: transparent electrodes in liquid crystal displays, energy-saving or heat-protecting windows, and electronics as thin-film transistors and light-emitting diodes.

Zinc oxide crystallizes in two main forms, hexagonal wurtzite.[4] and cubic zinc-blende. The wurtzite structure is most stable at ambient conditions and thus most common. The zinc-blende form can be stabilized by growing ZnO on substrates with cubic lattice structure. In both cases, the zinc and oxide centers are tetrahedral, the most characteristic geometry for Zn (II). ZnO converts to the rock-salt motif at relatively high pressures about 10 GPa.[3] The many remarkable medical properties of creams containing ZnO can be explained by its elastic softness, which is characteristic of tetrahedral coordinated binary compounds close to the transition to octahedral structures .[5]

ZnO has also been considered for spintronics applications: if doped with 1–10% of magnetic ions (Mn, Fe, Co, V, etc.), ZnO could become ferromagnetic, even at room temperature. Such room temperature ferromagnetism in ZnO: Mn has been observed. [6] But it is not clear yet whether it originates from the matrix itself or from secondary oxide phases.

General Introduction

ZnO has a rich defect and dopants chemistry that can significantly alter properties and behavior of the material. [7]. Doping ZnO nanostructures with other elements and molecules leads to a variety of material characteristics, because the addition or vacancy of atoms changes the energy levels in the band gap. [8]. Native defects due to oxygen and zinc vacancies or zinc interstitials create its n-type semiconductor properties. Carriers created by doping have been found to exhibit a strong dominance over native defects. [7]

My research is dedicated to examination of the effect of (C and Si) Co-doped ZnO with intrinsic point defects, performing the different simulation techniques based on the useful concept of “Density Functional Theory”.

The principal objectives of this thesis are:

*To study and understand the structural, electronic and optical properties of ZnO Co-doped Carbon and Silicon.

**To understand how the microscopic properties of the Co-doping material deviates with its intrinsic defect.

**To test the effectiveness of the simulations employed using the functional GGA.

Our brief will be structured around three chapters:

The first chapter includes the results of a bibliographic search exclusively directed towards the study of the properties of ZnO, experimental and theoretical Background and intrinsic defects points and conductivity control.

In the next chapter, we discuss thoroughly the density functional theory and its evolution. This chapter 2 is written in the aim of getting insight about the fundamentals of the density functional theory, which is crucial as our entire computations are based on it.

The third chapter is divided into two parts. The first part is showed our results of the structural, electronic and optical properties of Co-doped ZnO films and the second part of this chapter has been dedicated to the view the impact of native point defects on the various properties of Co-doped ZnO films.

During this scientific research, i got an Erasmus + grant from the European Union, where i headed to “Jan Dlugosz university” ,faculty of science and technology, department of theoretical physics in Czestochowa, Poland to do a training on: investigations optical properties of solids by computational methods.

The detailed program of this traineeship period is:

-Get acquainted with computational methods which would allow to predict the optical properties of materials from the chemical composition / crystal structure.

General Introduction

-Investigation relations between the electronic, optical, elastic and thermodynamic properties of chosen compounds to their structural parameters.

After the mobility, we demonstrated practical skills of using computational packages for independent solving of problems in the field of quantum chemistry of semiconductor materials for applications in solar cells; in particular the impact of crystal structure defects occurring in real materials. It has necessary theoretical basis for the interpretation of the obtained results.

Finally, we end this manuscript with a general conclusion on the theoretical analysis results obtained.

Bibliography:

- [1]S.S.Kumar, P.Venkateswarlu, V.R.Rao, G.N. Rao, Synthesis, characterization and optical properties of zinc oxide nanoparticles,J. International Nano Letters,2013,P 2-6,<https://doi:10.1186/2228-5326-3-30>.
- [2]R.Kessler, Engineered Nanoparticles in Consumer Products: Understanding a New Ingredient,J. Environmental Health Perspectives ,V 119,P A120-A125,<https://doi:10.1289/ehp.119-a120>.
- [3]Ü.Özgür, Y.Alivov, C.Liu, A.Teke, M.A.Reshchikov, S.Doğan, V.Avrutin, S.J.Cho, A.Morkoç, A comprehensive review of ZnO materials and devices,J. Applied Physic,2015,V 98,P 041301-1- 041301-103,<https://doi:10.1063/1.1992666>.
- [4]J.Fierro, Metal Oxides: Chemistry & Applications,J. CRC Press,2006.
- [5]J.Phillips, Ionicity of the Chemical Bond in Crystals,J. Reviews of Modern Physics,1970,V 42,P 317-356,<https://doi:10.1103/RevModPhys.42.317>.
- [6]A.C.Mofor, A.El-Shaer, A.Bakin, A.Waag, H.Ahlers, U.Siegner, H.Ahlers, S.Sievers, M.Albrecht, W.Schoch, N.Izyumskaya, V.Avrutin, S.Sorokin, S.Ivanov, J.Stoimenos, Magnetic property investigations on Mn-doped ZnO Layers on sapphire,J. Applied Physics Letters,2005,V 87,P 062501-1 - 062501-3,<https://doi:10.1063/1.2007864>.
- [7]L.S.Mende, G.L.M.Driscoll, ZnO – nanostructures, defects, and devices,J. Materials Today,2007,V 10,P 40-48,[https://doi:10.1016/S1369-7021\(07\)70078-0](https://doi:10.1016/S1369-7021(07)70078-0).
- [8]J.B.Cui, M.A.Thomas, H.Kandel, C.Y.Soo, T.P.Chen, Low temperature doping of ZnO nanostructures,J. Science in China Series E: Technological Sciences,2009,V 52,P 318-323,<https://doi:10.1007/s11431-008-0353-9>.

Chapter 1

Fundamentals of ZnO

This chapter is devoted to a general description of zinc oxide ZnO. In part one, presenting us with a state of the art of its main properties. Then we let's look at its fields of application.

1.1 Crystal Structure:

Zinc oxide (ZnO) is a challenging material to study for any beginner in material science. The principal reason is that it is a multifunctional material with multiple properties, many of which are unique and distinct. It is one of the most studied semiconductors and thus investigation on this material provides a solid foundation to study any other material in future [1] due to its excellent properties for various applications.

ZnO exists in wurtzite, rock-salt, and zinc-blende crystal structures; however, at ambient conditions, the thermodynamically stable phase is the wurtzite structure, Fig.1 (A) with ionicity at the borderline between covalent and ionic semiconductors. The hexagonal wurtzite crystal structure belongs to the P6₃mc class in the Hermann–Mauguin notation or to the class in the Schoenflies notation. The ZnO primitive unit cell contains two formula units, which each zinc ion surrounded by four oxygen ions Fig.1(B) in a tetrahedral coordination and vice versa [2]. The non-Centro-symmetric tetrahedral coordination in ZnO results in the piezoelectric properties, crystallographic polarity, and is also a key factor in crystal growth and defect generation.

The wurtzite ZnO has four common crystal faces, including the polar Zn-terminated (0001) and O-terminated (000 $\bar{1}$) faces (c-axis oriented), and the non-polar (11 $\bar{2}$ 0) (a-axis) and (10 $\bar{1}$ 0) faces which both contain an equal number of Zn and O atoms. The polar and the (1010) surfaces are found to be stable; however, the (11 $\bar{2}$ 0) face is less stable [3]. The lattice parameters, commonly measured at room temperature by X-ray diffraction (XRD), are $a = 3.25 \text{ \AA}$ and $c = 5.20 \text{ \AA}$ with the ratio $c/a = 1.6$ in an ideal wurtzite structure. The a-parameter typically ranges from 3.2475 to 3.2501 \AA and from 5.2042 to 5.2075 \AA for the c-parameter. The variation in lattice parameters depends on the concentration of foreign atoms, defects, external strains, and temperature [2].

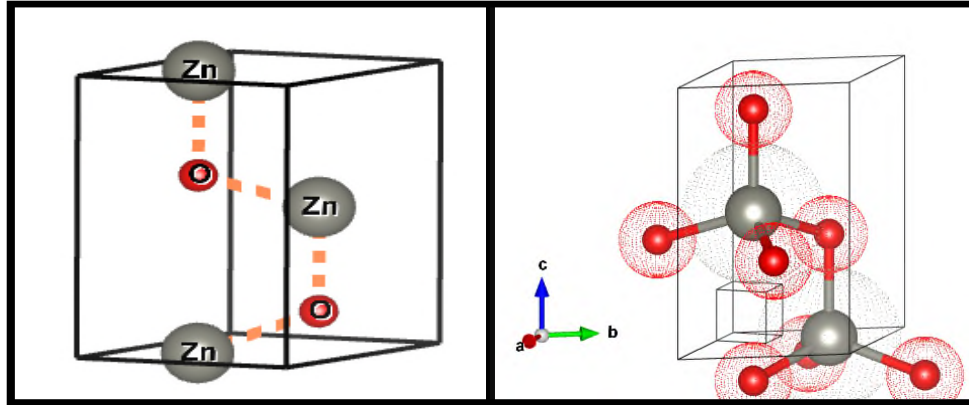


Fig.1: The hexagonal unit cell of ZnO (A) and (B) tetrahedral coordination where the green atoms are Zn and the red atoms are O.

Physical Parameter	Value
Crystal structure	Wurtzite
Lattice constant	$a=b=3.24 \text{ \AA}$ and $c=5.20 \text{ \AA}$
Molar mass	81.3g/mol
Density	5.606g/cm^3
Melting point	2248K
Bond length	$1.977\mu\text{m}$
Energy gap	3.4 eV direct
Refractive index	2.008,2.029
Dielectric constant	$\epsilon_0=8.75$ and $\epsilon_\infty=3.75$
Effective mass	Electron=0.24 and hole=0.59
Exciton bending energy	60meV
Electron-hole mobility	$200\text{cm}^2\text{V}^{-1}\text{s}^{-1}$
Ionicity	62%
Thermal conductivity	60W/mK
Heat capacity	$C_p=9.6\text{cal/mol.K}$
Breakdown voltage	$5 \times 10^6\text{Vcm}^{-1}$
Heat of crystallization	62KJ/mol
Yung modulus(bulk ZnO)	111.24.7 GPa
Bulk modulus(polycrystalline ZnO)	142.23GPa

Table.1: The physical parameters of ZnO.

1.2 Physical Properties: The physical parameters of ZnO at room temperature (300K) are shown in **Table.1** [63]

1.3 Electronic Properties:

ZnO has been widely investigated due to their excellent electronic and optical properties, non-toxicity, and low cost [4–5]. As a kind of II-VI compound semiconductor, ZnO can also serve as a high-activity semiconductor photo catalyst because it has high chemical stability, high carrier mobility, large exciting binding energy (60meV), mature synthesis technology, and tunable properties [6–7]. However, the wide band gap (3.37 eV) of ZnO will result in low absorbability (4%) under sunlight irradiation [8], which is not conducive to the photo catalytic utilization of ZnO in the visible light region.

The band structure and electronic states of wurtzite ZnO have been calculated by several theoretical approaches and determined experimentally [2]. Fig.2 shows the band structure calculation using the Local Density Approximation (LDA) and incorporating atomic self interaction corrected pseudo potentials (SIC-PP) [9 -10]. In the valence band, bands located between -10 and -5 eV correspond to the Zn 3d levels, while the upper 6 bands from -5 eV to 0 eV are mainly O 2p orbital's. The first two bands in the conduction band (CB) correspond to empty Zn 4s levels. The band gap value obtained from this calculation was reported 3.77 eV [9]. Further studies on other properties of ZnO; have been reviewed by other researchers [11-12]

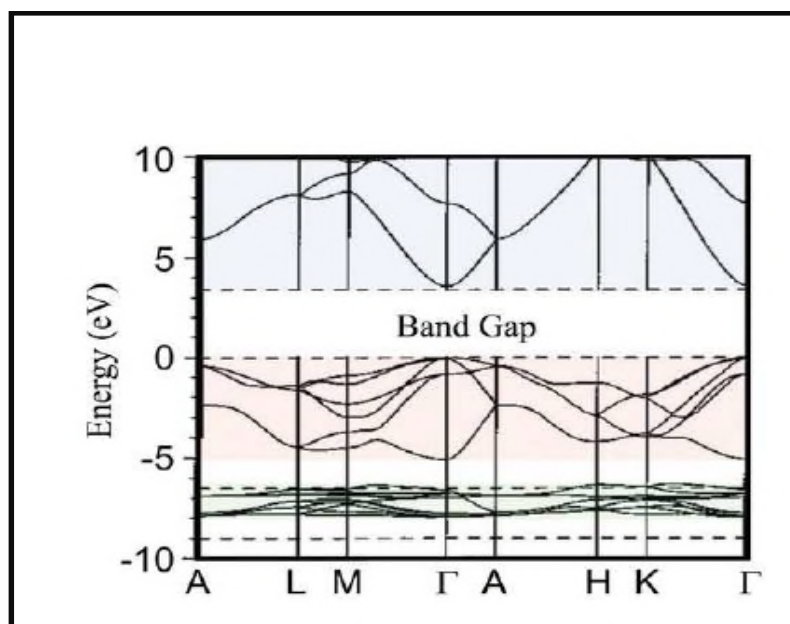


Fig.2: Band Structure of ZnO Wurtzite using LDA method [9 -10].

We notice that the maximum of the valence band and the lowest of the minimum of the conduction band at point Γ ($k = 0$), indicating that ZnO is a direct gap semiconductor. The advantage associated with this band gap is the use of ZnO as a material in intense electric fields, circuit breakers. [13], in nanometric-scaled applications such as bio-logical tracers and optoelectronic devices, as we shown in Fig.3. [14-15].

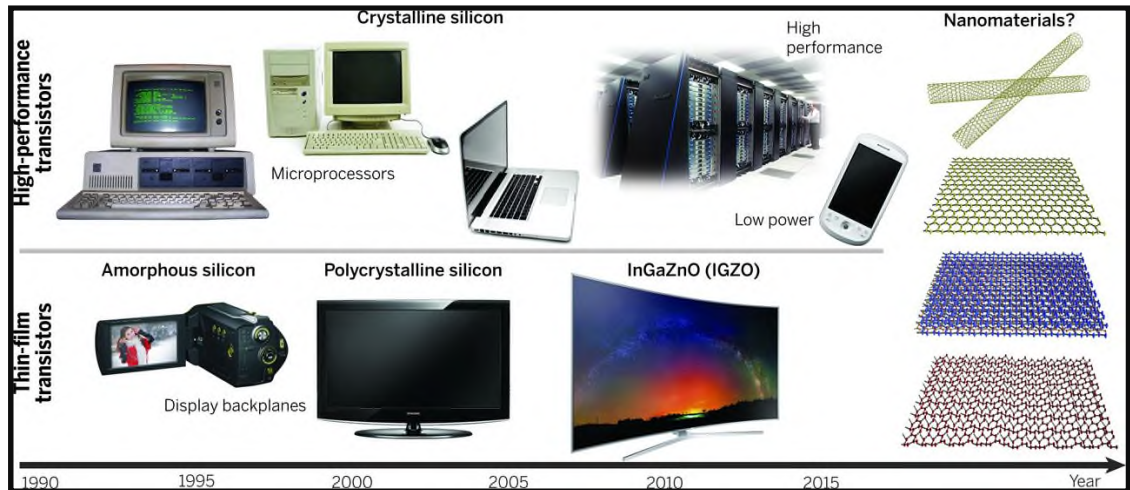


Fig.3: Technologies enabled by high-performance and thin-film transistors over the past 25 years. **(Top)** Silicon transistors have driven the microprocessors used in computational devices ranging from low-power gadgets to large servers. **(Bottom)** Various forms of cheaper silicon enabled the display revolution, now being shared by IGZO. **(Right)** Nano-materials may be the next transistor material for enabling a new generation of technologies [15].

1.4 Optical properties:

The fundamental optical properties of ZnO, such as refractive index and dielectric constants, have been determined by a number of previous studies [16-17]. The measurements are performed using ellipso-metry. The determined values of the dielectric constants of ZnO are summarized in Table.2 [17], and the refractive index of ZnO under the wurtzite structure is $m_o=2.008$ et $n_e=2$. [18].

		Film	Bulk
ϵ_0	$E \perp c$	7.46	7.77
	$E \parallel c$	8.59	8.91
ϵ_∞	$E \perp c$	3.70	3.60
	$E \parallel c$	3.78	3.66

Table.2: Values of static (ϵ_0) and high frequency (ϵ_∞) dielectric constants [17].

The work of Meyer et al, gives us a very clear treatment and an analysis of the spectrum of exciton emissions obtained for massive ZnO, n-type ZnO, and certain defects reported in the spectral characteristics, such as the emission of donor-acceptor pairs (DAP) [19].

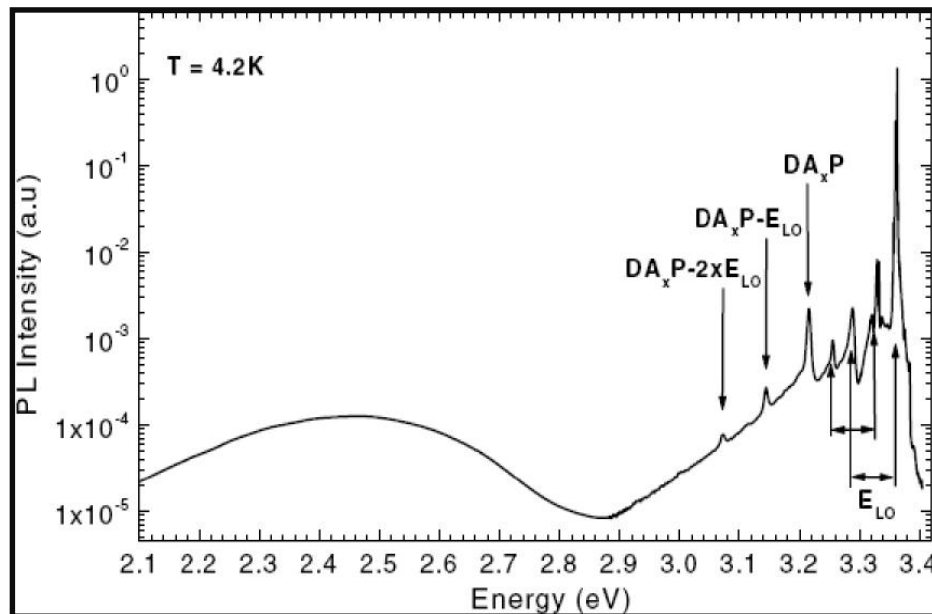


Fig.4: Photoluminescence spectrum of massive n-type ZnO (He-Cd excitation) showing donor-acceptor pairs [19].

1.5 Electrical Properties:

ZnO is an intrinsically n-type semiconductor due to the deviation from stoichiometry and the presence of intrinsic defects such as oxygen vacancies (VO), zinc interstitials (Zn_i), and zinc vacancy (V_{Zn}). Doping of ZnO provides a method for controlling its structure, and consequently optical, electrical, and magnetic properties, which leads to a range of changes, including band gap value, transparency, room-temperature ferromagnetism, piezoelectricity and magneto-optical properties [20-21-22].

The n-type doping of ZnO with a donor state, achieved by replacing atoms with one or more electrons in the outer shell compared to the substituted element (Zn or O) in ZnO. Consequently, the substitution of group-III elements on Zn sites and group-VII elements on O sites, produces highly conductive n-type ZnO. These group VII elements, F, Cl, Br and I are also donor dopants by substituting for oxygen atoms. It has been reported that fluorine F doping can increase the conductivity of ZnO by chemical spray techniques [23]. The p-type doping of ZnO with an acceptor level is provided by substitution of group-I elements on Zn sites and group-V on O sites. Although, ZnO can be easily n-type doped, efforts to obtain reliable p-type doping are still a problem due to the low solubility, much higher ionization and formation energy of p-type dopants [24-25].

1.6 p-types Conductivity:**1.6.1 Historical Background:**

The increase in the world population and industrial growth has led to an increased need for new technology, another direction to solve environmental problems and a clear future vision. Obtaining p-type doping in ZnO has proved to be a very difficult task [26], one reason is that the fact there is very few candidate shallow in ZnO. Now, several groups have p-type ZnO reported. [27]

Theoretically, the group I elements, Li and Na, are good acceptors for ZnO when they occupy Zn sites, but it is often stated that doping with Li always produces semi-insulating (SI) ZnO [28]. This is due to the interstitial Li Li_i has a formation energy than Li_{Zn} in n-type ZnO, and Li_i is a donor. Therefore, a sample with a high concentration of Li may have a self-compensation problem, placing itself between Li_{Zn} and Li_i , giving a Fermi level very close to the middle of the gap, and thus producing a semi-insulating material. The same problem arises for the Na

The elements of group V, N, P, As and Sb, are important for the realization of the p-type ZnO. Nitrogen N can be a good acceptor, since its core electronic structure and ionic radius are similar to those of oxygen O and it easily replaces O atoms.

However it seems difficult to make p-type ZnO through doping by N atoms. It would be very promising to produce good p-type materials using other group V elements such as P, As and Sb with different mechanisms. Using density functional theory (DFT), Limpijumnong et al find that a complex, AsZn-2VZn, has a low energy of formation to act as acceptors in the host structure of ZnO [29].

Experimentally, Joseph et al [30] have reported p-type ZnO through codoping using N (in the form of N₂O) with Ga as a codopant. They reported suspiciously high hole concentrations of $4 \times 10^{19} \text{ cm}^{-3}$ and low room temperature resistivity of 2_Ωcm. Yan et al [31] have proposed an alternative interpretation of the results, in terms of the chemical potentials of the gases used during growth. More recently, Yan et al [32] suggested that co-doping would be effective in the case of ZnO only for very high Ga and N concentrations so that an impurity band (caused by neutral Ga +N complexes) would form above the ZnO valence band, leading to a significant reduction of the ionization energy of the excess N impurities. We note, however, that the experimental results for co-doping in ZnO have not been reproduced.

More interesting, the co-doping has been suggested to be an effective method of achieving p-type conductivity in ZnO. The term co-doping means that, along with the acceptors that are incorporated to produce holes, donors are also incorporated during the growth [33].

1.7 ZnO as a photo-catalyst:

ZnO nanostructures with different morphologies and properties have attracted much attention for photo-catalytic applications, in both environment and energy fields.

Up to now, more than 2500 papers have been published on the photo-catalytic performance of ZnO nanostructures. All of this research investigated the influence of different factors, such as preparation method, composition, morphology, size, specific surface area, porosity, and crystalline phase. Fig.5 shows the trend of publications of ZnO nanostructures as a photo-catalyst in the last 15 years. It shows an evolution and an exponential growth of research for both pure and doped ZnO nanostructures. [34]

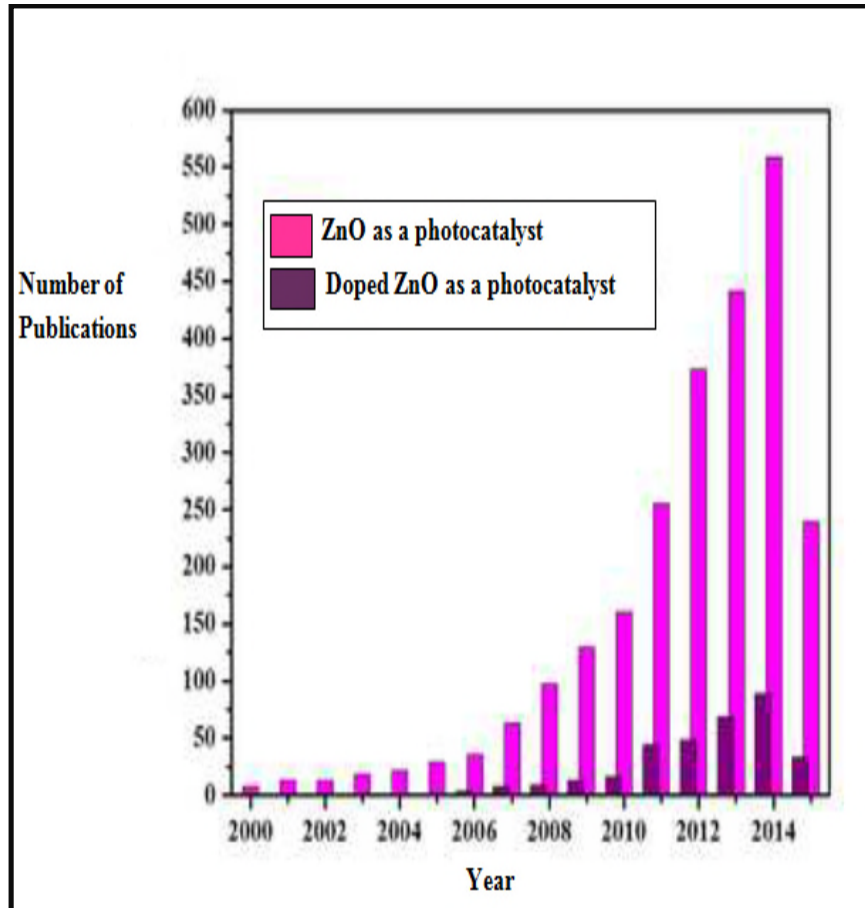


Fig.5: The photo-catalytic applications of the ZnO nanostructures in the environment and energy fields. (b) The number of publications of ZnO and doped ZnO as a photocatalys from 1 January 2000 to 22 May 2015 in the Scopus citation database using keywords in title section "photo-cataly" and "Zinc Oxide" or ZnO.

1.8 ZnO on Spintronic:

In the current time, spin-tronics is an emerging technology that exploits not only the out also the spin of the electron to encode information. The spin, which was totally d in the applications of classical microelectronics, gives rise to new physical ana which offer interesting perspectives in terms of integrability, speed of ication, consumption and non-volatility of information. It is in this sense that ics have aroused great interest in the scientific community as an alternative to onal electronics which today face major physical obstacles due to further reduction in of the components. In 1988, the teams of Albert Fert and Peter Grünberg discovered giant magneto-resistance (GMR), which can be considered as the starting point of the field.

Traditionally, ZnO is used as important diluted magnetic semiconductors. A large number of experimental studies [35–36] have shown that the ferromagnetism of ZnO strongly depends on the preparation of samples, and the point defects in the systems may play an

important role. Thus, how to effectively control the point defects in the experiment becomes a very interesting and challenging problem. [37]

Spin-tronics has important applications, the most widespread being the reading of hard disks by the giant magneto-resistance (GMR), the tunnel magneto-resistance (TMR: Tunnel Magneto-Resistance) and writing magnetic memories (MRAM: Magneto-resistive Random Access Memories) in our computers.

1.9 Nonmetal Doping of ZnO:

Nonmetal doping of ZnO, which is expected to substitute for oxygen atoms, has been intensively investigated. In this regard, hybridization of nonmetal dopants orbital and O 2p states of ZnO raise the upper edge of the valence band and thus narrow the band gap. Elements with lower electro-negativity than oxygen and similar size to that of lattice O atoms are two main requirements for effective nonmetal dopants [38]. ZnO doping with nonmetals, such as carbon (C), nitrogen (N), and sulfur (S) can lead to the formation of intermediate energy levels and extend the valence band [39-40]. Details of ZnO doping process by one most popular nonmetals Carbon and consequent results are discussed in the third chapter.

1.9.1 Carbon doped ZnO:

Carbon doping is the one most popular approach for nonmetal doping of ZnO and has received considerable interest during recent years. Pan et al. [41] have studied the structural and magnetic properties of pure and C-doped ZnO by DFT calculations. The formation energies of carbon doping have been calculated and the results show that carbon incorporation occurs with carbon oxidation number ranging from -4, by replacing an oxygen atom (C_O), to +4 by the formation of carbonate species (C_{Zn+2O_i}). [34]. Carbon substitutional doping on Zn sites (C_{Zn}) and interstitial carbon (C_i) are also observed [42]. Tan et al. [42] calculated the formation energy of C doping by ab initio methods and showed that the formation energy of C_{Zn} and C_{Zn+2O_i} increased with decreasing of oxygen partial pressure and the formation of CO/CO₂ species occurred in an oxygen rich ambient.

Comparing XRD lattice constants showed a lattice expansion in C doped ZnO, which indicated that C^{4-} with larger ionic radius of 260 pm is substituted instead of smaller O^{2-} with 140 pm ionic radius [43-44]. In contrast, in the other work, the lattice constant of C doped ZnO became smaller, which indicated C^{4+} with an ionic radius of 16 pm is substituted for the larger Zn^{2+} with an ionic radius of 74 pm (see ref [45-46]). Moshfegh's group [45] recently utilized multi-walled carbon nano-tubes (MWCNTs) as a source of carbon doping in C-doped ZnO nano-fibers applied as a photo-catalyst.

As evidence for visible-light activity and band gap narrowing of C-doped ZnO, band gap energy was also calculated using Tauc's formula. Based on data analysis, band gaps of 3.13 and 3.01 eV are obtained for pure and MWCNT-doped ZnO.

Recently, Doping with non-metal elements such as C has been reported to reduce the band gap of a wide-band semiconductor by enhancing a number of properties but not limited to ferromagnetism, magnets to transport properties and p type conduction properties [47-48]

1.10 Transition metal Doping in ZnO:

Transition metal doping in ZnO crystal lattice is one of the well-known strategies for tuning the band gap of ZnO to modify the morphology, particle, crystallite size of ZnO host and make it a visible-light-active photo-catalyst [49-50]. It is well established that transition metal doping inhibits ZnO growth, which leads to the production of smaller nanostructures with higher surface area [51]. Substitutions of transition metal cations modify the environment of Zn in ZnO lattice and change its electronic band structure and introduce many crystal defects such as oxygen vacancies. Oxygen vacancies may act as efficient electron traps and lead to an enhancement in photo-generated electron/hole separation efficiency [52]. The ZnO optical absorption edge extends into visible-light region after transition metal such as Ag, Mn, Cu, Fe, Ni and Si doping. Actually, the transition-metal-doped Si, Ge, and Li semiconductors were hardly applied because their Curie temperatures were lower than room temperature. Studies on hexagonal wurtzite ZnO as diluted magnetic semiconductors are active, and effective transition-metal-doped ZnO can achieve a Curie temperature higher than room temperature [53-54]. Several studies confirm that the doping affects luminescence of ZnO, e.g. red emission in Co doped ZnO [55], yellow-orange-red emission in Mn doped ZnO [56], blue emission in Cu doped ZnO [57], orange emission in Si doped ZnO [58] etc.

1.10.1 Silicium doped ZnO:

In the previous report with pure Si doping (substitution $\leq 3\%$) it has been presented that Eg band gap increased from about 3, 28 to 3, 44 eV at different doping concentrations. [59]. In addition, the optical properties of doped ZnO, in particular with silicon Si, have been systematically investigated with ab initio calculations based on the density functional theory (DFT) [60].

1.11 Co-doping of ZnO:

Moreover, the co-doping of ZnO is one of the best chemical methods for advanced applications and may modify considerably its physical properties. Indeed, Park et al. [61] have noticed that the electrical properties were enhanced with aluminum–gallium co-doping of ZnO nano-fibers fabricated by electro spinning technique. [62]. In the final chapter, we will depicted the original ZnO:C:Si structure reveals promising optical and electronic properties, and it can be investigated as good candidates for practical uses as transparent and conducting electrodes in solar cell devices.

1.12 Intrinsic Defects points:

However, in real life, there is always deviation in the crystal lattice structure. Besides ionicity and lattice stability, the major cause of such deviation in a lattice structure is the defect or the deviation of the periodicity of atomic arrangement in the crystal. These defects are either point defects like zinc anti-sites and oxygen vacancies or extended defects like dislocations which increase the lattice constant of ZnO. The principal cause of defect in the crystal is the thermal agitation which increases anharmonicities in the lattice vibration and to maximize the entropy, atoms/ions may be delocalized from their lattice points. We are particularly interested in native point defects in ZnO, especially; vacuum, interstitial and the discussion of other kinds of defects are beyond the scope of this thesis. A defect in a crystal is a thermodynamic necessity. Such as the oxygen point defect in ZnO is the delocalization of an oxygen ion from its lattice point. Whenever an oxygen ion leaves its lattice point, it creates holes of charge plus two. As a result, the four zinc ions dangle within the lattice point causing anharmonicities in the overall lattice vibration. These holes in the lattice point create an electric potential in the crystal. Since, ZnO is an n-type semi-conductor; there is always the availability of the mobile electrons in the crystal. As a consequence, if this Coulomb's potential attracts two electrons, then the lattice point becomes neutral or zero charged; if it attracts one electron, then the lattice point charge becomes plus one. Otherwise, the lattice point charge becomes two plus if there is no interaction between holes and electrons [63]. Henceforth, the native oxygen point defect in ZnO is classified as three kinds:

- (i) Oxygen point defect with zero charged state.
- (ii) Oxygen point defect with plus one charged state.
- (iii) Oxygen point defect with plus two charged state.

Fig.6, Fig.7 and Fig.8 explain their formations. Among these three kinds of oxygen point defects,

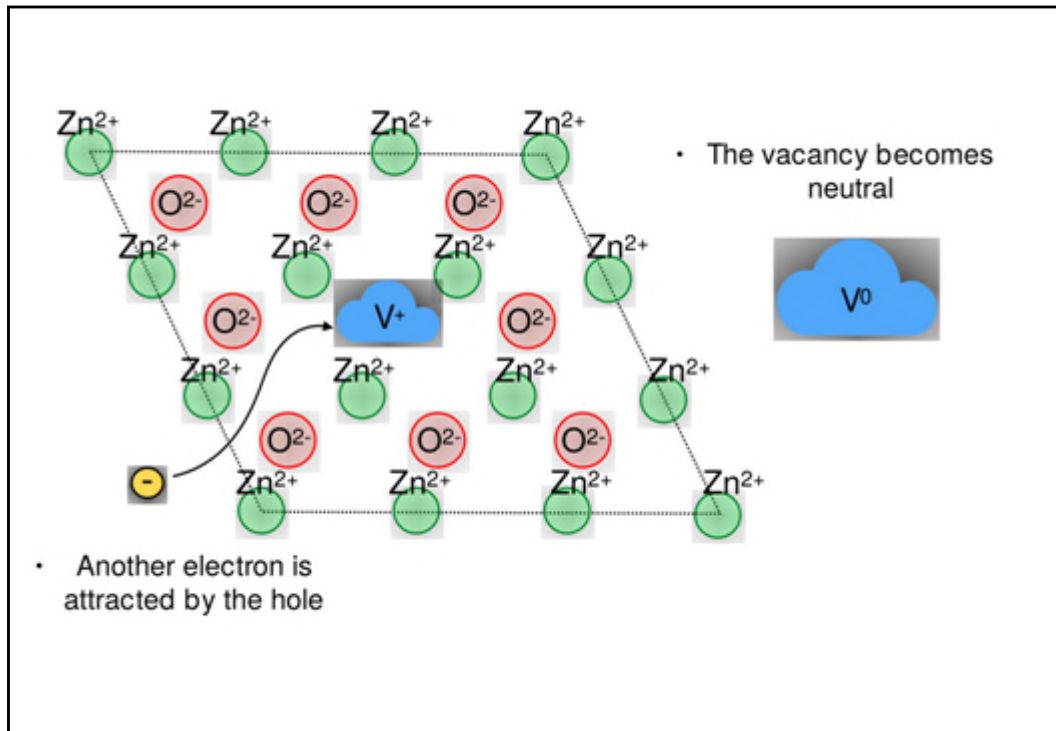


Fig.6: A systematic diagram of formation of the Zero ZnO (V^0_o).

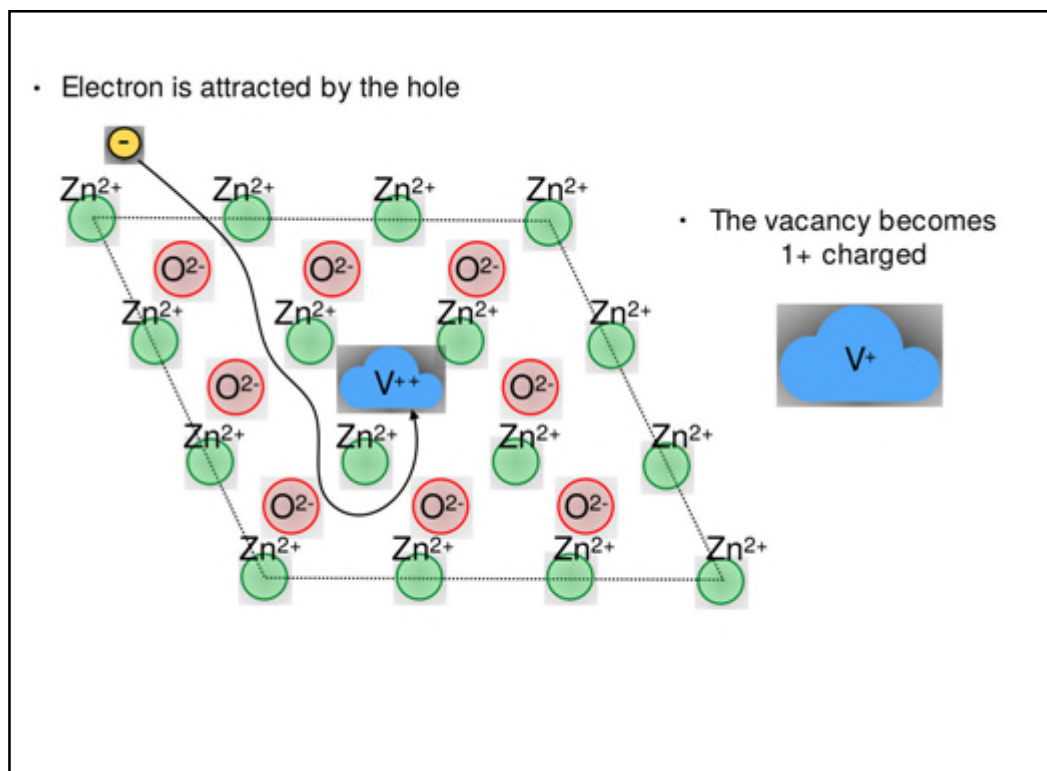


Fig.7: A systematic diagram of formation of the One ZnO (V^+_o).

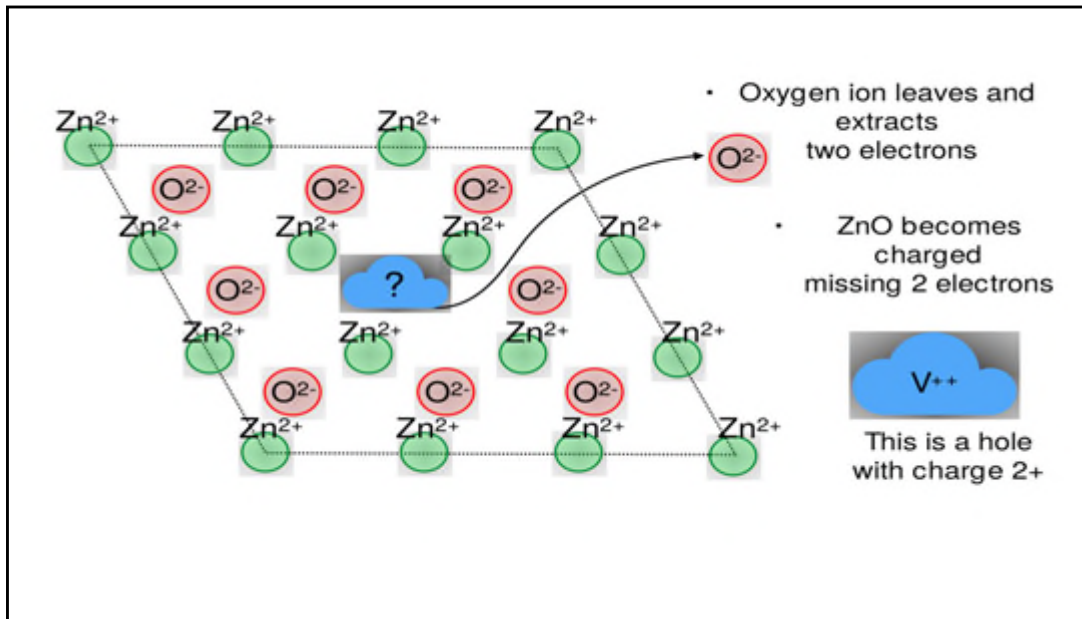
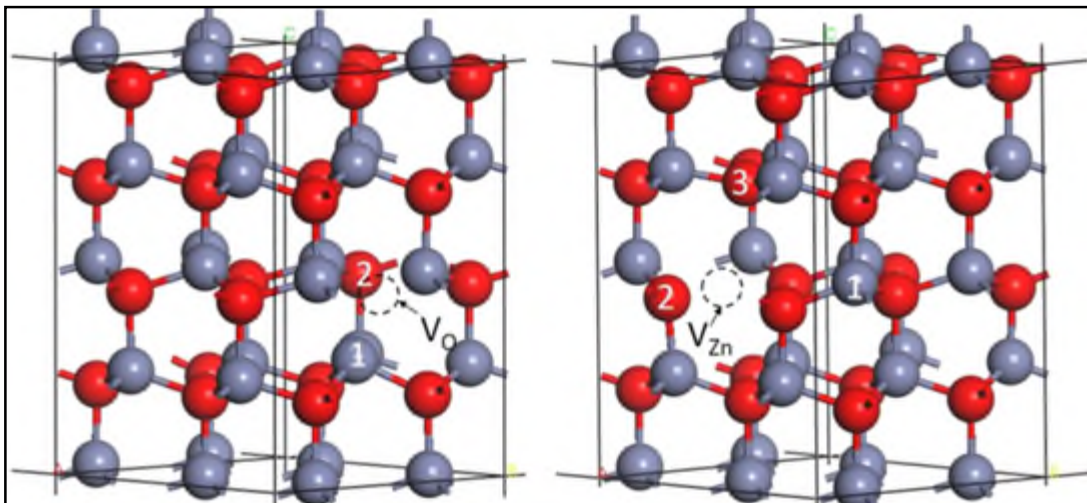


Fig.8: A systematic diagram of formation of the Two ZnO (V^{2+}_O) [63].

In our research, we are interested in the tow important native point defects:

1/Oxygen and Zinc Vacancies:



2/Oxygen and Zinc tetrahedral interstitials:

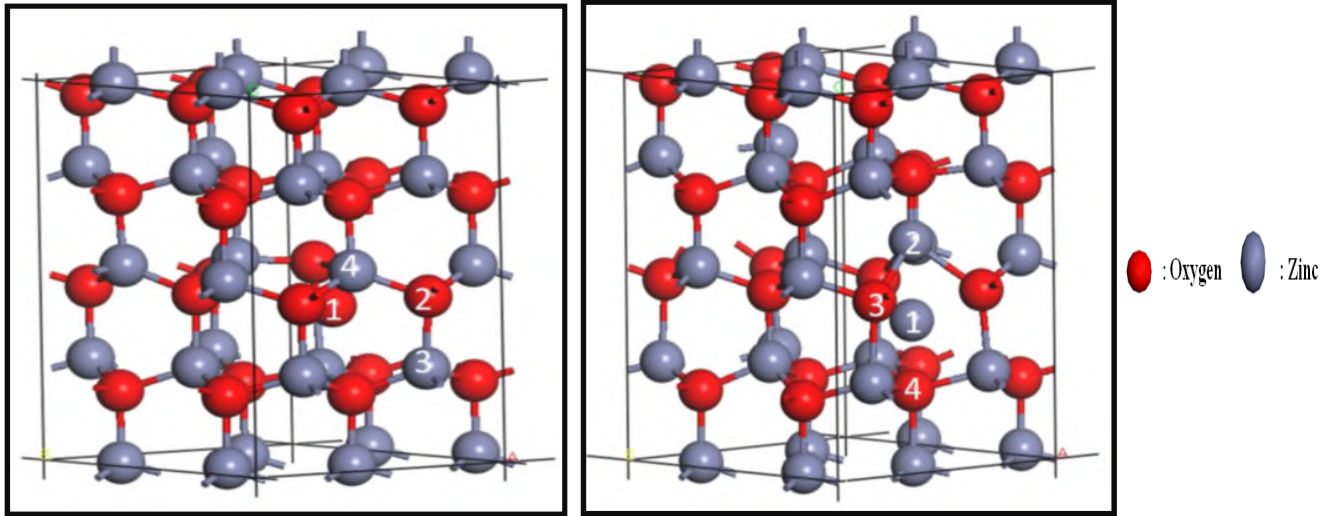


Fig.9: Different native points [64]

1.12.1 Some Experimental and Theoretical Background:

During preparation, ZnO will exhibit intrinsic defects, such as zinc vacancy (V_{Zn}) and oxygen vacancy (V_O), and the role of these vacancy defects in the optical properties of ZnO has been explored experimentally and theoretically [65–66]. It is suggested that zinc vacancies are a possible source of the often-observed green luminescence in ZnO [33]. Tang et al. [65] found that V_O narrowed the band-gap of ZnO, and the results of photo-catalytic experiments reflected that V_O can not only act as impurity levels in the band structure of ZnO but also function as electron traps to accept the photo-generated electrons. Wang et al. [67] prepared pristine ZnO films, and found that the introduction of the green luminescence is correlated with the formation of the Zn vacancy-related defect (V_{Zn}). Theoretical studies of the effect of vacancy defects in metal element-doped ZnO were performed in [68–69]. Bai et al. [68] studied the electronic and optical properties of 2D ZnO:Mg/Be with V_O or V_{Zn} . The results indicated that V_O will cause a blue-shift, whereas V_{Zn} will cause a red-shift in the optical absorption spectra. Alessandra et al. [70] presented a first-principles study on the effect of native point defects in Al:ZnO transparent conductive oxide. They found that V_O defects maintain the electrical properties but worsen the transparency of native Al:ZnO, whereas V_{Zn} defects are strong electron acceptors that can destroy the metal-like conductivity of the system. Meng et al. [71] studied the formation energies, electronic, and optical properties of pure ZnO and Er-doped ZnO with and without incorporating the intrinsic point

defects (IPDs). The strong interactions between the Er dopants and acceptor-type IPDs in ZnO were perceived as one of the important reasons for the strong light absorption in the visible and infrared regions. For the yttrium element, Li et al. [69] calculated the electronic and ferromagnetic properties of a Y-doped ZnO (0001)-Zn polar surface with and without point defects. The calculated results showed that V_{Zn} is an acceptor that can trap electrons to balance the electrovalence, and V_O can introduce an impurity level in the band-gap near the Fermi level.

Native or intrinsic defects are imperfections in the crystal lattice that involve only the constituent elements [68]. They include vacancies (missing atoms at regular lattice positions), interstitials (extra atoms occupying interstices in the lattice) and anti-sites (a Zn atom occupying an O lattice site or vice versa). Native defects can strongly influence the electrical and optical properties of a semiconductor, affecting doping, minority carrier lifetime and luminescence efficiency, and are directly involved in the diffusion mechanisms connected to growth, processing and device degradation [68–71].

The other native defects (zinc anti-sites, oxygen interstitials and oxygen anti-sites) have higher formation energies and, therefore, are not expected to play a role in ZnO under near-equilibrium conditions. The ZnO anti-site is a double donor in n-type ZnO, but its high formation energy indicates that it is an unlikely source of unintentional n-type conductivity. Recent first-principles calculations revealed a large off-site displacement of the Zn atom by more than 1Å from the substitutional lattice site toward two next-nearest-neighbor oxygen atoms along the $[1\ 0\ .1\ 0]$ direction, as shown in fig.9 [72]. The resulting ZnO–O inter-atomic distances are only 8% larger than the equilibrium Zn–O bond length. At this equilibrium configuration we find three ZnO–Zn distances of $\sim 2.4\text{Å}$ and one ZnO–Zn distance of $\sim 2.8\text{Å}$.

Most of the calculations agree that oxygen vacancies and zinc vacancies are the lowest energy defects, followed by the Zn interstitial and the ZnO anti-site. Oxygen interstitials and O_{Zn} anti-sites were found to be high in energy [33].

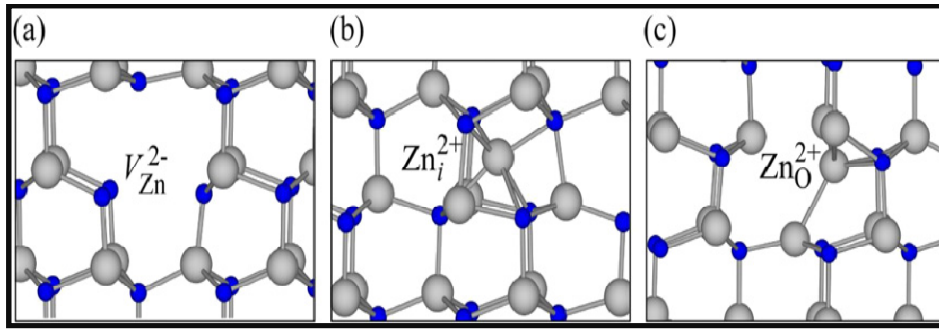


Fig.10: Calculated local atomic geometry for (a) the Zn vacancy; (b) the zinc interstitial and (c) Calculated local atomic geometry of the zinc anti-site .[33] ,where the blue atom is O and the green atom is Zn.

1.12.2 Intrinsic Defects Points and Conductivity Control:

Due to the native defects in ZnO, n-type conductivity can be readily acquired while obtaining p-type ZnO is still a challenge. Nowadays, the complexity of doping behavior in ZnO has attracted much attention. Group I and group III are popular dopants for fabricating p-type and n-type ZnO, respectively. [73-74]. Carbon is a group IV element that can be expected acting as a donor or double acceptor in ZnO depending on the doping concentration and the growth conditions.[75] To investigate carbon impurities is of importance since it cannot be avoided during the sample fabrication processes. Up to now, not many studies were focused on the effect of carbon impurities on the properties of ZnO [76].

Understanding the incorporation and behavior of point defects in ZnO is therefore essential to its successful application in semiconductor devices. Native defects are, in general, related to the compensation of the predominant acceptor or donor dopants, i.e. donor defects are easier to form in p-type material [33].

1.13 Experimental approach and Ab initio approach:

The different methods used for the production of undoped and doped ZnO thin films are: the sol gel method, chemical vapor deposition, molecular beam epitaxy (MBE), pulsed laser ablation (PLD) and sputtering. ab initio calculations are used to predict the type of materials and determine the nature of the electronic interactions brought into play. Much software has been explored to compute these properties such as: Espresso, ab initio, Vasp, Elker, Wien2k and Materials Studio into CASTEP code.

In the second chapter, we choose the Materials studio based on DFT approximation as a primary method in our research.

1.14 Conclusion:

In this chapter we have presented the main properties and applications of Zinc Oxide: electronic, optical and electrical, .We then discussed the main applications of this transparent semiconductor: optoelectronic, photocatalys and spintronic. Doped ZnO appears to be a promising candidate for the development of metal-oxide semiconductors (MOS) because of its high performance, good stability, transparency, and flexibility and their influences on the p type order. Experimental and theoretical work carried out so far on the electronic properties of ZnO doped with different non metals and transition metals and especially Carbon and Silicium have been cited.

Bibliography:

- [1] P.Kumar, H.K.Malik, A.Ghosh, R.Thangavel, K.Asokan, An insight to origin of ferromagnetism in ZnO and N implanted ZnO thin films: Experimental and DFT approach, *J. Alloys and Compounds*, 2018, V 768, P 323-328, <https://doi.org/10.1016/j.jallcom.2018.07.097>.
- [2] H.Morkoç, Ü.Özgür, Zinc oxide: fundamentals, materials and device technology, John Wiley & Sons, New York, 2008, ISBN:97835274081393527408134.(Book)
- [3] C.Jagadish, S.Pearson, Zinc oxide bulk, thin films and nanostructures: processing, properties, and applications, J. Elsevier, Amsterdam, 2011, ISBN 13:978-0-044722-3, ISBN 10:0-08-044722-8.(Book)
- [4] S.Fu, J.Chen, H.Han, W.Wang, H.Shi, J.Fu, Y.Jia, ZnO@Au@Cu₂O nanotube arrays as efficient visible-light-driven photoelectrod, *J. Alloys Compound*, 2019, V 799, P183–192, <https://doi.org/10.1016/j.jallcom.2019.05.340> 799.
- [5] S.Chen, F.Liu, M.Xu, J.Yan, F.Zhang, W.Zhao, Z.Zhang, Z.Deng, J.Yun, R.Chen, C.Liu, First-principles calculations and experimental investigation on SnO₂@ZnO hetero-junction photo-catalyst with enhanced photo-catalytic performance, *J. Colloid Interface Science*, 2019, V 553, P 613–621, <https://doi.org/10.1016/j.jcis.2019.06.053>.
- [6] N.Tu, H.Bui, D.Trung, A.Duong, D.Thuy, D.Nguyen, K.Nguyen, P.Huy, Surface oxygen vacancies of ZnO: A facile fabrication method and their contribution to the photoluminescence, *J. Alloys Coumpound*, 2019, V 791, P 722-729, <https://doi.org/10.1016/j.jallcom.2019.03.395>.
- [7] G.Singh, S.Kumar, V.P.Singh, R.Vaish, Transparent ZnO crystallized glass ceramics for photocatalytic and antibacterial applications, *J. Applied Physics*, 2019, V 125, P 175102-1-175102-12, <https://doi.org/10.1063/1.5081988>.
- [8] W.Mohamed, A.Abu-Diefb, Synthesis, characterization and photocatalysis enhancement of Eu₂O₃- ZnO mixed oxide nanoparticles, *J. Physics and Chemistry of Solids*, 2018, V 116, P 375-385, <https://doi.org/10.1016/j.jpcs.2018.02.008>.
- [9] D.Vogel, P.Krüger, J.Pollmann, Ab initio electronic-structure calculations for II-VI semiconductors using self-interaction-corrected pseudo-potentials, *J. Physics Review*, 1995, V 52, P 314-319, <https://doi.org/10.1103/PhysRevB.52.R14316>.
- [10] R.M.Pasquarelli, D.S.Ginley, R.O'Hayre, Solution processing of transparent conductors: from flask to film, *J. Chemical Society Review*, 2011, V 40, P 5406–5441, <https://doi.org/10.1039/C1CS15065K>.

- [11] S. Pearton, D. Norton, K. Ip, Y. Heo, T. Steiner, Recent progress in processing and properties of ZnO, *J. Progress in Materials Science*, 2005, V 50, P 293-340 <https://doi.org/10.1016/j.pmatsci.2004.04.001>.
- [12] J. Li, S. Ma, X. Liu, Z. Zhou, C. Q. Sun, ZnO meso-mechano-thermo physical chemistry, *J. Chemical Reviews*, 2012, V 112, P 2833–2852, <https://doi.org/10.1021/cr200428m>.
- [13] Ü. Özgür, Y. L. Alivov, C. Liu, A. Teke, M. A. Reshchikov, S. Doğan, V. Avrutin, S. J. Cho, H. Morkoç, A comprehensive review of ZnO materials and devices, *J. Applied Physics Reviews*, 2005, V 98, P 041301-1-041301-103, <https://doi.org/10.1063/1.1992666>.
- [14] H. Hong, J. Shi, Y. Yang, Y. Zhang, J. E. Engle, R. Nickles, X. Wang, W. Cai, Cancer-Targeted Optical Imaging with Fluorescent Zinc Oxide Nanowires, *J. Nano Letters*, 2011, P 3744–3750, <https://doi.org/10.1021/nl201782m>.
- [15] A. D. Franklin, Nanomaterials in transistors: From high-performance to thin-film applications, *J. Science*, 2015, V 349, P aab2750-1-aab2750-9, <https://doi.org/10.1126/science.aab2750>.
- [16] X. W. Sun, H. S. Kwok, Optical properties of epitaxially grown zinc oxide films on sapphire by pulsed laser deposition, *J. Applied Physics*, 1999, V 86, P 408-411, <https://doi.org/10.1063/1.370744>.
- [17] N. Ashkenov, B. N. Mbenkum, C. Bundesmann, V. Riede, M. Lorenz, D. Spemann, E. M. Kaidashev, A. Kasic, M. Schubert, M. Grundmann, Infrared dielectric functions and phonon modes of high-quality ZnO films, *J. Applied Physics*, 2003, V 93, P 126-133, <https://doi.org/10.1063/1.1526935>.
- [18] S. Pearton, D. Norton, K. Ip, Y. Heo, T. Steiner, ~~RETRACTED~~: Recent progress in processing and properties of ZnO, *J. Progress in Materials Science*, 2005, V 50, P 293-340, <https://doi.org/10.1016/j.pmatsci.2004.04.001>.
- [19] B. K. Meyer, H. Alves, D. M. Hofmann, W. Kriegseis, D. Forster, F. Bertram, J. Christen, A. Hoffmann, M. Straßburg, M. Dworzak, U. Habocek, A. V. Rodina, Bound exciton and donor–acceptor pair recombinations in ZnO, *J. physica status solidi (b)*, 2004, P 231-260, <https://doi.org/10.1002/pssb.200301962>.
- [20] C. Klingshirn, J. Fallert, H. Zhou, J. Sartor, C. Thiele, F. Flaig, D. Schneider, H. Kalt, 65 years of ZnO research - old and very recent results, *J. physica status solidi (b)*, 2010, P 1424–1447, <https://doi.org/10.1002/pssb.200983195>.
- [21] H. Wenckstern, H. Schmidt, M. Brandt, A. Lajn, R. Pickenhain, M. Lorenz, M. Grundmann, D. Hofmann, A. Polity, B. Meyer, H. Saal, M. Binnewies, A. Börger, K. Becker, V. Tikhomirov,

- K.Jug, Anionic and cationic substitution in ZnO, *J. Progress in Solid State Chemistry*, 2009, V 37, P 153-172, <https://doi.org/10.1016/j.progsolidstchem.2009.11.008>.
- [22] J.Fan, K.Sreekanth, Z.Xie, S.Chang, K.Rao, p-Type ZnO materials: Theory, growth, properties and devices, *J. Progress in Materials Science*, 2013, V 58, P 874-985, <https://doi.org/10.1016/j.pmatsci.2013.03.002>.
- [23] P.Kumar, C.Kartha, K.Vijayakumar, F.Singh, D.Avasthi, Effect of fluorine doping on structural, electrical and optical properties of ZnO thin films, *J. Materials Science and Engineering: B*, 2005, V 117, P 307-312, <https://doi.org/10.1016/j.mseb.2004.12.040>.
- [24] W.Li, Q.Hou, Z.Xu, C.Zhao, Study of point defect on the stability and magneto-optical properties of ZnO:Cu by first-principles, *J. Molecular Physics*, 2019, P 1-14, <https://doi.org/10.1080/00268976.2018.1556406>.
- [25] L.P.Dai, H.Deng, F.Y.Mao, J.D.Zang, The recent advances of research on p-type ZnO thin film, *J. Materials Science: Materials in Electronics*, 2008, V 19, P 727-734, <https://doi.org/10.1007/s10854-007-9398-y>
- [26] D.Look, Recent advances in ZnO materials and devices, *J. Materials Science Engineering: B*, 2001, V 80, P 383-387, [https://doi.org/10.1016/S0921-5107\(00\)00604-8](https://doi.org/10.1016/S0921-5107(00)00604-8).
- [27] A.Tsukasaki, A.Ohtomo, T.Onuma, M.Ohtani, T.Makino, M.Sumiya, K.Ohtani, S.Chichibu, S.Fuke, Y.Segawa, H.Ohno, H.Koinuma, M.Kawasaki, Repeated temperature modulation epitaxy for p-type doping and light-emitting diode based on ZnO, *J. Nature Materials*, 2005.
- [28] X.S.Wang, Z.C.Wu, J.F.Webb, Z.G.Liu, Ferroelectric and dielectric properties of Li-doped ZnO thin films prepared by pulsed laser deposition, *J. Applied Physics A: Materials Science and Processing*, 2003, P 561-565, <https://doi.org/10.1007/s00339-002-1497-2>.
- [29] S.Limpijumnong, S.B.Zhang, S.Weiland, C.H. Park, Doping by Large-Size-Mismatched Impurities: The Microscopic Origin of Arsenic- or Antimony-Doped p-Type Zinc Oxide, *J. Physical Review Letters*, 2004, V 92, P 155504-1-155504-4, <https://doi.org/10.1103/PhysRevLett.92.155504>.
- [30] M.Joseph, H.Tabata, T.Kawai, p-Type Electrical Conduction in ZnO Thin Films by Ga and N Codoping, *J. Japan Society of Applied Physics*, 1999.
- [31] Y.Yan, S.B.Zhang, S.Pantelides, Control of Doping by Impurity Chemical Potentials: Predictions for p-Type ZnO, *J. Physical Review Letters*, 2001, V 86, P 5723-5726, <https://doi.org/10.1103/PhysRevLett.86.5723>.

- [32] Y. Yan, J. Li, S. Wei, M. Al-Jassim, Possible Approach to Overcome the Doping Asymmetry in Wideband Gap Semiconductors, *J. Physical Review Letters*, 2007, V 98, P 135506-1-135506-4, <https://doi.org/10.1103/PhysRevLett.98.135506>.
- [33] A. Janotti, C. V. de Walle, Fundamentals of zinc oxide as a Semiconductor, *J. Reports on Progress in Physics*, 2009, V 72, P 1-29, <https://doi:10.1088/0034-4885/72/12/126501>.
- [34] M. Samadi, M. Zirak, A. Naseri, E. Khorashadizade, A. Moshfegh, Recent progress on doped ZnO nanostructures for visible-light photocatalysis, *J. Thin Solid Films*, 2016, V 605, P 2-19, <https://doi.org/10.1016/j.tsf.2015.12.064>.
- [35] M. Venkatesan, C. Fitzgerald, J. Coey, Thin films: unexpected magnetism in a dielectric oxide, *J. Nature*, 2004, V 430, P 630, <https://doi.org/10.1038/430630a>.
- [36] Y. Sun, X. Li, Y. Zong, Y. Lan, Z. Li, J. Feng, H. Fan, Z. Zhang, X. Zheng, Thermal decomposition synthesis of single-crystalline porous ZnO nanoplates self-assembled by tiny nanocrystals and their pore-dependent magnetic properties, *J. Ceramics International*, 2017, V 43, P 6029-6038, <https://doi.org/10.1016/j.ceramint.2017.01.143>.
- [37] Q. Hou, X. Jia, Z. Xu, C. Zhao, L. Qu, Effects of Li doping and point defect on the magnetism of ZnO, *J. Ceramics International*, 2018, V 44, P 1376-1383, <https://doi.org/10.1016/j.ceramint.2017.09.002>.
- [38] J. Coronado, F. Fresno, M. Alonso, R. Portela, Design of advanced photocatalytic materials for energy and environmental applications, *J. Springer*, 2013. (Book)
- [39] S. Kadam, V. Mate, R. Panmand, L. Nikam, M. Kulkarni, R. Sonawane, B. Kale, A green process for efficient lignin (biomass) degradation and hydrogen production via water splitting using nanostructured C, N, S-doped ZnO under solar light, *J. RSC Advances*, 2014, P 1-10, <https://doi.org/10.1039/C4RA10760H>.
- [40] L. Chen, Y. Tu, Y. Wang, R. Kan, C. Huang, Characterization and photoreactivity of N-, S-, and C-doped ZnO under UV and visible light illumination, *J. Photochemistry and Photobiology A: Chemistry*, 2008, V 199, P 170-178, <https://doi.org/10.1016/j.jphotochem.2008.05.022>.
- [41] H. Pan, J. Yi, L. Shen, R. Wu, J. Yang, J. Lin, Y. Feng, J. Ding, L. Van, J. Yin, Roomtemperature ferromagnetism in carbon-doped ZnO, *J. Physical Review Letter*, 2007, V 99, P 127201-1-127201-4, <https://doi.org/10.1103/PhysRevLett.99.127201>.
- [42] S. Tan, X. Sun, Z. Yu, P. Wu, G. Lo, D. Kwong, p-type conduction in unintentional carbondoped ZnO thin films, *J. Applied Physics Letters*, 2007, V 91, P 072101-1-072101-3, <https://doi.org/10.1063/1.2768917>.

- [43] Y. Zhu, M. Li, Y. Liu, T. Ren, Z. Yuan, Carbon-Doped ZnO hybridized homogeneously with graphitic carbon nitride nano-composites for photo-catalysis, *J. Physical Chemistry C*, 2014, V 118, P 10963–10971, <https://doi.org/10.1021/jp502677h>.
- [44] X. Zhou, Y. Li, T. Peng, W. Xie, X. Zhao, Synthesis, characterization and its visible-light induced photocatalytic property of carbon doped ZnO, *J. Materials Letters*, 2009, V 63, P 1747-1749, <https://doi.org/10.1016/j.matlet.2009.05.018>.
- [45] M. Samadi, H. Shivaee, M. Zanetti, A. Pourjavadi, A. Moshfegh, Visible light photocatalytic activity of novel MWCNT-doped ZnO electrospun nanofibers, *J. Molecular Catalysis. A: Chemecal*, 2012, V 359, P 42-48, <https://doi.org/10.1016/j.molcata.2012.03.019>.
- [46] Z. Zhan, L. Zheng, Y. Pan, G. Sun, L. Li, Self-powered, visible-light photodetector based on thermally reduced graphene oxide-ZnO (rGO-ZnO) hybrid nanostructure, *J. Materials Chemistry*, 2012, V 22, P 2589–2595, <https://doi.org/10.1039/C1JM13920G>.
- [47] K. Badreddine, I. Kazah, M. Rekaby, R. Awad, Structural, Morphological, Optical, and Room Temperature Magnetic Characterization on Pure and Sm-Doped ZnO Nanoparticles, *J. Nanomaterials*, 2018, P 1-11, <https://doi.org/10.1155/2018/7096195>.
- [48] X. Zhang, J. Qin, R. Hao, L. Wang, X. Shen, R. Yu, S. Limpanart, M. Ma and R. Liu, Carbon-Doped ZnO Nanostructures: Facile Synthesis and Visible Light Photocatalytic Applications, *J. Physical Chemistry C*, 2015, P 20544-20554, <https://doi.org/10.1021/acs.jpcc.5b07116>.
- [49] S. Rehman, R. Ullah, A. Butt, N. Gohar, Strategies of making TiO₂ and ZnO visible light active, *J. Hazardous Materials*, 2009, V 170, P 560-569, <https://doi.org/10.1016/j.jhazmat.2009.05.064>.
- [50] C. Wu, L. Shen, Y. Zhang, Q. Huang, Solvothermal synthesis of Cr-doped ZnO nanowires with visible light-driven photocatalytic activity, *J. Materials Letters*, 2011, V 65, P 1794-1796, <https://doi.org/10.1016/j.matlet.2011.03.070>.
- [51] K. Barick, S. Singh, M. Aslam, D. Bahadur, Porosity and photocatalytic studies of transition metal doped ZnO nanoclusters, *J. Microporous and Mesoporous Materials*, 2010, V 134, P 195-202, <https://doi.org/10.1016/j.micromeso.2010.05.026>.
- [52] G. Thennarasu, A. Sivasamy, Metal ion doped semiconductor metal oxide nanosphere particles prepared by soft chemical method and its visible light photocatalytic activity in degradation of phenol, *J. Powder Technology*, 2013, V 250, P 1-12, <https://doi.org/10.1016/j.powtec.2013.08.004>.

- [53] T. Dietl, H. Ohno, F. Matsukura, J. Cibert, D. Ferrand, Zener Model Description of Ferromagnetism in Zinc-Blende Magnetic Semiconductors, *J. Science*, 2000, V 287, P 1019-1022, <https://doi.org/10.1126/science.287.5455.1019>.
- [54] S. Méndez, C. Rodríguez, K. Venegas, J. Aquino, F. Magaña, Magnetism and decarburization-like diffusion process on V₂O₅-doped ZnO ceramics, *J. Ceramics International*, 2015, V 41, P 6802-6806, <https://doi.org/10.1016/j.ceramint.2015.01.127>.
- [55] T. Loan, N. Long and L. Ha, Photoluminescence properties of Co-doped ZnO nanorods synthesized by hydrothermal method, *J. Physics D: Applied Physics*, 2009, V 42, P 1-7, <https://doi.org/10.1088/0022-3727/42/6/065412>.
- [56] F. Romeiro, J. Marinho, A. Silva, N. Cano, N. Dantas, R. Lima, Photoluminescence and Magnetism in Mn²⁺-Doped ZnO Nanostructures Grown Rapidly by the Microwave Hydrothermal Method, *J. Physical Chemistry C*, 2013, P 26222-26227, <https://doi.org/10.1021/jp408993y>.
- [57] H. Zhu, J. Iqbal, H. Xu, D. Yu, Raman and photoluminescence properties of highly Cu doped ZnO nanowires fabricated by vapor-liquid-solid process, *J. Chemical Physics*, 2008, V 129, P 124713-1-124713-5, <https://doi.org/10.1063/1.2981050>.
- [58] T. Srivastava, S. Kumar, P. Shirage and S. Sen, Reduction of O²⁻ related defect states related to increased bandgap in Si⁴⁺ substituted ZnO, *J. Scripta Materials*, 2016, V 124, P 11-14, <https://doi.org/10.1016/j.scriptamat.2016.06.038>.
- [59] H. Qin, H. Liu and Y. Yuan, Si doped ZnO thin films for transparent conducting oxides, *J. Surface Engineering*, 2013, V 29, P 70-76, <https://doi.org/10.1179/1743294412Y.0000000072>.
- [60] R. Chowdhury, S. Adhikari, P. Rees, Optical properties of silicon doped ZnO, *J. Physica B: Condensed Matter*, 2010, V 405, P 4763-4767, <https://doi.org/10.1016/j.physb.2010.08.072>.
- [61] M. Park, S. Han, Enhancement in conductivity through Ga, Al dual doping of ZnO nanofibers, *J. Thin Solid Films*, 2015, V 590, P 307-310, [doi:10.1016/j.tsf.2015.02.069](https://doi.org/10.1016/j.tsf.2015.02.069).
- [62] A. Abbassi, A. El Amrani, H. Zahraoui, A. Benyoussef, Y. El Amraoui, First-principles study on the electronic and optical properties of Si and Al co-doped zinc oxide for solar cell devices, *J. Applied Physics A*, 2016, P 2-7, <https://doi.org/10.1007/s00339-016-0111-y>.
- [63] A. Lamichhane, Quantum-mechanical ab-initio calculations of the properties of wurtzite ZnO and its native oxygen point defects, 2018. (Thesis)
- [64] Q. L. Lin, G. P. Li, N. N. Xu, H. Liu, D. J. E. C. L. Wang, A first-principles study on magnetic properties of the intrinsic defects in wurtzite ZnO, *J. Chemical Physics*, 2019, V 150, P 094704-1-094704-8, <https://doi.org/10.1063/1.5063953>.

- [65] Y. Tang, H. Zhou, K. Zheng, J. Ding, T. Fan, D. Zhang, Visible-light-active ZnO via oxygen vacancy manipulation for efficient formaldehyde photodegradation, *J. Chemical Engineering*, 2015, V 262, P 260-267, <https://doi.org/10.1016/j.cej.2014.09.095>.
- [66] M. Lahmer, The effect of growth conditions and vacancies on the electronic, optical and photocatalytic properties of the ZnO (1010) surface, *J. Materials Chemistry and Physics*, 2016, V 182, P 200-207, <https://doi.org/10.1016/j.matchemphys.2016.07.024>.
- [67] Z. Wang, S.C. Su, M. Younas, F.C.C. Ling, W. Anwand, A. Wagner, The Zn-vacancy related green luminescence and donor-acceptor pair emission in ZnO grown by pulsed laser deposition, *J. Royal Society of Chemistry*, 2015, V 5, P 12530-12535, <https://doi:10.1039/C4RA13084G>.
- [68] L. Bai, Z. Lin, M. Wen, H. Dong, Z. Liu, H. Chen, F. Wu, Vacancies inducing electronic and optical properties in 2D ZnO:Be/Mg, *J. Physica B: Condensed Matter*, 2019, V 555, P 47-52, <https://doi.org/10.1016/j.physb.2018.11.064>.
- [69] C. Li, Q. Hou, Effects of Y doping with point defects on the ferromagnetic properties of ZnO(0001)-Zn polar surface, *J. Applied Surface Science*, 2018, V 459, P 393-396, <https://doi.org/10.1016/j.apsusc.2018.08.012>.
- [70] A. Catellani, A. Ruini, A. Calzolari, Optoelectronic properties and color chemistry of native point defects in Al:ZnO transparent conductive oxide, *J. Materials Chemistry C*, 2015, P 1-7, <https://doi.org/10.1039/C5TC01699A>.
- [71] Z. Meng, X. Mo, X. Cheng, Y. Zhou, X. Tao, Y. Ouyang, Interactions between Er dopant and intrinsic point defects of ZnO: A first-principles study, *J. Materials Research Express*, 2017.
- [72] A. Janotti, C.V. de Walle, New insights into the role of native point defects in ZnO, *J. Crystal Growth*, 2006, V 287, P 58-65, <https://doi.org/10.1016/j.jcrysgro.2005.10.043>.
- [73] J.B. Yi, C.C. Lim, G.Z. Xing, H.M. Fan, L.H. Van, S.L. Huang, K. Yang, X.B. Qin, B.Y. Wang, T. Wu, L. Wang, H.T. Zhang, X.Y. Gao, T. Liu, A.T.S. Wee, Y.P. Feng, J. Ding, Ferromagnetism in Dilute Magnetic Semiconductors through Defect Engineering: Li-Doped ZnO, *J. Physical Review Letters*, 2010, P 137201-1-137201-4, <https://doi.org/10.1103/PhysRevLett.104.137201>.
- [74] X. Jiang, F.L. Wong, M.K. Fung, S.T. Lee, Aluminum-doped zinc oxide films as transparent conductive electrode for organic light-emitting devices, *J. Applied Physics Letters*, 2003, V 83, P 1875-1877, <https://doi.org/10.1063/1.1605805>.

[75]K.Matsumoto, K.Kuriyama, K.Kushida, Electrical and photoluminescence properties of carbon implanted ZnO bulk single crystals,J. Nuclear Instruments and . Methods in Physics Research Section B: Beam Interactions with Materials and Atoms,2009,V 267,P 1568-1570,<https://doi.org/10.1016/j.nimb.2009.01.128>.

[76]L.T.T.seng, J.B.Yi, X.Y.Zhang, G.Z.Xing, H.M.Fan, T.S.Herng, X.Luo, M.Ionescu, J.Ding, S.Li, Green emission in carbon doped ZnO films,J. AIP Advances,2014,V 4,P 067117-1-067117-7,067117-2-067117-7,[https://doi: 10.1063/1.4882172](https://doi:10.1063/1.4882172).

Chapter 2

Fundamentals of the Density Functional Theory

As a start, the discipline condensed matter physics is widely described as material science, thus, making the latter an interdisciplinary subject. After the Second World War, the role of computer simulation in testing various mathematical models generates attention in various disciplines of science. The integration of computer simulation is very pronounced in material science for computing the properties as well as visualizing and mimicking the structure of the material. The innovation of different varieties of software and computing tools has swiftly augmented theoretical research in material science. Many complex structures of crystal can be computed with great accuracy with the aid of a supercomputer. This structure involves the many body Schrödinger problem and the analytical solution of it is mostly a cumbersome process. In the year 1964, Hohenberg and Kohn introduced "Density Functional Theory" [1], which approximates many body Schrödinger problem with the numerical solution.

Between the years 1989 to 2004, the development of computer simulation packages were built and upgraded, which are widely used in modeling material in the atomic domain. In the early twenty-first century and then, this simulation package is used as an important tool for theoretical scientists to calculate the electronic, optical, vibrational, thermal and magnetic properties of the various materials. Likewise, many other powerful computational tools are evolving in this century. As a result, a lot of research journals in the field of material science are published with the aid of these computational tools and thus, creating a new discipline called computational material science. Today, it is one of the prime branches of science [2].

2.1 Some history of science:

The calculations of the electronic structure are the major backbone problem of the material scientists. After the discovery of the electron in 1896-1897, the theory of electronic structure is the central issue for all the theoretical physicists. In the year 1897, J.J. Thomson not only discovered the electron at the Cavendish Laboratory in Cambridge [3] but also came up with the conclusion that the electron is a negatively charged particle. Based on this study, he proposed the "plum pudding model" of the electronic structure which was soon modified by his student Ernest Rutherford.

In 1910 Rutherford showed that the atom was made of a small positively charged nucleus and number of negatively charged electrons revolving around the nucleus making the atom electrically neutral, he presented a model of an atomic structure known as nuclear atom [4]. His model was like the planetary model where the gravitational force is analogous to the electrostatic force. However, there were several experimental issues that are incompatible with this model. Among them, the most important issue was the violation of Maxwell's law

which states that the accelerated charged particle radiates electromagnetic energy. An electron revolving around the nucleus should lose energy by emitting electromagnetic radiation and finally collapse into the nucleus making the atom unstable. In the year 1913, Neil Bohr tried to solve the contradiction of Rutherford model by simply stating that the physics of atomic scale could not be addressed by the classical mechanics and electromagnetism, but required a set of new laws which later became quantum mechanics [5]. Bohr postulated that the electron revolves around the nucleus only in specific orbit having specific energy and radius and that in such quantum orbits it does not emit radiation. This postulate was in accordance with the Planck's theory of black body radiation and verification of the dependency of frequency absorbed/emitted by electrons with the difference in the energy levels of the orbits provide a robust foundation for the development of the quantum mechanics.

Thus, it is always paradoxical that the search for the electronic structure creates quantum mechanics or the quantum mechanics is created for the search of electronic structure. Nevertheless, the electrons serve as the testing ground for the quantum mechanics. In the year 1926, Schrödinger formulated the mathematical language of quantum mechanics which is the basis for the electronic structure calculation and it was soon applied to multi-electronic atoms (Heitler and London, 1927) and polyatomic systems (Bloch, 1928) [6]. With the quantum theory, many intrinsic properties of the electrons were discovered as well as tested experimentally. In 1930s, the band theory for independent electrons was formed [7] leading to the classification of the materials as conductors, insulators and semiconductors. The use of Schrödinger equation in calculating the many-body systems is quite cumbersome and impractical in real life. For instance, in order to calculate the electronic configuration of CO₂, the Schrödinger equation becomes a 66 dimensional problem (if we neglect the nuclear dynamics) as the total number of electrons in CO₂ is 22 and for three degree of spatial orientation (neglecting spins), the configuration is represented by the wave function $\psi(r_1; r_2; \dots; r_{66})$. Since, the presence of one electron in space influences the behavior of the other electrons, the wave function cannot be expressed as the product of the wave functions of the individual electrons, i.e., $\psi(r_1; r_2; \dots; r_{66}) \neq \psi(r_1) \times \psi(r_2) \times \dots \times \psi(r_{66})$. Such difficulty in quantum mechanics is often described as the quantum many-body problem. Thus, the exact solution of Schrödinger equation in the case of CO₂ involves an equation in 66 degrees of freedom. Further, it is always complicated to understand the two body Coulomb interaction in this multiple number of electrons.

As a result, the solution of Schrödinger equation in quantum many-body problem must resort to some approximations. The first approximations to be used is Born Oppenheimer

approximation which states that atoms have heavy nuclei and therefore can consider them as stationary sources of electrostatic potential. This approximation is vital to reduce the nuclei factor from the Hamiltonian function of the quantum multi-body system. After that, one may use either Hartree-Fock Method (HF) or Density Functional Theory (DFT). In HF method, one can treat the many body wave function as the combination of some standard base functions, i.e., $\psi(1; 2; \dots; N) = \varphi(1) \times \varphi(2) \times \dots \times \varphi(N)$ and can make the Hamiltonian function as separable. Though this method does not treat the anti-symmetric condition for electrons wave function, one can easily use the Slater determinant to incorporate the Pauli Exclusion Principle [8]. On the other hand, DFT approximates the many body wave functions to electron probability density function which is only the function of spatial coordinates and thus reducing any N dimensional problem to a 3 dimensional problem. The mathematical details of this reduction of N dimensional problem to 3 dimensional functions are shown in step-wise details subsequently in further sections.

Density functional theory was proposed by Hohenberg-Kohn in 1960 [9] and due to the unavailability of the powerful computer between 1960 and 1990, the use of DFT in the calculation of electronic structure of the material is limited. However, after 1990, due to the advent of the powerful supercomputer, the DFT has revolutionized the field of material science by not only calculating the properties of the materials but also providing an alternate method of investigation instead of using traditional experimental ways. In the current time, DFT undoubtedly one of the techniques most used in computing electronic structures.

The major benefits of DFT calculations can be summarized as follows:

- 1* DFT calculation is the first-principle or ab-initio calculation as it calculates the properties of the material without using any adjustable parameters.
- 2* DFT can obtain the structure of the materials beyond the capabilities of experiments.
- 3* DFT predicts the properties on a microscopic scale and to such a depth which is currently inaccessible to experiments.

In this chapter, we will outline the foundations on which DFT is based, discussing the different levels of approximations required to solve the Schrödinger equation. In the following, the approximations used for the calculation of the energy and the exchange-correlation potential will be presented. Finally, the foundations and various examples of the pseudo-potential approximation will be described.

The principle of DFT consists in reformulating a quantum problem with N bodies, in a mono-body problem (function of the spin) with the electron density as variable.

2.2 Quantum Many-Body Problem:

From a mathematical point of view, the Schrödinger equation appears to be a separate problem, quite delicate, since it has both parabolic and hyperbolic aspects [10].

Understanding the structural, electronic, optical and magnetic properties of materials involves studying the system of electrons and strongly interacting nuclei that constitute it. In 1929, Dirac declared that solving the Schrödinger equation for such a system is extremely difficult

$$\hat{H}\psi = E\psi \quad (1)$$

Where \hat{H} is the Hamiltonian operator, ψ is the wave function and E is the total energy of the system.

A solid is a collection of positively charged heavy particles (nuclei) and negatively charged light particles (electrons). If we have N cores, we are faced with a problem of $(N + ZN)$ particles in electromagnetic interaction. It's a multi-body problem. For a system composed of N ions of \vec{R}_j coordinates of charge Z , of mass M and of n electrons of \vec{r}_i coordinates and of mass m , the exact Hamiltonian for this system is:

$$\mathbf{H} = \sum_{i=1}^N \frac{\nabla_i^2}{2M_i} + \sum_{i=1}^n \frac{\nabla_i^2}{2m} + \sum_{i>j} \frac{1}{|\vec{r}_i - \vec{r}_j|} + \sum_{I>J} \frac{Z_I Z_J}{|\vec{R}_I - \vec{R}_J|} - \sum_{i,I} \frac{Z_I}{|\vec{R}_I - \vec{r}_i|} \quad (2)$$

The first two terms represent the kinetic energies of ions and electrons respectively and that the following terms denote the potential energies of Coulomb electron-electron interaction (v_{e-e}) ion-ion (v_{N-N}) and (v_{e-N}) electron-ion respectively.

The equation (2) allowing to calculate the internal energy of the system is a $(N + n)$ body problem. Its solution is only possible analytically for a two-body system and is only numerically feasible for a very small number of particles (considering the system and is only numerically feasible for a very small number of particles (considering the current means of calculation). The rest of this paragraph will therefore present reasonable approximations allowing the resolution of this problem. [11].

2.3 The Born-Oppenheimer approximation:

The **BO** approximation treats this system as the electrons in the potential of the stationary nuclei by assuming nuclei are massive and slow in motion with respect to electrons and suppose there is a large difference in mass between nuclei and electrons and a difference in scale of time between electronic and nuclear movements. Therefore, it is possible to decouple the motion of nuclei from that of electrons and write the wave function as the product of two wave functions, one nuclear and the other electronic:

$$\Psi(\vec{x}, \vec{R}) = \Psi(\vec{x}, \vec{R})\chi(\vec{R}) \quad (3)$$

Where:

$\Psi(\vec{x}, \vec{R})$ is the wave function of electrons.

$\chi(\vec{R})$ is the wave function associated with the nuclei.

So:

Total energy is written then as the sum of a nuclear and electronic contribution:

$$\mathbf{E} = \mathbf{E}_{\text{nucl}}(\vec{R}) + \mathbf{E}_{\text{elec}}(\vec{R}) \quad (4)$$

This therefore amounts to calculating the energy by solving the electronic Schrödinger equation:

$$\left[\sum_{i=1}^n \frac{\nabla_i^2}{2m} + \sum_{i>j} v_{e-e}(\vec{r}) - \sum_{i,l} v_{e-N}(\vec{x}, \vec{R}) \right] \Psi(\vec{x}, \vec{R}) = \mathbf{E}_n(\vec{R}) \Psi(\vec{x}, \vec{R}) \quad (5)$$

Solutions of this equation (eq 5) represent the energies \mathbf{E}_n of the electronic states n.

These depend on the positions \vec{R} of the ions (here considered as external parameters) and for a given atomic configuration, the electrons are assumed to be in their ground state which corresponds to the energy \mathbf{E}_0 of the system (adiabatic approximation).

Hence, the importance of BO approximation lies in the separation of motion of electrons and nuclei. The picture of electrons dynamics in the static potential of the nuclei is the beginning point for DFT.

Several methods exist for solving equation (5). The first are those of Hartree-Fock [12] based on the free electron hypothesis. These methods are very used in quantum chemistry to process atoms and molecules, but they are less precise for solids. DFT turns out to be a more modern method and probably more powerful. Its history goes back to the first thirties of the 20th century but it was formally established in 1964 by the two theorems of Hohenberg and Kohn [13]. These authors demonstrated that all aspects of the electronic structure of a system in a state non degenerate fundamental are completely determined by its electron density at place of its wave function.

2.4 Hartree and Hartree-Fock approximations:

Historically, the resolution method proposed by Hartree is at the origin of more recent methods used especially in solid-state chemistry. This approximation is based on a different vision. In Hartree-Fock, the central element is the mono-electronic wave function. [14]

The introduced approximation consists in writing the electronic wave function as the product of the mono-electronic wave functions:

$$\Psi = \Phi_1 \Phi_2 \Phi_3 \dots \Phi_n = \prod_{i=1}^n \Phi_i \quad (6)$$

Note that this form of the electron wave function would be correct for a system of independent electrons (from a statistical point of view). Equation (5) is then transformed into a system of mono-electronic equations:

$$\left[-\frac{1}{2} \nabla_i^2 + v_{e-N}(\vec{r}, \vec{R}) + v_{e-e}(\vec{r}) \right] \Phi_i(\mathbf{x}, \vec{R}) = E_i(\vec{R}) \Phi_i(\mathbf{x}, \vec{R}) \quad (7)$$

$v_{e-e} = v_H = \int \frac{|\Phi_j(\vec{r}')|^2}{|\vec{r}-\vec{r}'|} d^3 r' = \int \frac{\rho(\vec{r}')}{|\vec{r}-\vec{r}'|} d^3 r'$: is the potential associated with the Coulomb interaction with the other electrons of the gas (also called "Hartree potential") and v_{e-N} that with the ions.

Writing a relation such as (equation 7) goes against the Pauli exclusion principle and if we try to calculate the probability of finding two electrons at the same position at the same time, we will find it non-zero. The Hartree-Fock method then introduces these quantum effects designated under the nomenclature "exchange".

In this method, the wave function Ψ can be described as a Slater determinant:

$$\Psi_{1,n}(\mathbf{x}_1, \dots, \mathbf{x}_n) = \frac{1}{\sqrt{n!}} \begin{vmatrix} \Phi_1(\mathbf{x}_1) & \Phi_1(\mathbf{x}_2) & \dots & \Phi_1(\mathbf{x}_n) \\ \Phi_2(\mathbf{x}_1) & \Phi_2(\mathbf{x}_2) & \dots & \Phi_2(\mathbf{x}_n) \\ \dots & \dots & \dots & \dots \\ \Phi_n(\mathbf{x}_1) & \Phi_n(\mathbf{x}_2) & \dots & \Phi_n(\mathbf{x}_n) \end{vmatrix} \quad (8)$$

This way of expressing the wave function of an n-electron system from the single-electron wave functions satisfies the **Pauli Exclusion Principle** because ψ is antisymmetric with respect to the exchange of two electrons. Equation (5) is, in this case, replaced by a system of Hartree-Fock equations:

$$\left[-\frac{1}{2} \nabla^2 + v_{e-N}(\vec{r}, \vec{R}) + \int \frac{\rho(\vec{r}')}{|\vec{r}-\vec{r}'|} d^3 r' \right] \Phi_i(\vec{r}) - \sum_{j \neq i} \delta_{\sigma_i, \sigma_j} \int \frac{\Phi_j^*(\vec{r}') \Phi_i(\vec{r}')}{|\vec{r}-\vec{r}'|} d^3 r' \Phi_j(\vec{r}) = E \Phi_i(\vec{r}) \quad (9)$$

While the Hartree method does not take into account the impossibility for two electrons of the same spin to be in the same quantum state, the Hartree-Fock method fills this gap by introducing an exchange term (last term of equation (9)). Each electron then tends to surround itself with an electron hole and this repulsion decreases the energy of the system. The difference between the ground state energy of the system determined from equation (7) and that determined from equation (9) is the exchange energy.

Recall that electron-electron interactions are described, in the model, as the interactions of each electron with an average field due to the other electrons. This does not take into account the strong correlation that exists between two electrons of opposite spins and that keeps them at a distance from each other. The difference between the true ground state energy and that determined from equation (9) is the correlation energy. A "post Hartree-Fock" treatment allows filling in the lack of correlation by refining the model with a linear combination of Slater determinants to describe the poly-electronic wave function.

The Hartree-Fock method quickly becomes numerically very expensive when the number of electrons increases. The different terms involved in the solution of the electronic Schrödinger equation (kinetic energy of a system of non-interacting electrons, Hartree potential, exchange and correlations) were introduced by the Hartree-Fock method. They will be taken up in the Density Functional Theory which is less costly.

2.5 Density Functional Theory:

The Density Functional Theory, DFT, was introduced in the mid-sixties by Hohenberg and Kohn [13], Kohn and Sham [15]. The contribution of Walter Kohn through the density functional theory in the explanation of electronic properties, in particular in condensed matter physics, was rewarded by the Nobel Prize in Chemistry in 1998[11]. This theory allows an efficient application of the basic principles of quantum mechanics in numerical calculation codes called ab-initio to determine the electronic properties of atomic groupings [16].

The electronic structure is fundamental because it determines directly or indirectly all the properties of a group of atoms, in particular the energy of its fundamental state.

The basis of the density functional theory (DFT) was developed in 1927 by Thomas [17-18] and Fermi [19] who calculated the energy of an atom by representing its kinetic energy as a function of the electron density. In 1928, Dirac [20] introduced the exchange term predicted by Hartree but there was still no account of the electronic correlation that was finally added by Wigner, but this theory established by Hohenberg and Kohn 1964 [13-21] is improved in 1965 by Kohn and Sham [22], its main purpose is the modeling of the electron-electron interaction, it describes the behavior of electrons strongly bound in the presence of the electrostatic field of ions. Thus the electron is immersed in a non local effective potential. As a result, many electronic calculations are performed with the DFT, making it very popular in the investigation of the structure and properties of the matter. Walter Kohn was awarded with Nobel Prize for DFT in 1998.

In DFT, the total energy is decomposed into three contributions:

1*The kinetic energy.

2*The coulomb energy: due to electronic interactions between all charged particles in the system.

3*The exchange and correlation term: due to multi-electron interactions.

So, the principal of the DFT theory indicates that each state has a total energy of a system of interacting electrons in an external potential that is represented as an electron density functional ρ of the ground state.

This decomposition is formally accurate, but the expression of the exchange and correlation term is unknown. In this theory the electrons are considered as electron densities constructed from the wave functions of an electron (LDA) [23-24]. These wave functions of an electron are similar to those of the Hartree-Fock theory. Several works performed using LDA [25-26], have shown that this approach gives good results and provides better information on the properties of metals and transition metal.

It is therefore possible to express the energy as a simple functional of $V_{\text{ext}}(r, R)$:

$$E_0 = [\Phi_0 | H | \Phi_0] \quad (10)$$

$$E_0 = \int [T_e + V_{ee} + V_{\text{ext}}] \rho_0 d^3 r_\alpha \quad (11)$$

The Hohenberg and Kohn functional is defined by (eq12), if we dropping the zero indices:

$$E_{V_{\text{ext}}} = F[\rho] + \int \rho(\mathbf{r}) V_{\text{ext}} d\mathbf{r} \quad (12)$$

More interesting, the DFT allows not solving the problem. But to reformulate it. Therefore, other approximations on $F[\rho]$ are needed.

2.6 Equations of Kohn and Sham:

The Kohn-Sham approach imposes on the exchange-correlation term to take in charge, in addition to all this the correction of the kinetic energy term. Indeed, even if the density of the considered fictitious system is the same as the real one, the determined kinetic energy determined is different from the real energy, because of the artificial independence of the wave functions. The Kohn-Sham theory [15] is based on the hypothesis that it is possible to reproduce the density of the fundamental state of a system of N interacting particles by an auxiliary system of independent particles. The real system of interacting electrons is replaced by a set of fictitious and independent particles evolving in an effective an effective potential. Kohn and Sham propose a writing of $F[\rho]$ in three terms [15]:

$$F[\rho] = T_s[\rho] + E_H[\rho]E_{XC}[\rho] \quad (13)$$

Where the first two are calculable and explainable by simple approximations and the third contains all the complicated and difficult to evaluate elements.

E_H or Hartree energy is associated with the self-interaction of each electron is defined by:

$$E_H[\rho] = \frac{1}{2} \int \frac{\rho(\mathbf{r}')\rho(\mathbf{r})}{|\mathbf{r}-\mathbf{r}'|} d^3\mathbf{r}' d^3\mathbf{r} \quad (14)$$

T_s is the kinetic term of a fictitious system of non-interacting electrons immersed in an effective potential which is that of the real system:

$$V_{\text{eff}} = (V_H + V_{XC} + V_{\text{ext}})[\rho(\mathbf{r})] \quad (15)$$

The Hamiltonian is written:

$$\left[-\frac{\hbar^2}{2m} \nabla^2 + V_{\text{eff}}(\mathbf{r}) \right] \Phi_i(\mathbf{r}) = E_i \Phi_i(\mathbf{r}) \quad (16)$$

Then, the density of states is written:

$$\rho(\mathbf{r}) = \sum_i f_i |\Phi_i(\mathbf{r})|^2 \quad (17)$$

Where f_i and Φ_i are the occupation number and eigenvalue associated with the state Φ_i respectively.

The exchange and correlation term E_{XC} is defined by the associated potential.

$$V_{XC} = \frac{\partial E_{XC}[\rho]}{\partial n(\mathbf{r})} \quad (18)$$

$$V_{XC} = (V_{ee} - V_H)[\rho] + (T - T_s)[\rho] \quad (19)$$

It is the only one that cannot be treated exactly. The term "exchange" comes from the necessity for a system containing fermions to have anti-symmetric wave functions with respect to the exchange of any pair of fermions of the same nature (for example two electrons). This anti-symmetry in turn results in a spatial separation between wave functions of electrons of the same spin which contributes to the energy of the system. In general, the wave functions of the electrons are spatially separated because of the columbic interactions between the electrons. The associated energy is called electronic correlation. Equations (20), (21) and (22) are called: **Kohn-Sham equations**. The table.1 displays the three Kohn-Sham equations.

Now, the calculation of the energy and the exchange-correlation potential is based on a number of number of approximations.

1* The generalized gradient approximation (GGA): $E_{XC}^{GGA}[\rho] = \int f[\rho(\mathbf{r}), \nabla_n(\mathbf{r})] d^3\mathbf{r}$ (23)

2* The local density approximation (LDA): $E_{XC}^{LDA}[\rho] = E_X[\rho] + \int \rho(\mathbf{r})E_C[\rho(\mathbf{r})]d^3\mathbf{r}$ (24)

“The quantum Monte-Carlo calculations by Ceperley and Alder [27] have also enabled to obtain precise values of the $E_{XC}^{LDA}[\rho]$.”

3* The approximations of the local density and the generalized gradient with the Hubbard correction (LDA+U and GGA+U). **Fig.1** has shown the different approximations basis.

<p>The first approximate solution of equation was obtained in 1928 by Hartree [28]:</p> $\mathbf{H} = \mathbf{T}_e(\mathbf{p}) + \mathbf{V}_{ee}(\mathbf{r}) + \mathbf{V}_{\text{ext}}(\mathbf{r}, \mathbf{R})$	
<p>Making the approximation that electrons experience only an average effective potential resulting from all of their neighbors, the N-electron wave function is separable into a product of single-electron wave functions $\Psi_i(\mathbf{r}_i)$ for which the Hamiltonian is written:</p>	$\left[-\frac{\hbar^2}{2m} \nabla^2 + \mathbf{V}_{\text{ext}} + \Phi_i \right] \Psi_i(\mathbf{r}) = E_i \Psi_i(\mathbf{r}) \Psi_i \quad (20)$
<p>The term being the Coulomb potential obtained by the Poisson equation:</p>	$\nabla^2 \Phi_i = 4\pi^2 \sum_{j \neq i} \Psi_j ^2 \quad (21)$
<p>In 1930 Fock [29] showed that the solutions of this Hamiltonian reject the Pauli exclusion principle because it is not anti-symmetric with respect to the exchange of any two electrons. He proposed to add a fourth term representing the exchange potential which according to Fock [29] is written:</p>	$\mathbf{V}_X \Phi_i(\mathbf{r}) = \sum_{j \neq i} \int \frac{\Phi_j(\mathbf{r}') \Phi_i^*(\mathbf{r}') \Phi_j^*(\mathbf{r})}{ \mathbf{r} - \mathbf{r}' } \delta_{s_i, s_j} d^3 \mathbf{r}' \quad (22)$

Tab.1: The three Kohn-Sham equations.

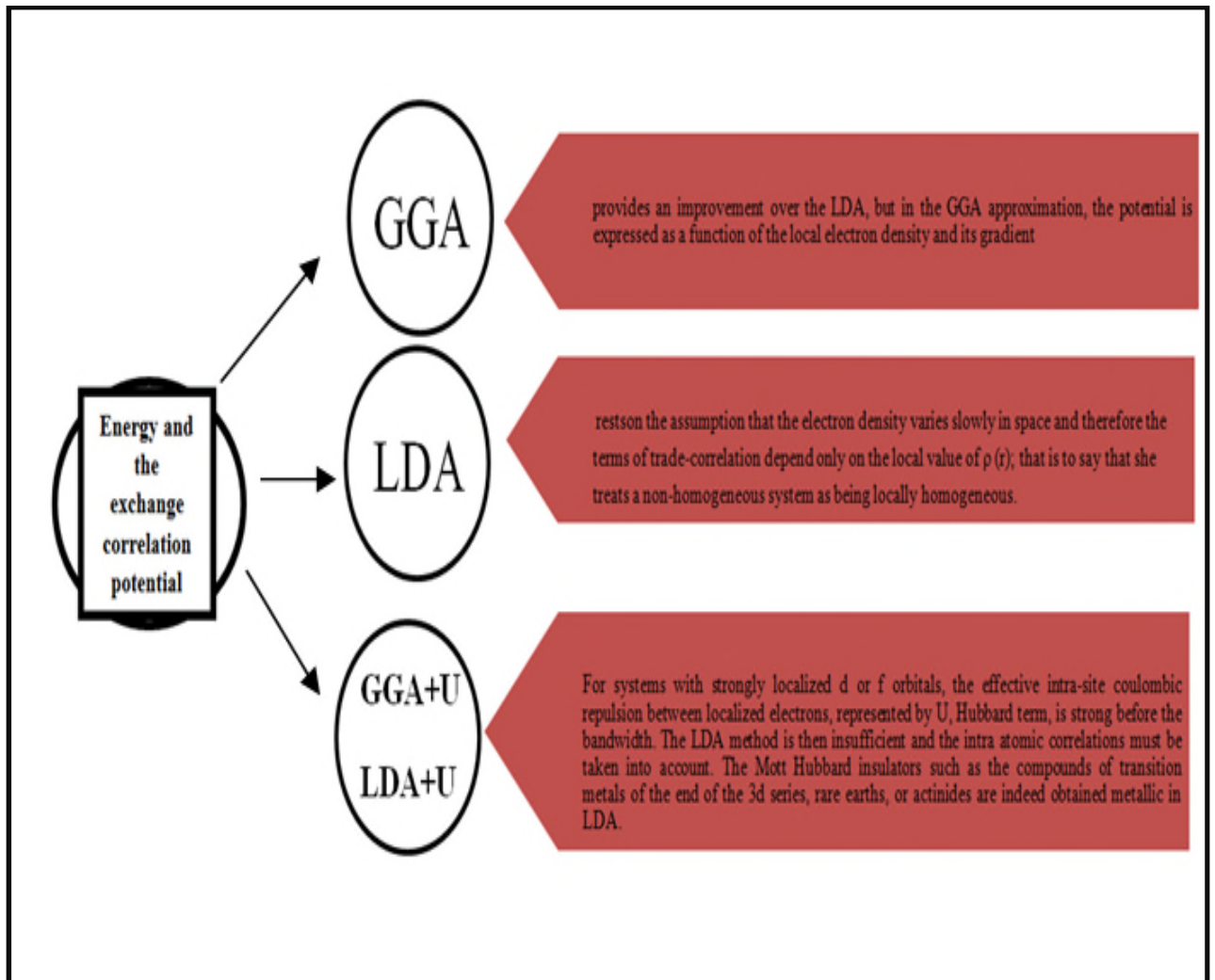


Fig.1: The different approximations basis.

2.7 Hubbard Correction U : In strongly correlated systems where 3d, 4d, 4f and 5f electrons are localized and very close to Fermi energy, the LDA and GGA approximations fail as these approximations are independent of the electrons states. The electrons in these states are self interacting and to account for this-orbital dependent potentials are introduced for these d and f electrons. The main aim of Hubbard correction U is to correct the effects of self interaction due to the localization of the states. The effective value of U is chosen in such a way that these localized states are pushed away from the Fermi level so that these states have no interaction with the bonding states [2]. The strong intra-site Coulomb screened interactions between d electrons have been introduced according to the approach referred to as the DFT+U method which combines the DFT method (LSDA or GGA with spin polarization) with a Hubbard Hamiltonian, \hat{H}_{hubbard} [30-31]. Thus, we used a simple version of DFT+U, proposed by Dudarev et al. [32] based on a Hamiltonian of the form:

$$\hat{H}_{\text{Hubbard}} = \frac{U}{2} + \sum_{m,m',\sigma} \hat{n}_{m,\sigma} \hat{n}_{m',-\sigma} + \frac{(U-J)}{2} \sum_{m \neq m',\sigma} \hat{n}_{m,\sigma} \hat{n}_{m',-\sigma} \quad (25)$$

Where $\hat{n}_{m,\sigma}$ is the operator which gives the number of electrons occupying a number orbital magnetic quantum m and spin σ at a particular site, U is the Hubbard parameter spherically averaged, which describes the energy cost to place an electron additional on a particular site. $U = E(f^{n+1}) + E(f^{n-1}) - 2E(f^n)$. J represented the energy of exchange screened. U depends on the spatial extension of the wave functions and screening, J is an approximation of the Stoner exchange parameter. U and J parameters characterize intra-site Coulomb repulsion.

The Mott-Hubbard Hamiltonian contains the contributions of energy already recorded by the DFT function. After subtracting terms counted twice from the energy given by the classical DFT method, the energy of the functional DFT+U in spin polarization of Dudarev et al. [31-32] is obtained:

$$E_{\text{DFT+U}} = E_{\text{DFT}} + \frac{(U-J)}{2} \sum_{m\sigma} (\hat{n}_{m,\sigma} - \hat{n}_{m\sigma}^2) \quad (26)$$

In this approach U and J do not intervene separately but by their difference ($U_{\text{eff}} = U - J$).

However, experience shows that the best results are achieved when the U parameter is allowed to vary depending on the property of interest. CASTEP therefore does not calculate the value of U but uses it as an input parameter.

This chapter 2 is written in the aim of getting insight about the accurate differences in the computational capacities of these functionals.

2.8 Kohn and Hohenberg theorem:

This theorem shows that there is a one-to-one correspondence between the ground state $\Phi(r_1, r_2, \dots, r_n)$ and the local charge density $\rho(r)$ defined by:

$$\Phi(\mathbf{r}) = \sum_j \int \delta(\vec{r} - \vec{r}_j) |\Phi|^2 d\tau_0 \quad (27)$$

and therefore that $E = \langle \Phi | H | \Phi \rangle$ also. Thereby:

$$E[\rho] = T[\rho] + E_{e-i}[\rho] + E_H[\rho] + E_X[\rho] + E_{i-i}[\rho] \quad (28)$$

T is the kinetic energy.

$$\left\{ \begin{array}{l} E_{e-i} \text{ the electron-ion interaction term.} \\ E_X \text{ the exchange term of purely quantum origin.} \\ E_H \text{ the classical electronic interaction term} \\ E_{i-i} \text{ the term of ion-ion interaction.} \end{array} \right.$$

So, by minimizing the functional, the fundamental energy becomes:

$$G[\rho] = E[\rho] - \mu \left(\int \Phi(\mathbf{r}) d^3\mathbf{r} - M \right) \quad (29)$$

2.9 The solution of the one-particle Kohn-Sham equations:

Kohn and Sham; in order to get around the difficulty of writing the terms E_X and T as functionals of the density $\Phi(\mathbf{r})$, will introduce an equivalent particle system, without interaction, and whose ground state is characterized at all points by the same form:

$$H_S = \sum_j -\frac{1}{2\Delta_j} + V_{\text{eff}}(\mathbf{r}_j) \quad (30)$$

The wave function of such a system can be expressed in the form of the product of N individual functions. These individual functions make it possible to determine the electron density at any point in space. Kohn-Sham orbitals are described by:

$$\Phi_i(\mathbf{r}) = \sum C_{i\alpha} \phi_\alpha(\mathbf{r}) \quad (31)$$

Where:

$C_{i\alpha}$ Are the coefficients of the expansion and ϕ_α are the basic functions.

Finally, this iterative procedure is continued until energy or charge convergence is achieved. Once convergence is reached, the energy of the ground state of the system is determined. The whole of this procedure is shown in Fig.2, (the solving is done iteratively using an “auto iteration cycle coherent”).

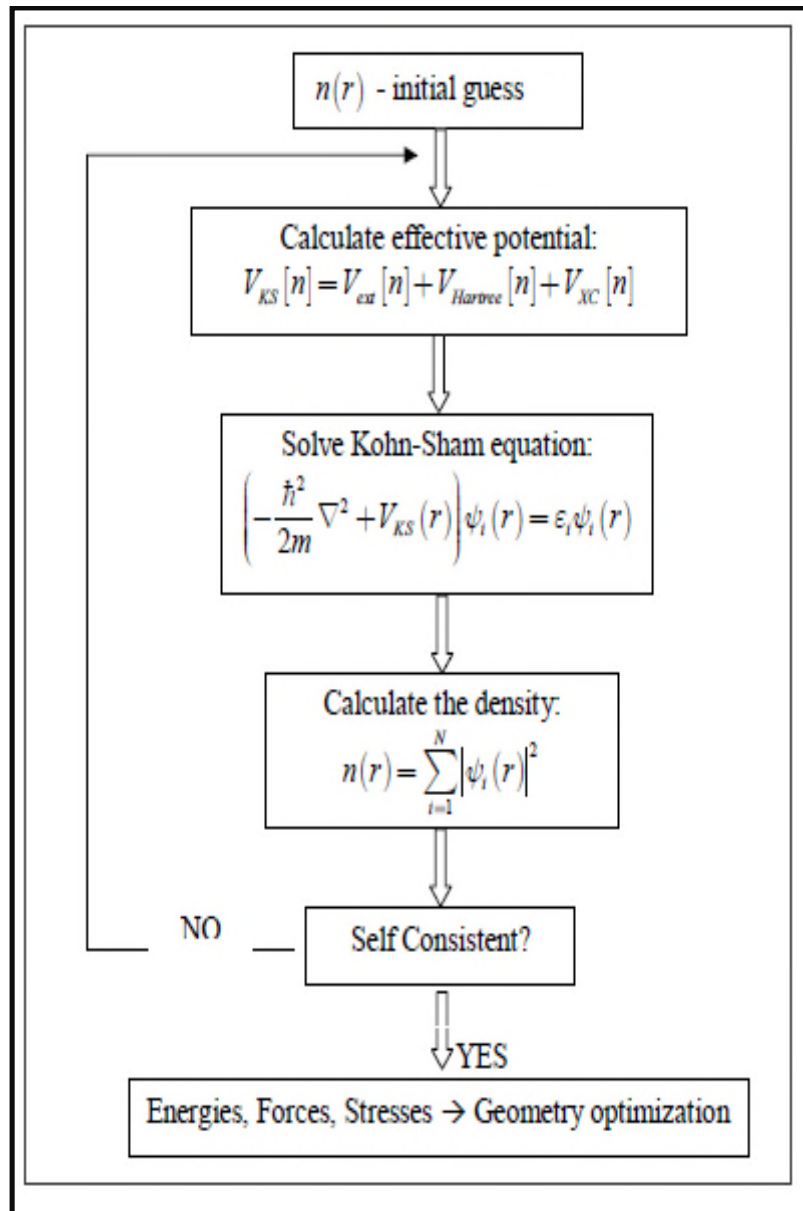


Fig.2: The self consistent calculation scheme of the density functional [45].

2.10 Bloch's theorem and plane waves:

One of the fundamental characteristics of a crystal is translational symmetry. In a crystal the ions are arranged in such a way that the crystal structure repeats itself periodically and infinitely in space. The system of infinite size can therefore be described in a finite way thanks to the notion of periodicity [33].

If $\mathbf{V}_{\text{eff}}(\vec{r})$ the potential, $\boldsymbol{\Psi}(\vec{r})$ wave functions, $\boldsymbol{\rho}(\vec{r})$ electron density and $\vec{\mathbf{L}}$ denotes a lattice vector crystal lattice obey :

$$\left. \begin{aligned} \mathbf{V}_{\text{eff}}(\vec{\mathbf{r}} + \vec{\mathbf{L}}) &= \mathbf{V}_{\text{eff}}(\vec{\mathbf{r}}) \\ \Psi(\vec{\mathbf{r}} + \vec{\mathbf{L}}) &= \Psi(\vec{\mathbf{r}}) \\ \rho(\vec{\mathbf{r}} + \vec{\mathbf{L}}) &= \rho(\vec{\mathbf{r}}) \end{aligned} \right\}$$

The application of this condition of invariance by translation symmetry to the solutions of the Kohn-Sham equations allows us to write the wave functions in the form of Bloch function [34-35]:

$$\Psi_i(\vec{\mathbf{r}}) = \mathbf{f}(\vec{\mathbf{r}}) \mathbf{e}^{i\vec{\mathbf{k}}\vec{\mathbf{r}}} \quad (32)$$

Where: $\vec{\mathbf{k}}$ is a wave vector of the first Brillouin zone. The periodic function $\mathbf{f}(\vec{\mathbf{r}})$ can be decomposed by Fourier transform on a plane wave basis of wave vectors $\vec{\mathbf{G}}$ of the reciprocal lattice:

$$\mathbf{f}_i(\vec{\mathbf{r}}) = \sum_{\vec{\mathbf{G}}} \mathbf{C}_{i,\vec{\mathbf{G}}} \mathbf{e}^{i\vec{\mathbf{G}}\vec{\mathbf{r}}} \quad (33)$$

Then, we can write the wave function as a sum of plane waves:

$$\Psi_i(\vec{\mathbf{r}}) = \sum_{\vec{\mathbf{G}}} \mathbf{C}_{i,\vec{\mathbf{k}}+\vec{\mathbf{G}}} \mathbf{e}^{i(\vec{\mathbf{k}}+\vec{\mathbf{G}})\vec{\mathbf{r}}} \quad (34)$$

In summary, in the current above section showed some of the main equations that govern the electronic interaction in matter and also gave an overview of the density functional theory (DFT) which will be the framework for the problems discussed on the next chapters.

2.11 Pseudo-potential-plane wave method:

2. 11. 1 Principle:

In molecules and solid compounds, valence electrons are the only ones involved in chemical bonds. The core electrons, which are on the innermost layers, close to the nucleus, are not very sensitive to the environment and moreover it is difficult to represent their wave functions on a plane wave basis because they generally have strong oscillations around the nucleus. In the pseudo-potentials approximation, the coulombic potential of the nucleus and the core electrons e_n is fixed. This approximation consists in grouping the core electrons with their nucleus in a core ion whose electronic states will remain unchanged, whose electronic states will remain unchanged whatever the environment in which the atom is placed (this is the frozen core approximation). On the other hand, the pseudo-potential approximation allows developing valence wave functions on a reduced number of plane waves. reduced number of plane waves.

The overriding application in electronic structure is to replace the strong Coulomb potential from the tightly bound nuclei and core electron effects with an effective ionic potential acting on a set of pseudo-wave functions, rather than on the true valence wave functions. The ionic potential from the nuclei and electrons of the core is replaced by a pseudo potential that acts on a set of pseudo wave functions that replace the true wave functions. Beyond the core region, the pseudo-potential reduces to the ionic potential, so that the pseudo wave function is equal to the true wave function [36]. Fig 3 represents schematically the interest of replacing an "all electron" potential by pseudo-potential.

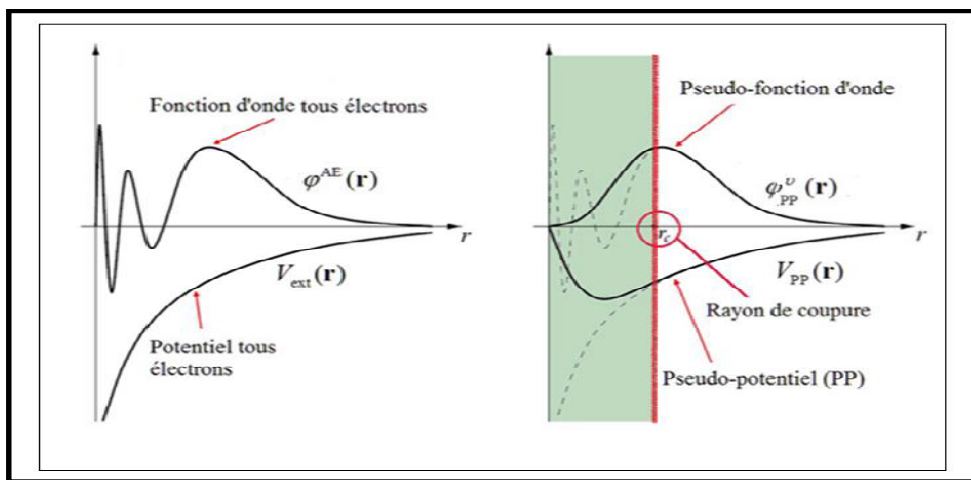


Fig.3: Representation of the replacement of an exact wave function all electrons and the associated potential by a pseudo wave function and pseudo-potential [36]

2.11.2 The pseudo-potentials types:

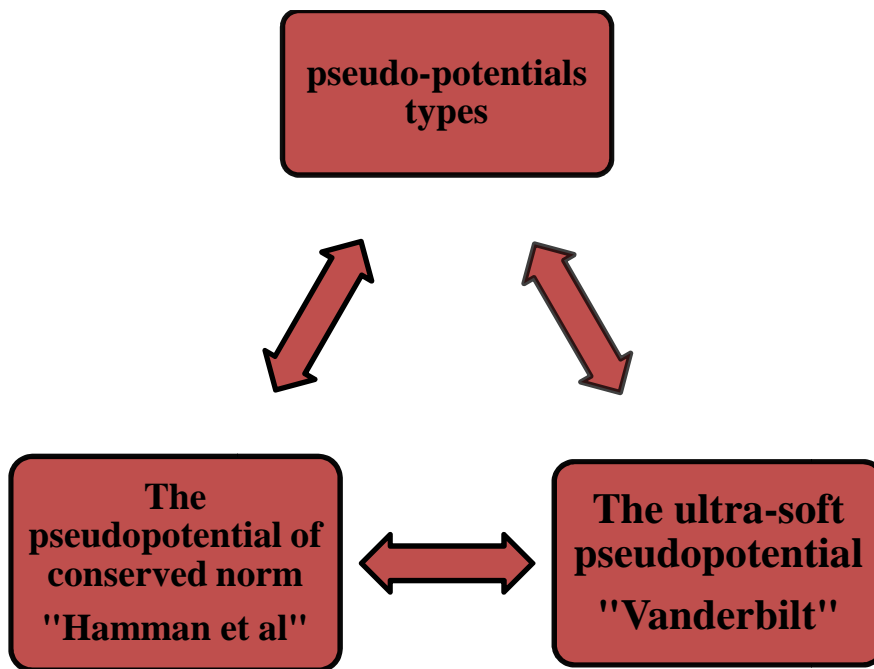


Fig.4: the two types of the pseudo-potentials.

1* **The conserved norm pseudo-potential:** has been proposed by Hamann et al. in 1979[37]. The concept of "conserved norm" occupies a special place in the development of ab initio pseudo-potentials because the effectiveness of the conserved norm pseudo-potential has evolved considerably and this evolution has been motivated by the following objectives:

- ◆ The conserved norm pseudo-potential must be softer, which means using the smallest possible number of plane waves to represent the pseudo wave function.
- ◆ It must be as transferable as possible, i.e. the pseudo-potential generated for one atomic configuration must exactly reproduce other configurations where the crystalline potential is necessarily different from that of a single atom.
- ◆ The charge density constructed using the pseudo-function must reproduce the valence charge density constructed using the real wave function with a high accuracy.

2* **The ultra-soft pseudo-potentials:** conservation of the norm finds its limits in the representation of localized valence orbitals where several plane waves are needed to describe them. Valence orbitals where several plane waves are needed to describe them in the vicinity of the nucleus. There is another formalism of pseudo-potentials, called ultra-soft, which differs by the suppression of the charge conservation constraint in the core region.

The first generation of ultra-soft pseudo-potentials was proposed by Vanderbilt [38].

This type (ultra-soft pseudo-potentials) main interest lies in reducing the number of plane waves needed for the calculations and calculations and consequently to keep a reasonable calculation time.

2.12 The PAW formalism:

Another method to generate ultra soft pseudo-potentials is the PAW (Projected Augmented Wave) method introduced by Blöch [39]. This method allows the generation of ultra-soft pseudo-potentials but for which the grid used to reconstruct the wave function around each atom is radial. These pseudo-potentials are more efficient, especially for magnetic systems [40]. This efficiency comes from the fact that the valence wave function reconstructed by PAW pseudo-potentials is exact, with all nodes in the core region and this for small cutoff radius.

The wave function is rewritten as follows:

$$|\Psi\rangle = |\Psi^{\text{ps}}\rangle = \sum_i |\phi_i^{\text{ps}}\rangle C_i + \sum_i |\phi_i\rangle C_i \quad (35)$$

Where:

$\sum_i |\phi_i^{\text{ps}}\rangle C_i$ is the development of $|\Psi^{\text{ps}}\rangle$ on a pseudo partial wave basis .

$\sum_i |\phi_i\rangle C_i$ is the development of $|\Psi\rangle$ on a partial wave basis, inside the spheres of volume $\Omega_{\vec{R}}$ around the atomic sites marked by \vec{R} .

The coefficients C_i are products of of pseudo wave functions and projection functions localized in the region Ω :

$$C_i = \langle p_i | \phi_i^{\text{ps}} \rangle \quad (36)$$

In the end, the exact wave function $|\Psi\rangle$ is expressed as a function of the pseudo-function $|\Psi^{\text{ps}}\rangle$ by:

$$|\Psi\rangle = |\Psi^{\text{ps}}\rangle - (\sum_i |\phi_i\rangle + - |\phi_i^{\text{ps}}\rangle) \langle p_i | \phi_i^{\text{ps}} \rangle \quad (37)$$

There are three objects in the PAW pseudo-potentials: The first is assimilated into the partial waves $|\psi\rangle$, obtained by radial integration of the Schrödinger equation for atomic energies E_i and which are orthogonal to the core functions, then the pseudo partial wave $|\psi^{\text{ps}}\rangle$ which coincides with partial exact outside the core region, last, The projection function $|p_i\rangle$, of each partial wave, localized in the region and $\Omega_{\vec{R}}$ which satisfies the relation $\langle p_i | \phi_i^{\text{ps}} \rangle$.

In our thesis, we have used pseudo-potentials of the Vanderbilt ultra-soft type [37]. From the CASTEP code library. The ultra soft potential allows a considerable reduction in the size of the plane wave basis compared to the norm-conserved potential [41].

2.13 Cambridge Serial Total Energy Package (CASTEP):

Materials science, also commonly termed materials science and engineering, covers the design and discovery of new materials, particularly solids. This field is so diverse that it interacts with other disciplines of sciences such as biology, particle physics, chemistry, engineering and metallurgy.

CASTEP was created by MC Payne and subsequently developed by academics in the UK, mainly from the Traditional Chinese Medicine Cambridge group. CASTEP is a state-of-the-art quantum mechanics-based program designed specifically for solid-state materials science. CASTEP from (Material Studios) of Accelrys Company and employs the density functional theory plane-wave pseudo-potential method, which allows you to perform first-principles quantum mechanics calculations that explore the properties of crystals and surfaces in materials such as semiconductors, ceramics, metals, minerals, and zeolites.

Typical applications involve studies of surface chemistry, structural properties, band structure and density of states (Fig.5 PDOS for 'BN, N'), and optical properties.

CASTEP can also be used to study the spatial distribution of the charge density, wave functions of a system and the super-Cell compounds (Fig.5 Schematic representation of the super-cell calculation of a substitutional impurity in a bulk and of a small molecule adsorption on a surface [42]). Milman et al, 2000 said that the process of geometry optimization generally results in a model structure that closely resembles the real structure [43] (see Fig.6), Walker et al have been calculated show The bulk modulus of the halite-sylvite mixture (NaCl/KCl) as a function of concentration by calculating the P-V equation of state for different Na concentration and fitting them with the third-order Birch-Murnaghan analytical expression. The results agree with the experimental data Fig.7 [44]. This researches indicate that this code has good agreement results with the experimental method.

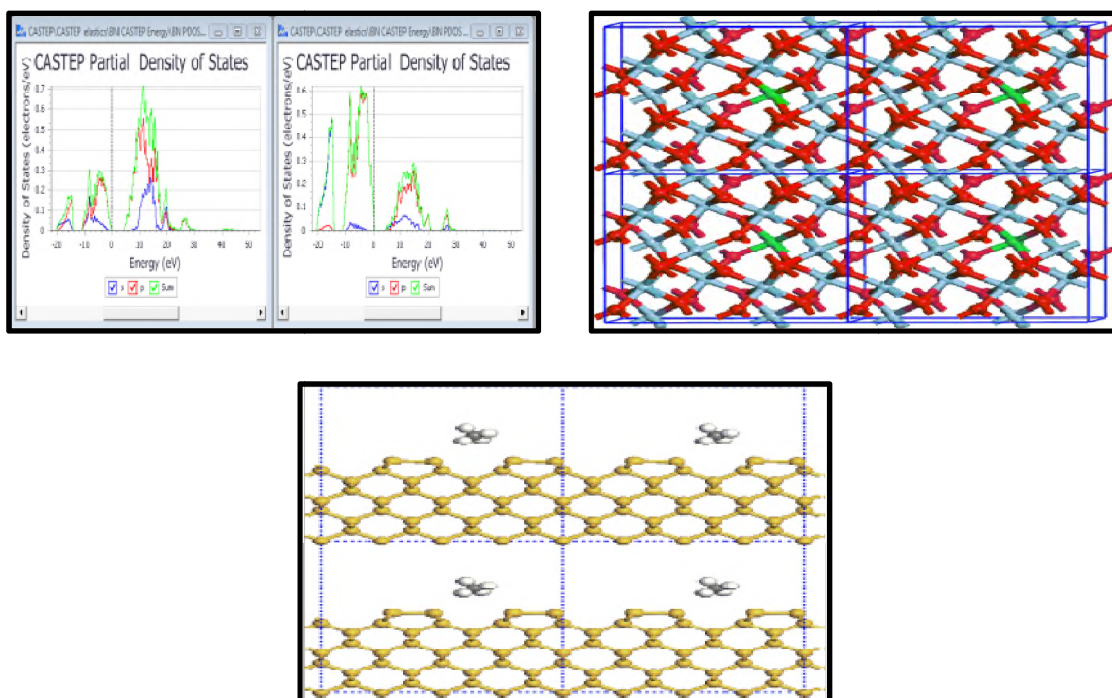


Fig.5:PDOS for BN. The left window is for ‘boron, nitrogen’ the right Schematic represents the super-cell calculation of a substitutional impurity in a bulk and the last: is the super-cell calculation of a small molecule adsorption on a surface [42].

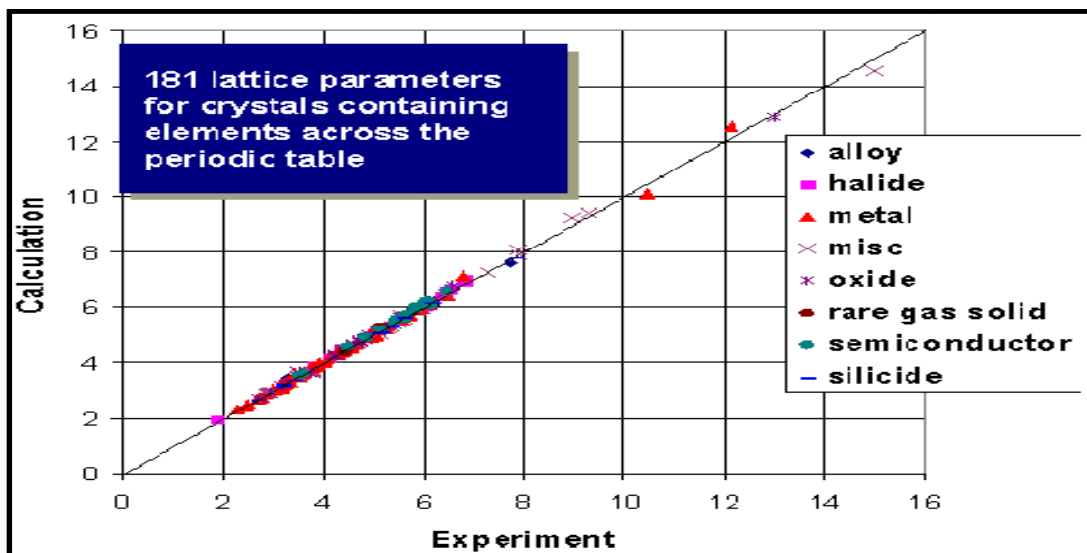


Fig.6: Experimental vs. CASTEP calculated lattice parameters [43].

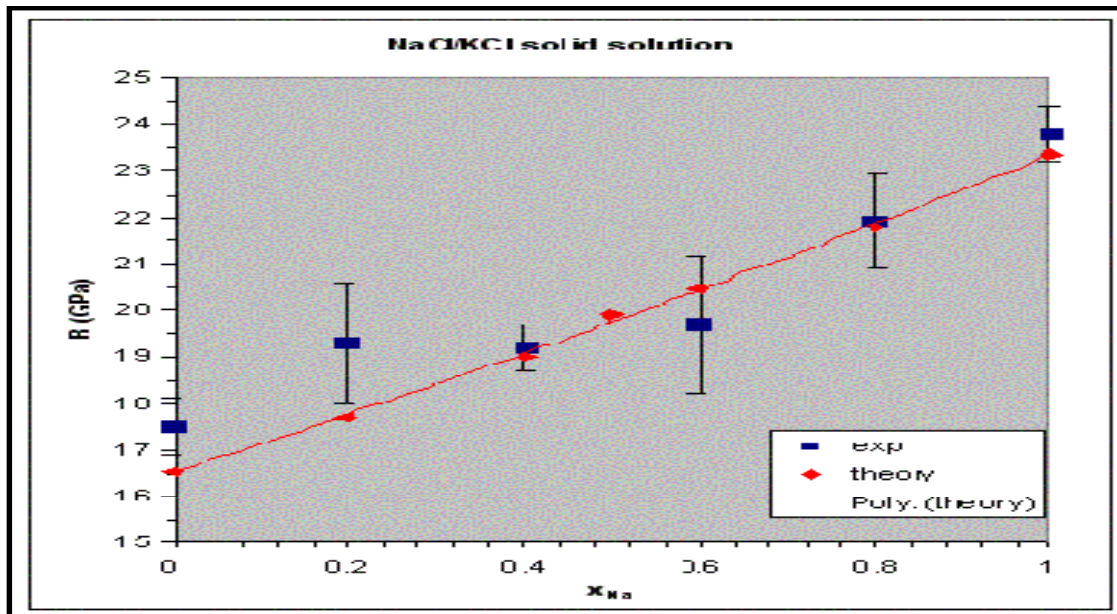


Fig.7: Dependence of the bulk modulus of the NaCl/KCl solid solution on concentration. Experimental data are from Walker et al. (2004). The solid line shows a polynomial fit to the calculated results [44].

2.14 Conclusion:

This chapter presents the main foundations of DFT, which allows approximating the electron density in the ground state of the electron gas without the need to calculate the microwave function. The different approximations used to calculate the energy and the cross-correlation potential, then we presented the quantum mechanical equations to solve the Schrödinger equation in the ground state. In this study, the DFT calculations were performed using a pseudo-potential approach. Its different foundations and types have been described. Finally, the Castep code capable of computing some physical properties of a finite atomic system is described.

Bibliography:

- [1]C.C.M.Rindt, S.V.G.Nedeia, Modeling thermochemical reactions in thermal energy storage systems,J. Advances in Thermal Energy Storage Systems,P 376-415,https://doi.org/10.1533/9781782420965.3.375.
- [2]A.Lamichhane, Quantum- mechanical Ab-initio calculations of the properties of wurtzite ZnO and its native oxygen point defects ,2018.(Thesis)
- [3]I.Falconer, J J Thomson and the discovery of the electron,J. Physics Education,1997.(Book)
- [4]S.Vallabhajosula, Atoms and Radiation,J. Molecular Imaging: Radiopharmaceuticals for PET and SPECT,2009,P 25-34,https://doi:10.1007/978-3-540-76735-0_3.
- [5]M.Whitaker, The bohr-moseley synthesis and a simple model for atomic x-ray energies,J. European Journal of Physics,1999,V 20,P 213-220,https://doi.org/10.1088/0143-0807/20/3/312.
- [6]J.Kohanoff, Electronic Structure Calculations for Solids and Molecules: Theory and Computational Methods,J. Cambridge University Press,2006.(Book)
- [7]J.Slater, Band theory,J. Physics and Chemistry of Solids,1959 ,V 8,P 21-25,https://doi.org/10.1016/0022-3697(59)90265-3.
- [8]C.Sherrill, An introduction to hartree-fock molecular orbital theory, School of Chemistry and Biochemistry,Georgia Institute of Technology,2000.
- [9]M.Casida and M.Rotllant, Progress in time-dependent density-functional theory,J. Annual Review of Physical Chemistry,2012,P 287-323, https://doi.org/10.1146/annurev-physchem-032511-143803.
- [10]T.Cazenave, Semi-linear Schrödinger equations,J. Courant Lecture Notes,2003,ISBN: 978-1-4704-1760-4.(Book)
- [11]M.Born and J.Oppenheimer, Zur Quantentheorie der Molekeln,J. Annalen der Physik,1927,P 458-484,https://doi.org/10.1002/andp.19273892002.
- [12]D.Hartree, The wave mechanics of an atom with non-coulombic central field: parts I, II, II,J. Mathematical Proceedings of the Cambridge Philosophical Society,1928.
- [13]P.Hohenberg and W.Kohn, In homogeneous electron gas,J. Physical Review B,1964.
- [14]R.Hoffmann, J.Malrieu, Simulation vs. Understanding: A Tension, in Quantum Chemistry and Beyond. Part B. The March of Simulation, for Better or Worse,J. Angewandte Chemie,2019,P 1-67,https://doi.org/10.1002/ange.201910283.

- [15]W.Kohn and L.Sham, Self-Consistent Equations Including Exchange and Correlation Effects,J. Physical Review, 1965,V 140,P 1133-1138,<https://doi.org/10.1103/PhysRev.140.A1133>.
- [16]K.Schwarz, Computation of Materials Properties at the Atomic Scale,J. Applications of Quantum Mechanics,2015,P 276-310,<https://doi.org/10.5772/59108>.
- [17]F.Fischer, M.Keller, T.Gerhard, T.Behr, T.Litz, H.Lugauer, M.Keim, G. Reuscher, T.Baron, A.Waag and G.Landwehr, Reduction of the extended defect density in molecular beam epitaxy grown ZnSe based II-VI heterostructures by the use of a BeTe buffer layer,J. Applied Physics,1998,V 84,P 1650-1654,<https://doi.org/10.1063/1.368234>.
- [18]L.Thomas, The calculation of atomic fields,J. Mathematical Proceedings of the Cambridge Philosophical Society,1927,P 542-548,<https://doi.org/10.1017/S0305004100011683>.
- [19]E.Fermi, Un Metodo Statistico per la Determinazione di alcune Proprietà dell'Atomo,J. Rend. Accad. Naz. Lincei,1927.
- [20]P.Dirac, Quantum Mechanics of Many-Electron System,J. Proceedings of the Royal Society A,1929,V 123,P 714-733,<https://doi.org/10.1098/rspa.1929.0094>.
- [21]T.Loucks, The Augmented Plane Wave Methode,J. New York, 1967.
- [22]E.Wimmer, H.Krakauer, M.Weinert, A.Freeman, Full-potential self-consistent linearized-augmented-plane-wave method for calculating the electronic structure of molecules and surfaces: O₂ molecule,J. Physical Review B,1981,V 24,P 864-875,<https://doi.org/10.1103/PhysRevB.24.864>.
- [23]G.Ortiz, Gradient-corrected pseudopotential calculations in semiconductors,J. Physical Review B,1992,V 45,P 11328-11331,<https://doi.org/10.1103/PhysRevB.45.11328>.
- [24]C.Bowen, G.Supiyama, B.Alder, Static dielectric response of the electron gas,J. Physical Review B ,1994,V 50,P 14838-14848,<https://doi.org/10.1103/PhysRevB.50.14838>.
- [25]E.Proynov, E.Ruiz, A.Vela, D.Salahub, Determining and extending the domain of exchange and correlation functional,J. International Journal of Quantum Chemistry ,1995,V 28,P 61-78,<https://doi.org/10.1002/qua.560560808>.

- [26] C. Filippi, D. Singh, C. Umringar, All-electron local-density and generalized-gradient calculations of the structural properties of semiconductors, *J. Physical Review B*, 1994, V 50, P 14947-14951, <https://doi.org/10.1103/PhysRevB.50.14947>.
- [27] D. Ceperly, B. Alder, Ground State of the Electron Gas by a Stochastic Method, *J. Physical Review Letters*, 1980, V 45, P 566-569, <https://doi.org/10.1103/PhysRevLett.45.566>.
- [28] D. Hartree, The Wave Mechanics of an Atom with a non-Coulomb Central Field. Part III. Term Values and Intensities in Series in Optical Spectra, *J. Mathematical Proceedings of the Cambridge Philosophical Society*, 1928, V 24, P 426-437, <https://doi.org/10.1017/S0305004100015954>.
- [29] V. Fock, Approximation method for the solution of the quantum mechanical multi-body problem, *J. Physics A*, 1930, P 126-148, <https://doi.org/10.1007/BF01340294>.
- [30] V. Anisimov, J. Zaanen, O. Andersen, Band theory and Mott insulators: Hubbard U instead of Stoner I, *J. Physical Review B*, 1991, V 44, P 943-954, <https://doi.org/10.1103/PhysRevB.44.943>.
- [31] S. Dudarev, A. Liechtenstein, M. Castell, G. Briggs, A. Sutton, Surface states on NiO (100) and the origin of the contrast reversal in atomically resolved scanning tunneling microscope images, *J. Physical Review B*, 1997, V 56, P 4900-4908, <https://doi.org/10.1103/PhysRevB.56.4900>.
- [32] S. Dudarev, G. Botton, S. Savrasov, C. Humphreys, A. Sutton, Electron energy loss spectra and the structural stability of nickel oxide : An LSDA+U study, *J. Physical Review B*, 1998, V 57, P 1505-1509, <https://doi.org/10.1103/PhysRevB.57.1505>.
- [33] S. Lardjane, Study of the structural, electronic and magnetic properties of electronic and magnetic properties of diluted magnetic semiconductor : Cobalt-doped ZnO, 2014, <https://tel.archives-ouvertes.fr/tel-01005359> (Thesis).
- [34] O. Gunnarsson, M. Jonson, B. Lundqvist, Descriptions of exchange and correlation effects in inhomogeneous electron systems, *J. Physical Review B*, 1979, V 20, P 3136-3164, <https://doi.org/10.1103/PhysRevB.20.3136>.
- [35] Y. Quéré, *Physique des matériaux*, Palaiseau Ecole Polytechnique, 1984.
- [36] Z. Souadia, Investigation of the physical properties of tellurides in metals M₂Te [M: Li, Na, K and Rb] alkalis via ab initio methods, Ferhat Abbas University, 2018. (Thesis)
- [37] D. Hamann, M. Schlüter, C. Chiang, Norm-Conserving Pseudopotentials, *J. Physical Review Letters*, 1979, V 43, P 1494-1497, <https://doi.org/10.1103/PhysRevLett.43.1494>.

- [38]D.Vanderbilt, Soft self-consistent pseudopotentials in a generalized eigenvalue formalism,J. Physical Review B,1990,<https://doi.org/10.1103/PhysRevB.41.7892>.
- [39]P.Blöchl, Projector augmented-wave method,J. Physical Review B,1994, ,V 50,P 17953-17979,<https://doi.org/10.1103/PhysRevB.50.17953>.
- [40]G. Kresse, D.Joubert, From ultrasoft pseudopotentials to the projector augmented-wave method,J. Physical Review B, 1999,V 59,P 1758-1775,<https://doi.org/10.1103/PhysRevB.59.1758>.
- [41]K.Schwarz, C.Draxl, P.Blaha, Charge distribution and electric-field gradients in YBa₂Cu₃O_{7-x},J. Physical Review B,1990,V 42,P 2052-2061,<https://doi.org/10.1103/PhysRevB.42.2051>.
- [42]M.Payne, M.Teter, D.Allan, T.Arias, J.Joannopoulos, Iterative Minimization Techniques for Ab Initio Total Energy Calculations: Molecular Dynamics and Conjugate Gradient, J Reviews of Moderne Physics,1992,V 64,P 1045-1097,<https://doi.org/10.1103/RevModPhys.64.1045>.
- [43]V.Milman, B.Winkler, J.White, C.Pickard, M.Payne, E.Akhmatskaya, R.Nobes ,Electronic structure, properties and phase stability of inorganic crystals: A pseudopotential plane-wave study,J. International Journal Quantum Chemistry ,2000,V 77,P 895–910 ,[https://doi.org/10.1002/\(SICI\)1097-461X\(2000\)77:5<895::AID-QUA10>3.0.CO;2-C](https://doi.org/10.1002/(SICI)1097-461X(2000)77:5<895::AID-QUA10>3.0.CO;2-C).
- [44]D.Walker, P.Verma, L.Cranswick, R.Jones, S.Clark, S.Buhre,Halite-sylvite thermoelasticity,J. American Mineralogist,2004,V 89,P 204-210, <https://doi.org/10.2138/am-2004-0124>.
- [45]A.Ciucivara, B.S, M.SS. Density functional studies of magnetic semiconductors and multiferroics, The University of Texas at Austin,2007, UMI Number: 3295228.

Chapter 3

Results and

Discussion

**Carbon and
Silicon co-
doping ZnO**

ZnO has been a very appealing candidate for optoelectronics, energy conversion, and photo-catalysis due to several unique features, low cost and high photosensitivity, including high electron mobility, a wide direct band gap with a large exciton binding energy, and electrochemical activity. However, ZnO is incapable of using visible light, which comprises around 43% of the solar spectrum, making it inefficient for solar cells and photo-catalysis [1].

ZnO has also many applications like: biological tracers [2], UV laser diodes [3] and polariton lasers as well as its integration into high-efficiency solar cells. In addition, ZnO is also studied for its great potential to solve environmental issues [4].

Over the past two decades, great efforts have been made in the synthesis of doped ZnO nano-materials to improve morphological, micro-structural and optoelectronic properties; in particular by modifying surface properties, band gap, specific surface, oxygen vacancies and crystal deficiencies [5-6].

Doping with non-metallic elements such as N or C would reduce the ZnO band gap, (ZnO has a wide band semiconductor) by improving a number of physical properties, like ferromagnetism, magnets with transport properties and p-type conduction properties [7-8].

Experimental studies showed that the incorporation of Si atoms in ZnO lattice have not an important effect on the band gap magnitude in the visible region where ZnO has the highest transmittance [9-10]. It was found that the concentration of Si doping significantly influences the transparency and, consequently, the absorbance values of the films. [11].

Experimentally, the evaluated band gap values shift to upper values relative to the pure ZnO films, depending on the Si doping concentration [11]. On the other hand, the volume of the unit cell and the network parameter for axis $a = b$ both decrease up to 0.6 % of Si content as expected if Si^{+4} (0.26 Å) replaces Zn^{+2} (0.6 Å). However, Si generates higher free carrier densities than those of other dopants like Al, Ga and In . This behavior can be attributed to both electron donor states and thus replace the Zn sites in the ZnO matrix [12-13]. Although ZnO co-doping by two different elements, has received much attention in recent years, experimental and theoretical studies to date are not conclusive to highlight the predominant type of defects and their mechanisms.

Driven by the aforementioned motivations, this chapter deals with theoretical studies of the co-effect of carbon and silicon on micro-structural and optoelectronic properties of ZnO, using first principles calculations based on density function theory (DFT). More interestingly, based on the results of the theoretical calculation; the structural, electronic and optical properties are calculated, discussed qualitatively because they were scarcely studied according to the published works. Therefore, the best strategy for obtaining high-performance

ZnO-based systems is to understand doping and co-doping mechanisms in order to improve carrier mobility and concentration, this will improve the optoelectronic and photovoltaic applications of ZnO-based devices.

1. Reminder on the calculation method

1.1 Convergence test:

This research work is performed using first principles calculations based on the density functional theory (DFT) using the plane wave method of pseudo-potentials [14] implemented in the CASTEP code.

Before embarking on long and costly calculations, it is necessary to optimize the input parameters that control the initial computational density. In general, there are two adjustments to be made:

- 1* The size of the plane wave basis by choosing the cutoff energy E_c (which allows a correct approximation of the wave functions).
- 2* The quality of the sampling of the Brillouin zone (by the number of points k).

All DFT calculations using the CASTEP code (Cambridge Serial Total Energy Package) in this work are based on the plane wave pseudo-potential method [14]. We also used generalized gradient approximation (GGA) with perdue-Burke-Ernzerhof (PBE). There is another approximation to be included in the research, (GGA+U) as an exchange correlation function [15-16-17]. It is well known that GGA is not sufficient to reproduce one of the important properties of semiconductors correctly, namely the energy of the band gap; therefore, the energy estimate of the impurity states in relation to the Fermi energy is generally only approximate [18]. For this reason, previous studies performed GGA+U calculation, $U-J = 10.5$ eV, was used for Zn d states [19], But it is not used here.

Calculations made with the CASTEP code "Cambridge Serial Total Energy Package" using an ultra-soft pseudo-potential for an effective calculation at lower energy cut-off energy. These pseudo-potentials are included in the code where they were generated by non-

relativistic calculations. The "ultrafine" choice of calculations ensures an accurate convergence of the total energy and rapidity in obtaining the different results.

The tests and inputs values which were carried out, led us to choose the parameters and inputs values mentioned in Table.1.

parameters	Values
The cut-off energy	380eV
The k-points were	$4 \times 4 \times 2$
convergence thresholds	2×10^{-5} eV/atom
The maximum force	> 0.03 eV. \AA^{-1}
Pressure	0.05 GPa
The maximum displacement	0.001 \AA
the self-consistent calculation SCF	$> 1 \times 10^{-6}$ eV/atom

Tab.1: Cutoff energy, number of k points and other impute values used in our calculation.

The valence electronic configuration of ZnO is: Zn $3p^6 3d^1 4s^2$ and O: $2s^2 2p^4$. Fig.1 (1.a, 1.b, 1.c and 1.d) represents 4 structures of undoped and (C, Si, C: Si) doped ZnO systems were done on $2 \times 2 \times 1$ super-cells, where C and Si atoms replace respectively O and Zn atoms.

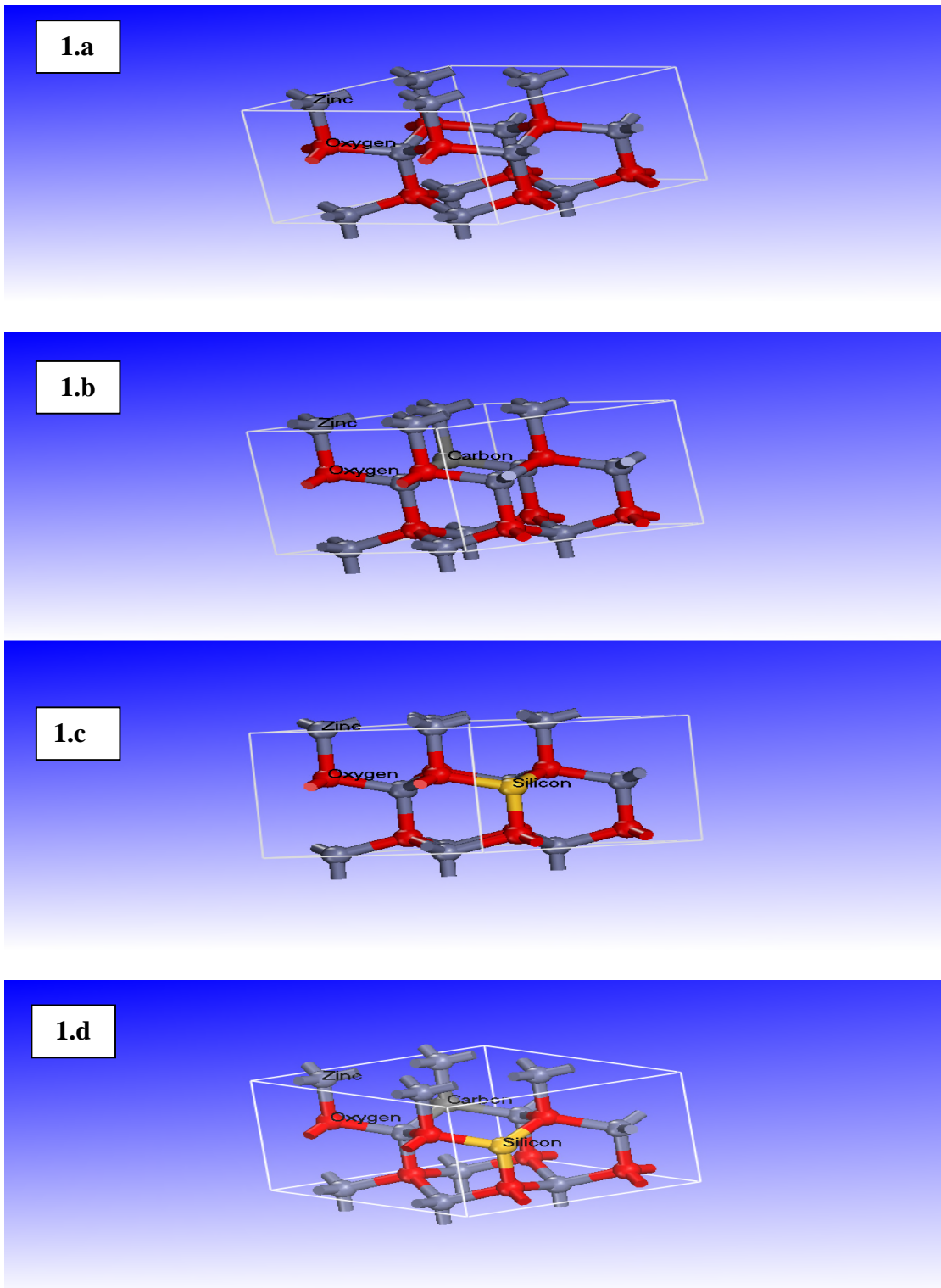


Fig.1: undoped ZnO, C doped ZnO, Si doped ZnO and C:Si doped ZnO (1.a, 1.b, 1.c and 1.d) respectively, on $2 \times 2 \times 1$ super cell.

For the previously studied systems in this research, electronic properties such as the density of state and optical properties such as dielectric function, absorption coefficient and refractive index were calculated. All these results were obtained for a carrier energy within the range (-23 eV, -10 eV) and (0 eV- 30 eV) respectively.

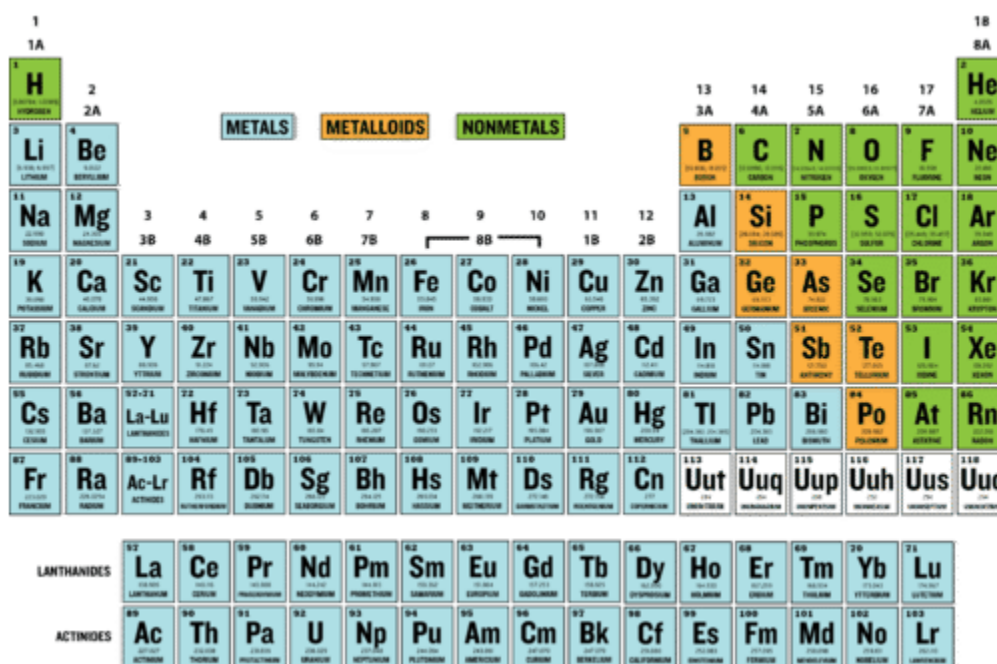
2. Results and discussion

2.1 Structural Properties:

We chose ZnO to be our field of study, Because it is highly doped with atomic impurities, and there now exists considerable academic research efforts to control ZnO doping to both improve existing physical properties and add new material dimensionalities, including varying the optoelectronic, magnetic , magneto-optic, electromagnetic, thermoelectric and piezoelectric properties . In this chapter, we used GGA approximation to explore the structural, electronic and optic properties of pure wurtzite ZnO phase and several compositions of X: ZnO for (X=C, Si, C: Si)

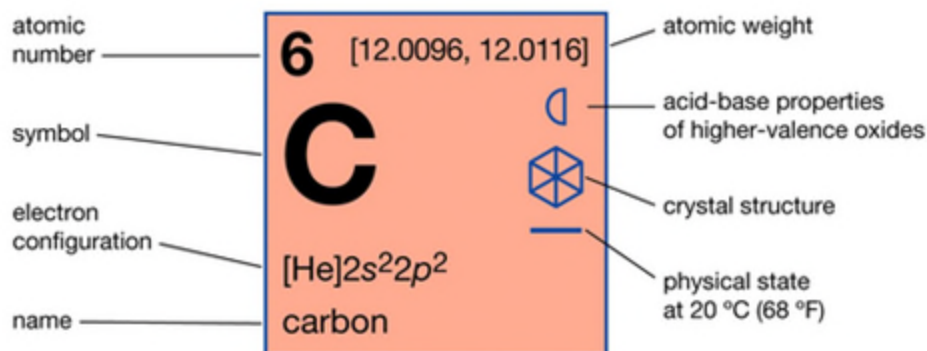
Recently, the ZnO presented an interesting subject for doping with various elements such as transition metals, noble metals. This is of course very suitable to improve the optoelectronic and photocatalytic properties because the incorporation of dopants generates lattice defects and changes consequently the band gap energy. In particular, the doping with metalloids and non metals elements has been extensively investigated, experimentally as well as theoretically.

(a)



(b)

Carbon



(c)

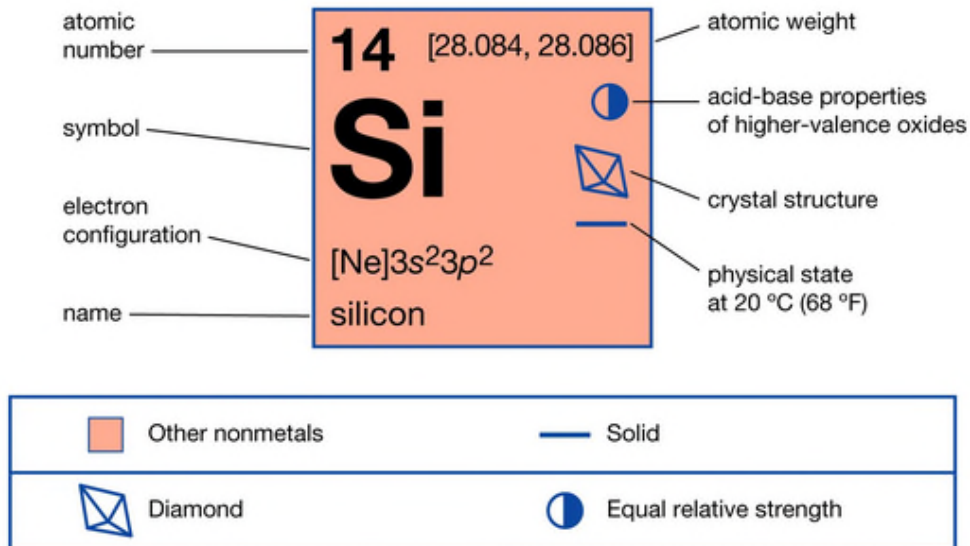
Silicon

Fig.2: (a) The parts of periodic table,(b) carbon characterizations and (c) silicon characterizations

The influence of the crystal structure on the physical properties of materials and the determination of structural properties play an important role in the physics of solid materials, as they provide information on the microscopic structure of materials and will therefore have a microscopic structure of materials and will therefore have a relatively necessity on the prediction of other properties.

Under normal atmospheric conditions, zinc oxide (ZnO) has a hexagonal structure with two atoms of Zn and two atoms of O in the primary cell, the lattice parameters are $a = b = 3.24 \text{ \AA}$, $c = 5.20 \text{ \AA}$, $\alpha = \beta = 90^\circ$ and $\gamma = 120^\circ$, with a space group (P63mc). The results obtained are then adjusted to Murnaghan's equation of state [20] which is given by the following expression:

$$E(V) = E_0 + [B_0 V / B_0' (B_0' - 1)] \times [B_0' (1 - V_0/V) + (V_0/V)^{B_0'} - 1] \quad (1)$$

Where E, V, B_0 and B_0' formulate respectively the total energy, equilibrium volume, bulk modulus and derivative of the bulk modulus of (C, Si and C: Si) doped ZnO when the formular between B_0, V is:

$$B_0 = V \partial^2 E / \partial V^2 \quad (2)$$

Using GGA, our calculated results for the total energy as a function of volume of (a) ZnO, (b) ZnO:C, (c) ZnO:Si and (d) ZnO:C:S represented in **Figure 3**. The würtzite structure of undoped ZnO is more stable than other compounds and the volume expand with the incorporation of C and Si content. Thus the bulk modulus of ZnO is (133.53 GPa) which is in agreement with other theoretical calculation [21], but there is a different with experimental data [22]. The lattice parameters optimized are shown in **Table 1**.

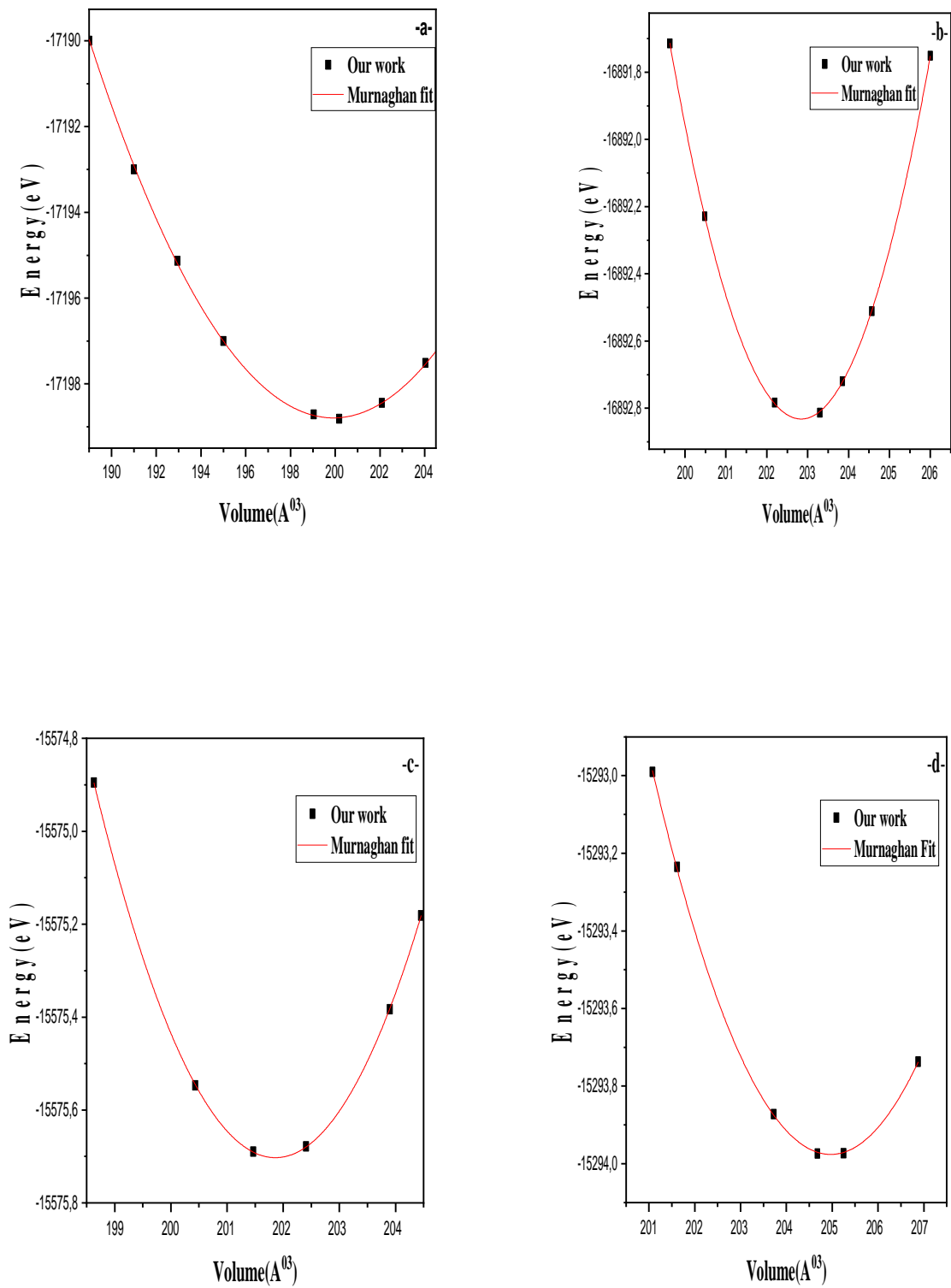


Fig.3: Calculated energy versus volume for pure ZnO (a), ZnO:C (b), ZnO:Si (c) and (d) ZnO:C:Si.

Lattice constants	Results	ZnO	C :ZnO	Si :ZnO	C:Si:ZnO
$a_0(\text{\AA})$	This work	3.3554	3.3564	3.3551	3.3712
	Theoretical results	3.276 ^a , 3.25 ^b 3.283 ^e , 3.326 ^k 3.284 ^l , 3.2832 ^g 3.2635 ^m , 3.283 ^q	3.263 ^{h, r}	----	----
	Experimental results	3.1728 ^f , 3.2497 ^j 3.244 ^k , 3.258 ^d	3.251 ⁱ 3.2558 ^o 3.242 ^p	3.0682 ^f	----
$c_0(\text{\AA})$	This work	5.2686	5.3337	5.25981	5.2443
	Theoretical results	5.258 ^a , 5.21 ^b 5.2983 ^c , 5.418 ^k 5.294 ^l , 5.29 ^m 5.288 ^q , 5.309 ^e	5.383 ^{h, r}	----	----
	Experimental results	5.195 ^f , 5.206 ⁱ 5.199 ^k , 5.220 ^d	5.210 ^t 5.2137 ^o 5.234 ^p	5.1516 ^f 5.31 ^s	----
μ	This work	0.383	0.37	----	----
	Theoretical results	0.38 ^a , 0.3767 ^m 0.3788 ⁿ , 0.3786 ^e	----	----	----
	Experimental results	0.382 ^d	----	----	----
$B_0(\text{GPa})$	This work	133.53	160.17	147.53	157.8
	Theoretical results	136 ^a , 148.1 ^b 138 ^g , 154 ^d 131.5 ^e	158.6 ^r	----
	Experimental results	173 ^d , 181 ^d 183 ^c	----

Tab.2: The equilibrium lattice parameters, internal parameter and bulk modulus in comparison with other theoretical and experimental works results.

^aRef[21], ^bRef[22], ^cRef[23], ^dRef[24], ^eRef[25], ^fRef[26], ^gRef[27],
^hRef[28], ⁱRef[29], ^jRef[30], ^kRef[31], ^lRef[32], ^mRef[33], ⁿRef[34],
^oRef[35], ^pRef[36], ^qRef[37], ^rRef[38], ^sRef[39]

As can be seen, a considered change of a_0 and c_0 parameters of ZnO observing with changing the doping elements. This variation is attributed to the change in doping of Zn^{+2} ions with Si^{+4} and O^{-2} with C^{-4} . The incorporation of the C and Si atoms in ZnO matrix, increases a_0 but decreases c_0 . These deviations are mainly related to the largest atomic radius of Carbon atoms (2.6 Å), Oxygen (1.4 Å) compared with that of Zinc atoms (0.74Å) and Silicon (0.26Å), and also with the electro negativity among the C, Si and Zn atoms. An earlier theoretical study showed that for C atom doping probably occurs by replacing O atoms in the ZnO matrix [40].

Moreover, our findings show that the Oxygen internal parameters μ of C: ZnO is less than the undoped ZnO. Another work suggests that carbon atoms may partially take interstitial positions in the ZnO matrix [41].

The lack of theoretical and experimental results is among the motivations for the choice of these materials. All this, gives us an opportunity to contribute to the scientific literature.

For B_0 , we note therefore; that the experimental values of the compressibility modulus are of very high values found by the PPsPW method with the functional PBE. What is certain is that the value of the stiffness modulus is much more sensitive to the method used than that of the equilibrium volume.

2.2 Elastic Properties

The single-crystal elastic constants C_{ij} are among the most important parameters that characterize the physical properties of crystals. From a practical point, the elastic constants measure the resistance of a solid to an external applied macroscopic stress and their abilities to recover and regain their original shape after stress. From the C_{ij} s, can be obtained some macroscopic elastic moduli like the bulk, Young, shear moduli, Poisson's ratio and C_{ij} , this moduli characterize the mechanical properties of solids.

For the examined systems, C_{11} , C_{12} , C_{13} , C_{33} , C_{44} , B and E to ambient pressure condition values, are quoted in Table 3.

In the first view, the stability conditions $C_{11} - C_{12} > 0$, $C_{11} + C_{12} > 0$ and $C_{44} > 0$ are very satisfied for the different systems. For ZnO,

We have also described the elastic constants of ZnO:C, ZnO:Si and ZnO:C:Si in ambient conditions. Respectively, we can showed that this constants decrease and became smaller than undoped ZnO, especially for carbon doped ZnO, where its values of bulk modulus and young modulus are decreased a lot. Therefore, it should be noted that there is an inverse relationship between the elastic properties and the doping. Using the following relations: $C_{11} > C_{12}$, $C_{44} > 0$, $(C_{11}C_{12})C_{33} > 2C_{13}^2$ and $(C_{11}-C_{12})C_{66} > 2C_{16}^2$, we confirm that all ZnO doping have a mechanical stabilities. The results of ones for GGA and the slight differences shifts may be results from the initials parameters introduce on the convergence criteria and the type of the interaction between atoms.

Elastic parameters (GPa)	C_{11}	C_{12}	C_{13}	C_{33}	C_{44}	B	E
ZnO	285	155	99	153	38	121.54	170
ZnO:C	134.98	105.38	91.83	90.42	12.13	115.398	39.836
ZnO:Si	147.74	90.219	71.304	158.52	32.14	100.24	86.45186
ZnO:C:Si	134.67	75.70	72.15	150.5	32.62	95.828	83.42

Tab.3: elastic constants of pure ZnO, C doped ZnO, Si doped ZnO and C:Si co-doped ZnO.

2.3 Electronic Properties

2.3.1 Band Structure

The ZnO band structures, C: ZnO, Si: ZnO and C: Si: ZnO are shown in **Figure 4** along the high symmetry points in the first Brillouin zone. The Fermi level is represented by a line based on GGA. It is recognized that the GGA method is inadequate to fully describe the electronic properties of materials; it generally underestimates the energy value of the band gap [42-43]. But, the GGA+U approach is generally used to improve the calculated band gap energy [44-45].

The calculated direct band gap for pure ZnO is 0.7 eV, which is close to the theoretical and experimental values [46-47-48] and 1.3 eV, 0.9 eV and 1.46 eV for C:ZnO, Si: ZnO and C:Si:ZnO respectively, reported on the **Table 4**, our results of the optical gap as well as those of other experimental and theoretical works [49-50].

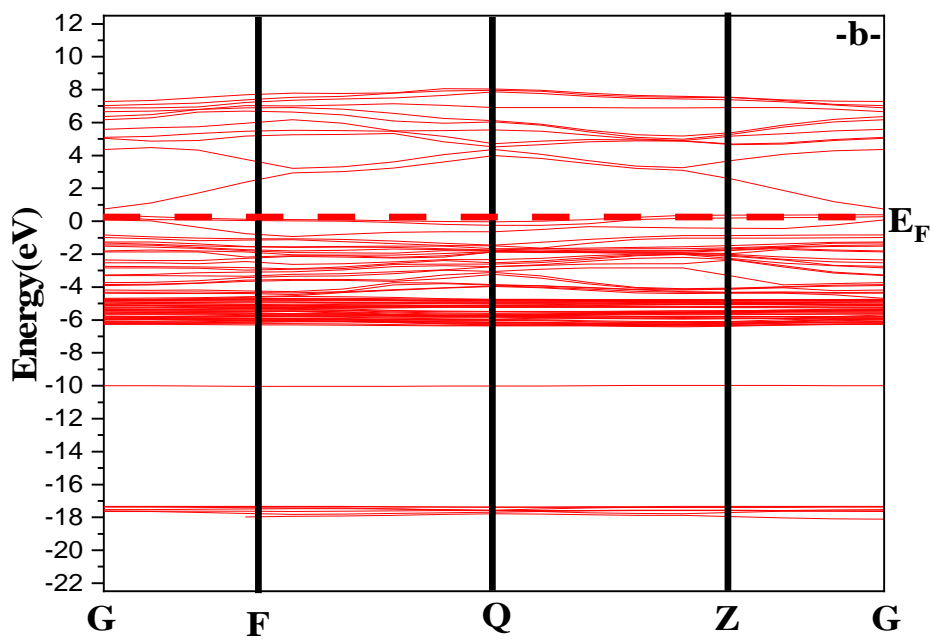
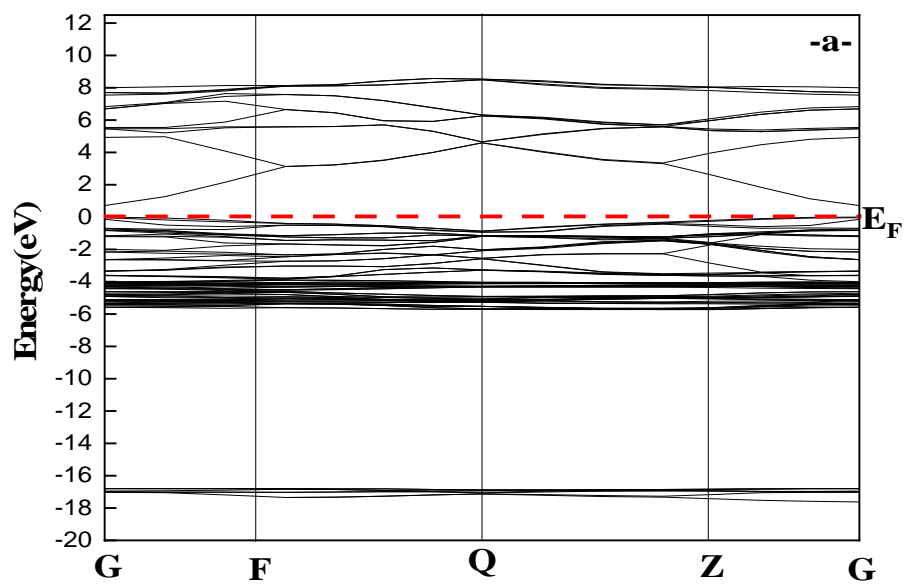
Compound	Eg (eV)		
	This work	Other theoretical results	Experimental results
ZnO	0.7	0.73 ^a	3.3 ⁱ
C:ZnO	1.30	0.9 ^h , 1.6 ^a	3.07 ^b , 2.98 ^c
Si:ZnO	0.9	1.5 ^f	3.4 ^d , 3.42 ^e , 3.52 ^g
C:Si:ZnO	1.46	----	----

Tab.4: Calculated band gap values in comparison with other theoretical and experimental works results.

^a Ref [46], ^b Ref [51], ^c Ref [52], ^d Ref [53], ^e Ref [54], ^f Ref [55], ^g Ref [56], ^h Ref [57], ⁱ Ref [58].

In fact, the position of the conduction band minimum (CBM) remains unchanged and the valence band maximum (VBM) move in the direction of high energy and all dopants have a direct band gap. At the dopants concentration of 12.5 % is already enough to lead to a degenerate semiconductor.

This is coherent with the appearance of new bands and the states of impurities in the valence band maximum (VBM). In addition, the gap between the Fermi level and the conduction band minimum (CBM) in the ZnO doped Si is smaller than the ZnO doped C and C: Si co-doped ZnO. Thus, it can be said reasonably that the doped Si on ZnO could have a strong effect on band structures and played the role of preferred dopants than C and C: Si co-doped ZnO, which may be due to the p-type doping character of Si. We note that vacant states are introduced into the band gap above the Fermi level, but the increase in this band gap may also be due to the reduction in lattice parameters caused by the enhancement of the valence band [46]. On the other hand, the energy contributions of our compound atoms play an irreplaceable role. The photon energy by taking of thermal excitation was also facility the transition of electrons .



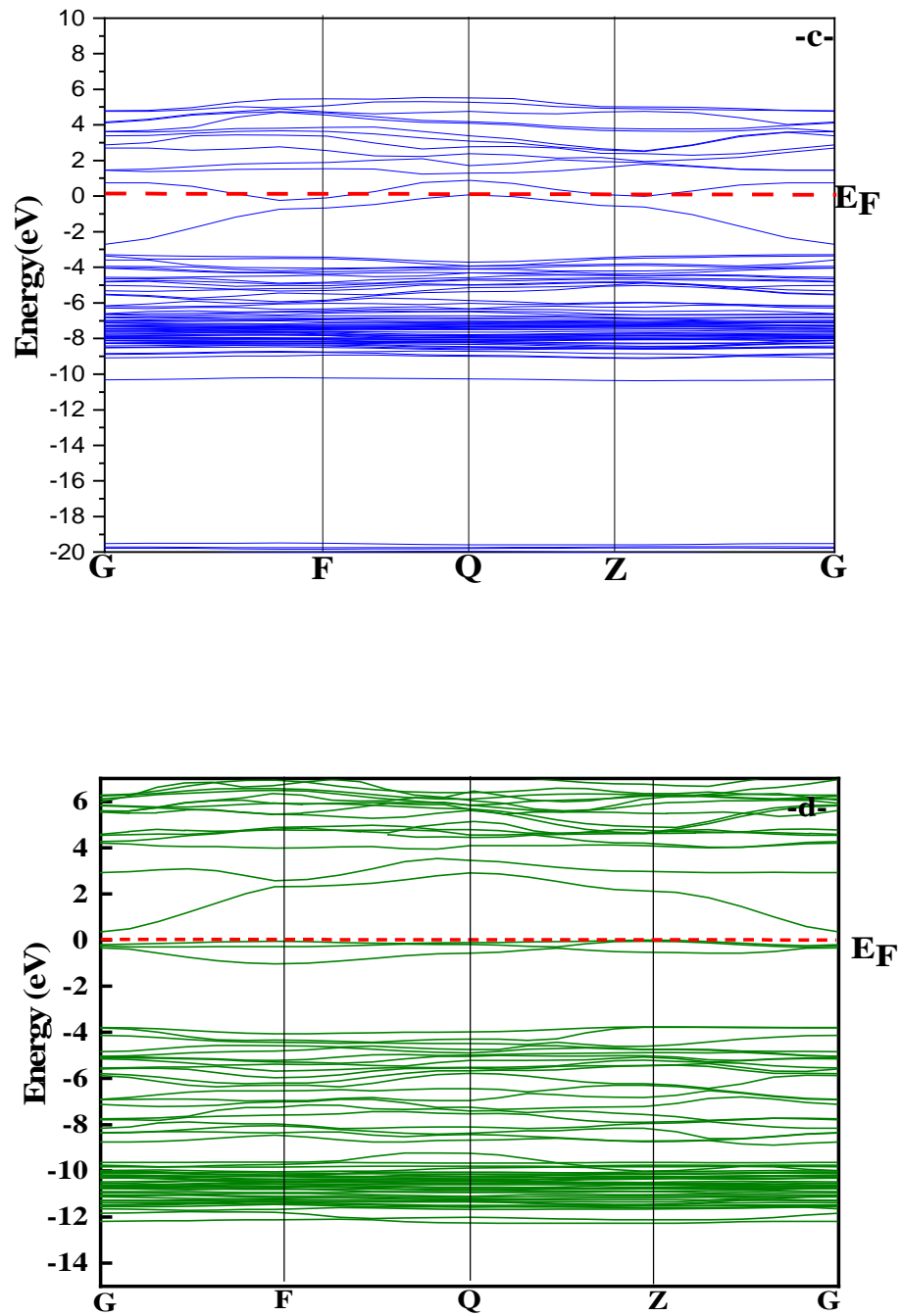
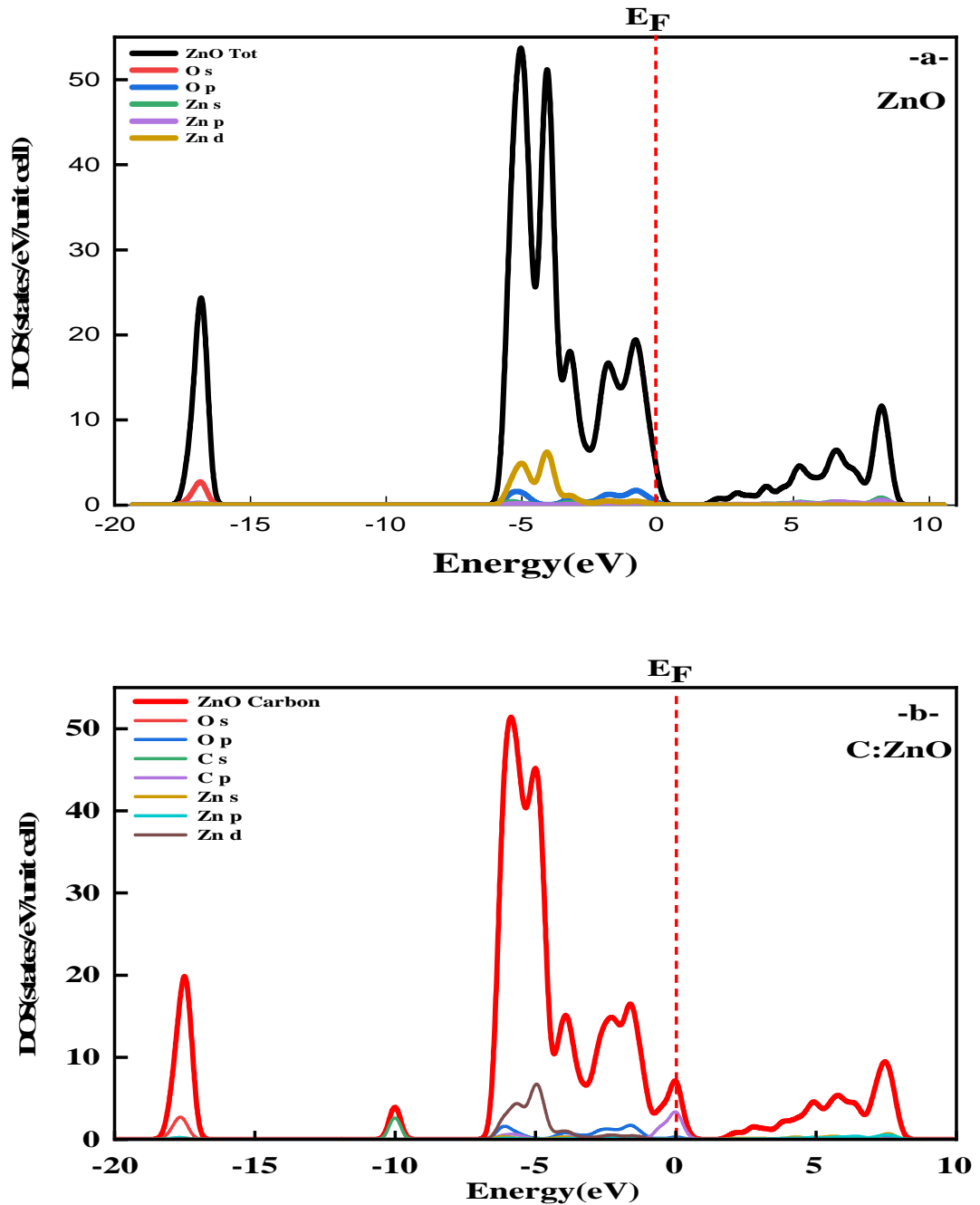


Fig.4: Band structures of (a) undoped ZnO and (b) C doped ZnO, (c) Si doped ZnO and (d) C:Si co-doped ZnO.

2.3.2 Density of state

Based on the DOS calculation found, **Figure 5** shows that the total state density (TDOS) and partial state density (PDOS) of the uncorrected ZnO, C: ZnO, Si: ZnO and C: Si: ZnO in the range (-23 eV–10 eV). The Fermi level is set to 0 eV. This property is more important to see the influence of the coexistence of different dopants in ZnO.



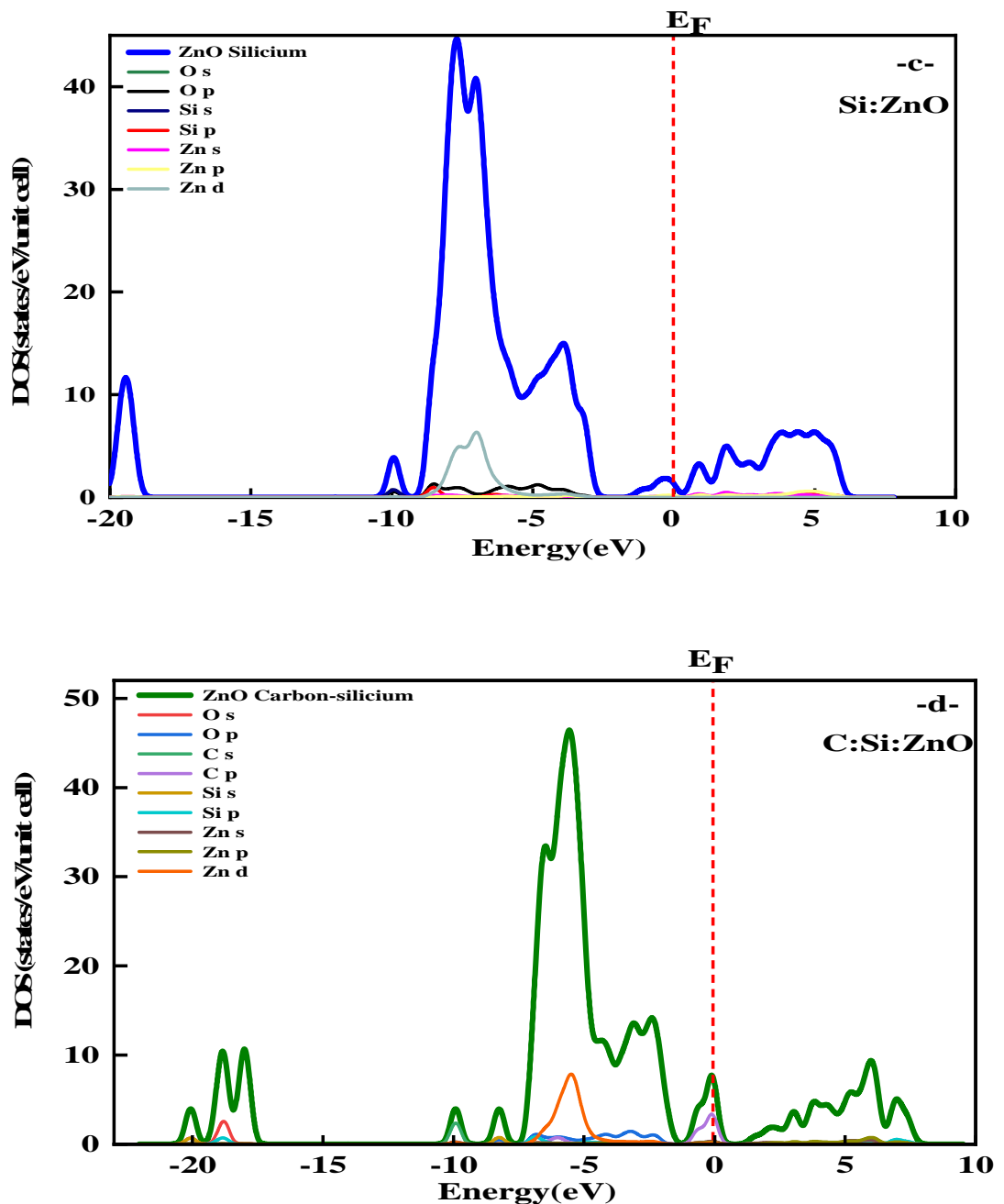


Fig.5: Density of states of (a) undoped ZnO and (b) C doped ZnO, (c) Si doped ZnO and (d) C:Si co-doped ZnO.

The peaks shown in **Figure 5** clearly show that the valence band consists of O-2p states and Zn-3d states, with a limited contribution from Zn-3p states. Thus, the ZnO conduction band is mainly composed of Zn-3p and 4s states with an almost equal contribution, mixed with some O-2s states.

The results indicate that the TDOS of the pure and doped ZnO have similar distributions of electronic states. However, the doping of atoms C and Si can indeed modify

the DOS and states close to the Fermi level in different ways. This phenomenon is recognized for its major influence on the optoelectronic properties of a semiconductor [29].

C: Si: ZnO co-doping creates more energy levels and moves the Fermi level in the (CBM), because the Si-2*p* state has a less energy than the Zn-4*d* state, constituting fully and half occupied states. The results also show the n-type conduction behavior of ZnO doped Si, because the minimum value band (VBM) of Si exceeds that of Zn [50]. When the (VBM) and (CBM) are very close, the conductivity of the co-doped ZnO is more higher with increasing Si concentration. Moreover, with the appearance of energy levels for $x = 3$ eV and $x = 7$ eV for C: Si: ZnO causes an electronic transition between occupied and unoccupied bands.

2.3.3 Electron Density distribution analyses

The way in which electrons are distributed in the crystal space is described by the electron density which is a measurable physical property. The type of the chemical bond is directly linked to ionicity which allows explaining and classifying the properties of solids. We note that the ionic character depends strongly on the total valence charge density.

It is well-known that the nature of bond character is highly dependent on the charge densities. To better elucidate the nature of bonding and access to information about the charge transfer.

Figure 6 shows the calculation of the charge densities for: (a) undoped ZnO and (b) C doped ZnO, (c) Si doped ZnO and (d) C:Si co-doped ZnO.

In the first time, we observed, the coexistence of both ionic and covalent bonding. The nature of chemical bonding, the atomic and bond populations obtained from first-principles calculations indicate that Zn-O band has a near ionic bond character; this is consistent with the distribution of charge density difference. While, the Zn-C band is strong covalent, Si-O is near covalent bond character, so there is a slight difference in the covalence between the bonds of ZnO:C and ZnO:Si. Blue, red, and yellow colors indicate electron depletion, electron accumulation, and regions with minimal difference, respectively. All bands spilling parameter for spin component 1 for ZnO and ZnO:C is $= 0.65\%$, but increases by $= 0.94\%$ for ZnO:Si and ZnO:C:Si.

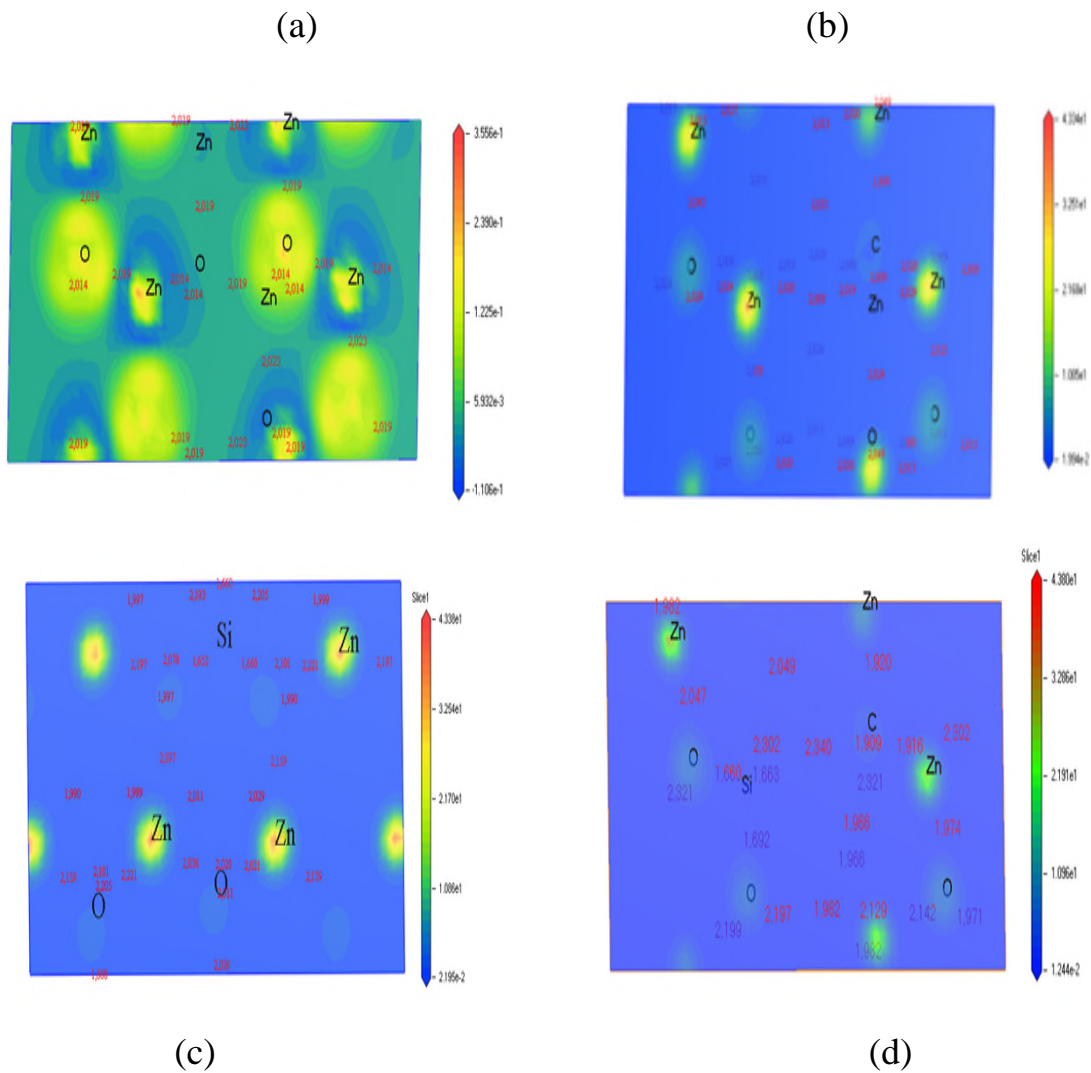


Fig.6: Charge densities for: (a) undoped ZnO and (b) C doped ZnO, (c) Si doped ZnO and (d) C:Si co-doped ZnO.

2.3.4 Mulliken population analysis

Table 5 shows the average Mulliken atomic and bond populations of atoms and bonds in different doping ZnO systems, which can explain charge transferring and bonding types. The atomic population value is positive for the loss of electrons, and the negative for the gaining of electrons. In addition, the larger bond population (maximum 1) indicates stronger covalent characteristics and smaller (minimum 0) indicates strong ionic properties.

Atomic Populations (Mulliken)

Species	s	p	d	Total	Charge (e)
C	1.47	3.60	0.00	5.08	-1.08
O	1.86	5.04	0.00	6.90	-0.90
Si	0.83	1.40	0.00	2.23	1.77
Zn	0.39	0.72	9.98	11.10	0.90

Population Analysis

Bond	Population	Length (Å ⁰)
O--Si	0.62	1.66327
C--Zn	0.82	1.90947
O--Zn	0.40	1.9714

Tab.5: Mulliken atomic and bond populations of C:Si:ZnO

For the intrinsic ZnO, the atomic population of Zn atom and O atom are 0.90 and -0.90, respectively, which means that the electrons lost by Zn atom are all obtained by O atom. In Si, the atomic population of Si atom is 1.77 and is larger than 0.90 of Zn atom, because the valence state of Si is higher than that of Zn. The atomic population of C atom is -1.08, smaller than that of other atoms, indicating that Ga atom contributes fewer electrons. And the bond population of C--Zn is 0.82, while the bond population of Si--O is 0.62, which are more than those in O--Zn, suggesting that the incorporation of C atom makes the ionic enhancement of the system.

2.4 Optical Properties

2.4.1 Dielectric function

Optical properties are a valid source of information on the quality of materials for their use in optoelectronic devices. It comes from photon-electron interactions. The CASTEP code calculates the optical properties from the dielectric function composed of the real and imaginary parts, which generate the calculation of all the other optical properties, including the absorption coefficient, reflectivity, refractive index and energy loss function (3), [59] as:

$$\boldsymbol{\varepsilon}(\boldsymbol{\omega}) = \boldsymbol{\varepsilon}_1(\boldsymbol{\omega}) + i\boldsymbol{\varepsilon}_2(\boldsymbol{\omega}) \quad (3)$$

Where $\boldsymbol{\varepsilon}_1$: the dispersion of the incident photons by the material, while $\boldsymbol{\varepsilon}_2$ corresponds to the energy absorbed by the material.

The **Figure 7** displays the dielectric function of undoped ZnO, C: ZnO, Si: ZnO and C: Si: ZnO in the energy range (0 eV–30 eV), (a) real parts and (b) imaginary parts. Compared to the undoped ZnO, $\boldsymbol{\varepsilon}_1$ (C: ZnO and Si: ZnO) has a reach maximum around 1eV, after, it moves to the lower energy above 3 eV and becomes negative reaching, this indicates the important effect of impurity doping [26], then it takes the same character with ZnO and Si: ZnO and become more stable.

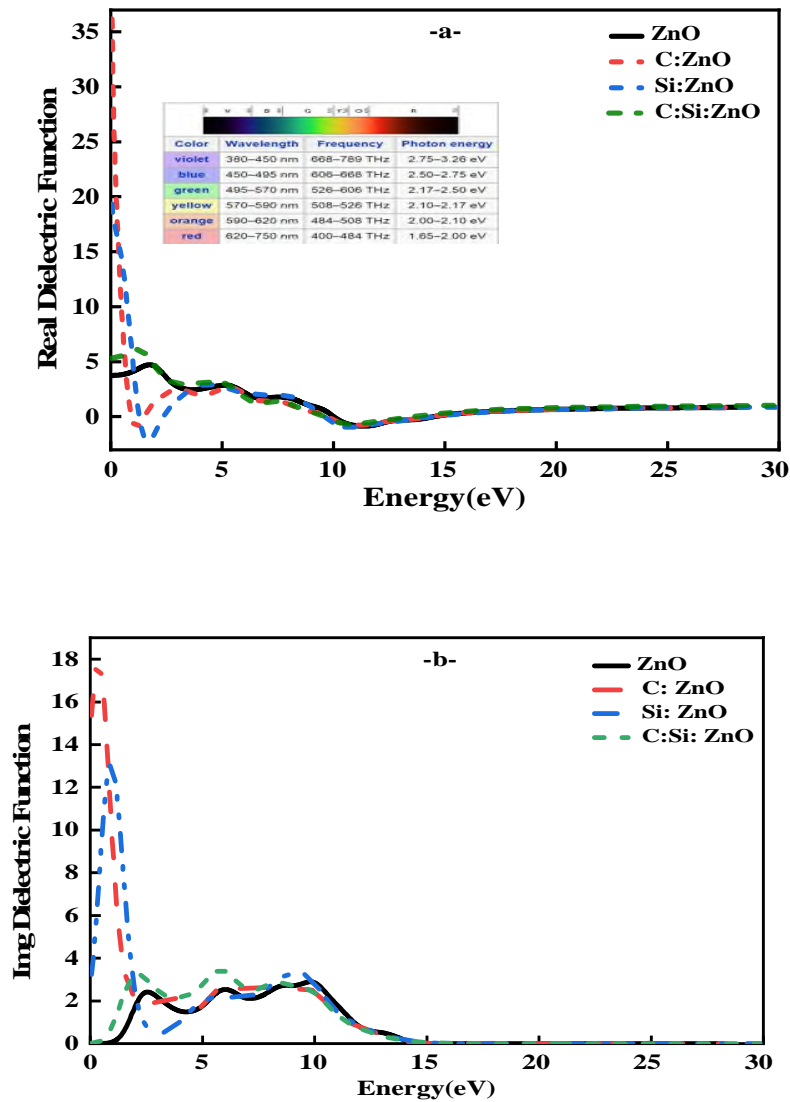


Fig.7: Dielectric Function of undoped ZnO and ZnO:C, ZnO:Si and ZnO:C:Si (0 eV – 30 eV): (a) real parts and (b) imaginary parts.

In addition, we observed a large energy zone ($h\nu$) in the visible and ultraviolet light regions for pure and doped ZnO, which improve the direct optical transitions between the maximum valence band and the minimum conduction band, which is the ZnO direct band gap.

There is a larger transition bands propagation ϵ_1 near 5 eV but decreased on Ultra-Violet region. ϵ_1 of the (Si: ZnO) system, had the same evolution over the energy rang (0 -10 eV) with undoped ZnO and there is a steep decrease between 10 eV and 12 eV.

The imaginary part of the dielectric function usually provides information about the photo-absorption properties of the materials [59-60]. From **Figure 7.a**, there are three peaks combined to (1 eV, 2 eV and 6 eV), related with the DOS. The first peak results from the electron transition between O-2*p* states and Zn-4*s* and between O-2*p* states and Zn-4*p*, but the second peak combined to the Zn-3*d* and O-2*p* states and the third peak due to the transition between O-2*s* states and Zn-3*d* states.

The ϵ_2 of all samples showed significant the absorption edges in the IR in the range and decrease in the UV-Vis region [61]. From the **figure 7.b**, we see that intrinsic ZnO has three main peaks, which is in good agreement with other *ab initio* calculation available [62]. The main peak of Si reached at about 1.3, which is similar to that found in the doped Si ZnO in the case of substitution 1.5 [63].

2.4.2 The absorption coefficient and reflectivity

Figure 8 presents a comparison between optical absorption spectra of undoped ZnO and C: ZnO, Si: ZnO and C: Si: ZnO and their reflectivity between 0 and 30 eV. As we observed, optical absorption coefficient for pure ZnO and ZnO doped with C, Si and C-Si is presented in **Figure 8.a**. ZnO has no absorption in the visible region (1.7 eV - 3.3 eV) and its absorption region is located in the UV region due to its intrinsic band gap (around 3.36 eV). All doped models have effectively moved the absorption edge of ZnO to visible region by creating states of impurity in the band gap, reducing the band gap and much stronger light absorption characteristics.

It is important to note that small changes occur near the red infrared region, especially for the C: ZnO system. After increasing and becoming more pronounced towards the upper visible region (3.5 eV), but has a limited effect on improving light absorption than Si: ZnO; this could be related to the impact of substitution doping. C-doped ZnO has a higher absorption in the near-ultraviolet region. Indeed, doped ZnO can be considered to have the most intense light absorption over the entire spectrum, leading to the fact that C-doping can alter the optical properties of ZnO, to a larger extent, mainly due to the effect of p-type doping characters on their electronic structures [29]. This result is very close to those of *Chen et al* [64].

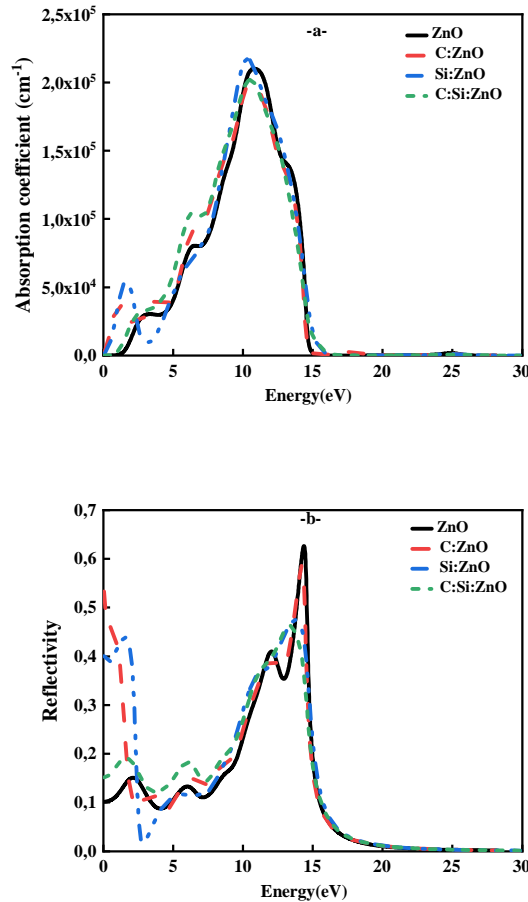


Fig.8: Simulation light absorption (a) and reflectivity (b) of pure ZnO, ZnO:C, ZnO:Si and ZnO:C:Si.

More careful observation in **Figure 8.a** the C: Si: ZnO system have $\alpha \sim 3 \times 10^4 \text{ cm}^{-1}$ in the range (0 eV-1.5 eV), and presents a significant improvement in their optoelectronic properties, which can contribute to a significant improvement in applications in the field of photovoltaic based on zinc oxide as a transparent semiconductor oxide [65].

Figure 8.b appears that the reflectivity data of different system doped ZnO. Carbon doped ZnO become inactive and has a slight increase compared with that of Si:ZnO, The incorporation of silicon, revealed the presence of different type electronic-vibrations during the diffusion on the surface of the material. This result corresponds with theoretical and experimental research [26]. Carbon has a small influence on reflectivity in the energy range of 2.5 eV - 5eV, when it decreases with the increase in C content, while it apparently increases after doping Si. In conclusion, it can play an important role in the field of optical devices of visible light.

Compound	Absorption coefficient $\alpha \times 10^4 \text{ (cm}^{-1}\text{)}$			Reflectivity R		
	Present work	Experimental Works	Theoretical works	Present work	Experimental works	Theoretical works
ZnO	2.4	2.5 ^d , 5.7 ^e	2 ^a , 2.1 ^c	0.15	0.18 ^g	0.13 ^a , 0.1 ^c
C:ZnO	2.5	-----	3 ^b	0.085	0.035 ^f	-----
Si: ZnO	2	-----	2 ^a	0.16	-----	0.08 ^a
C:Si:ZnO	4	-----	-----	0.17	-----	-----

Tab.5: Absorption coefficient α and reflectivity values of pure ZnO, C-doped, Si-doped and C: Si- doped ZnO.

^a Ref [66], ^b Ref [67], ^c Ref [26], ^d Ref [61], ^e Ref [69], ^f Ref [29], ^g Ref [68]

Table 5 summarizes our results as well as those of other works of the static absorption coefficient and the static reflectivity of pure, C-doped, Si-doped and C: Si doped ZnO in the visible scope of (1.7 eV -3.3 eV) are tabulating in.

2.4.3 Loss function energy

Electron energy loss function $L(\lambda)$ is an important parameter; it is used for describing loss in energy of a fast moving electron in a material from the top of a valence band to bottom of a conduction band [70]. This energy estimates the probability of inelastic diffusion, the distribution of energy loss distribution as well as the scattering angular distribution [71], and defined as:

$$\text{Im}[-1/\varepsilon(\mathbf{q}, \omega)] \quad (4)$$

The dielectric function $\varepsilon(q, \omega)$ in the energy loss function represents the response of an external electromagnetic disturbance to the material [72]. **Figure 9** depicts the results of bulk energy-loss function of undoped ZnO, C-doped, Si-doped and C: Si doped ZnO. We take the data from 0 eV to 30 eV. We could observe high loss energy along the range (12 eV - 15

eV) for both impurities; the weak peaks in the visible region for C: ZnO and Si: ZnO are mainly caused by the bulk phonon excitation.

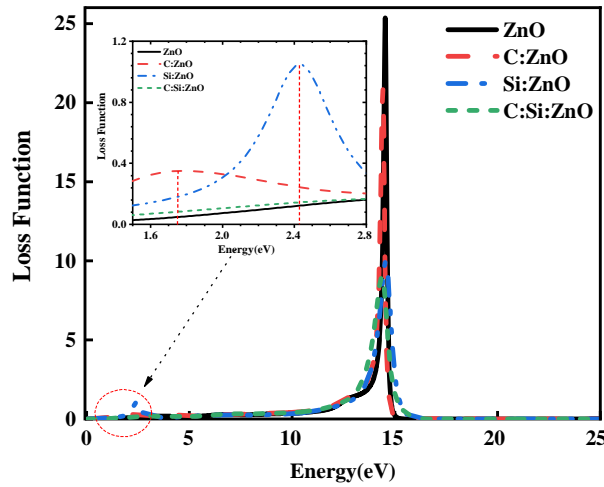


Fig.9: Loss function of undoped ZnO, C-doped, Si-doped and C: Si co-doped ZnO.

Undoped ZnO loss function tends to the sharp spectrum and its shoulder is around 14.5 eV, which is similar to the result found by *Chowdhury et al* [26].

Also peaks between (12 eV - 15 eV) in the energy loss spectra, which are related to the excitation of the plasmas resonance, in accordance with the results of *Sun et al*[72]. These peaks correspond to the edges of the reflection spectra and indicate the transition points from the metal characteristics to those of dielectrics of C: Si doped ZnO [62]. The loss energy between (3 eV - 10 eV) is not stable. It may be due to multiple inter-band transitions [71], while other ZnO doping locates at the low energy region.

2.4.4 Refractive index and extinction coefficient

Refractive index n of pure and doped ZnO, has been studied for its potential optical applications, it is important to determine the dispersion parameters, as they are closely related to the electronic polarization of ions and the local field within the material [73], it can be used to explain how light moves through a given medium. The refractive index is calculated by [74]:

$$n = \left(\frac{1+R}{1-R} \right) + \sqrt{\frac{4R}{1-R^2}} + k^2 \quad (5)$$

R is the reflectance and k the extinction coefficient.

Figure10.a and 10.b showed refractive index n of undoped ZnO, C-doped, Si-doped and C: Si co-doped ZnO versus energy, from **Figure10.a**, it was noticed that C doped ZnO has the same evolution with that of the Si doped ZnO and pure ZnO with C:Si doped ZnO in the interval (0 eV - 10 eV). From (0 eV - 1.8 eV) n spectra of C doped ZnO, Si doped ZnO

decreases strongly, where we found that n values reduce $n_C = 1.3$, $n_{Si} = 0.7$. This low energy zone can be explained by a resonant effect between polarization and electromagnetic radiation, caused by the co-doping of C-Si in the ZnO matrix. The resulting electrons are linked to an oscillating electric field in the ZnO [75]. The refractive index of undoped and co-doped ZnO sharply increase in this zone, $n_{ZnO} = 2.1$; $n_{C:Si} = 2.4$, indicating that their band gap is decreasing [62].

In the energy range (4 eV - 9 eV) all ZnO systems were very similar, with some slight changes. This may be due to a change in carrier concentration, which subsequently reduces and improves optical absorption [76-77]. Finally, at a higher energy, a decrease in the refractive index is directly related to the effect of band levels; surface optical polarity and optical losses. The findings are in accord with other research works [78-79].

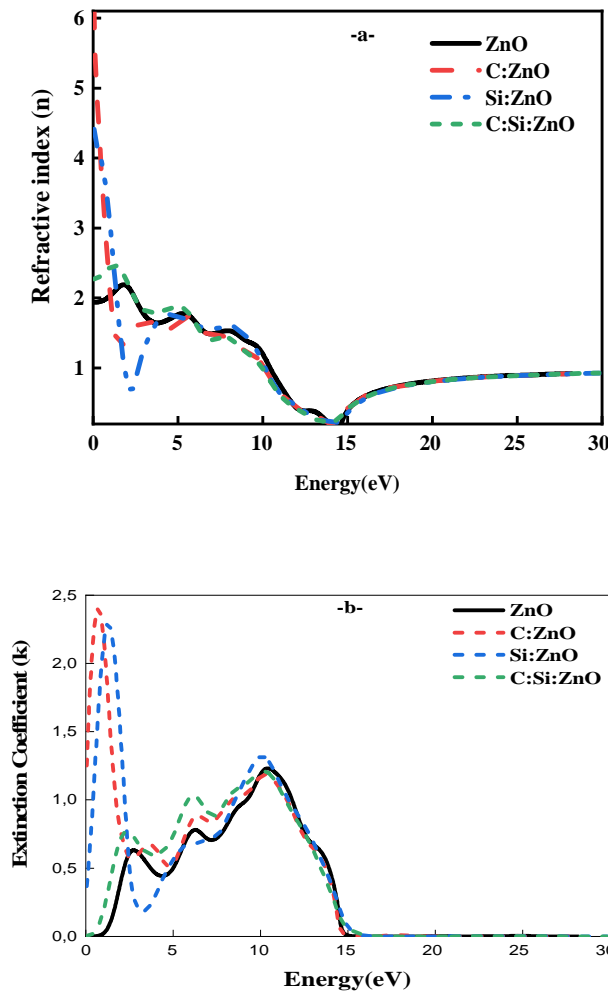


Fig.10: (a) Refractive index n and (b) Extinction Coefficient k of undoped ZnO, C-doped, Si-doped and C: Si co-doped ZnO versus energy.

2.4.5 Optical conductivity

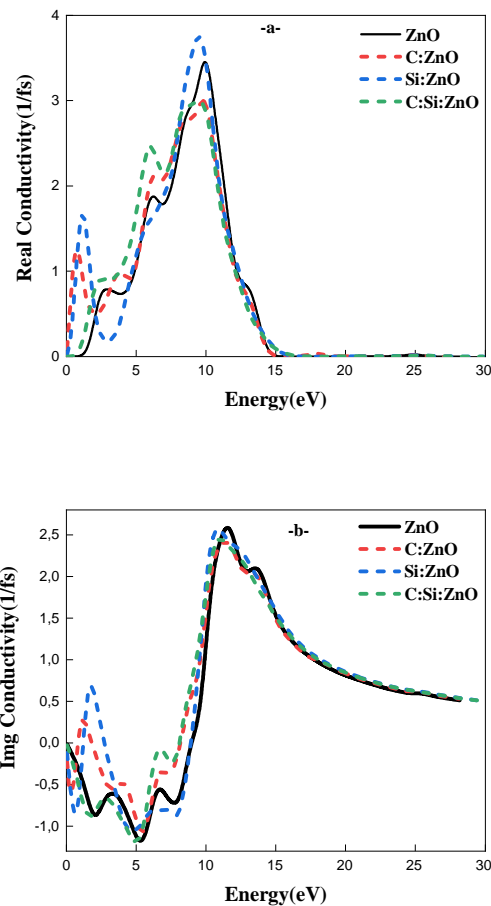


Fig.11: (a) real part and (b) imaginary part of optical conductivity for different systems: undoped ZnO, C-doped, Si-doped and C: Si co-doped ZnO

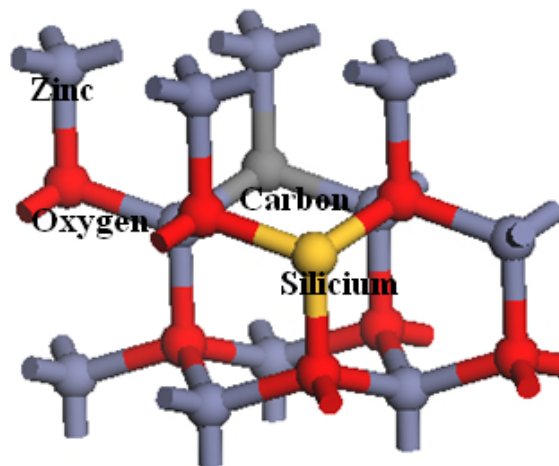
Figure11.a and 11.b showed real part and imaginary part of optical conductivity for different systems: undoped ZnO, C-doped, Si-doped and C: Si co-doped ZnO in terms of incident photon energy, from **Figure11.a**, in the visible region, the highest value of $\text{real}\sigma=1.8$ and $\text{img}\sigma=1.3$ back to Si doped ZnO. The spectra of ZnO and C:Si doped ZnO increases after 2 eV, which is related to optical transition from the highest states of valence band.

Point defects

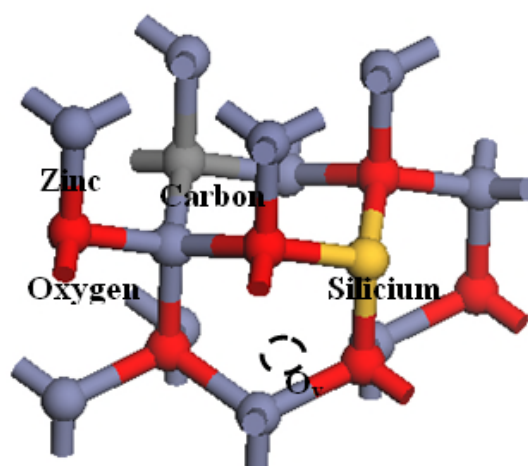
2.5 Point defects in C:Si:ZnO

We try to report in this section the achieved results in the effect of co-doping with native defects points on electronic structure and optical properties such as the energy gap, the dielectric constant and absorption coefficients of zinc oxide under the first principle study, using GGA approximation. Energy minimization is achieved by adopting the generalized gradient approximation (GGA) PBE [80]. Atomic Substitution Method (ASM) is used as a single point geometric defect model [19]. The cut-off energy equals to 380 eV within the choice of the Monkhorst Park scheme $4 \times 4 \times 2$ k-point mesh in reciprocal space, the maximum force converged to less than 10^{-6} eV/atom is used before the fully relaxation of all models.

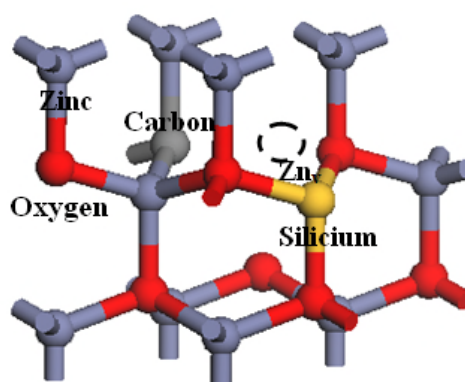
The following models are built as follows: undoped ZnO supercells, C doped ZnO, Si doped ZnO and C: Si co-doped ZnO was described and discussed above, in which Zn atom, is directly replaced by the Si atom, whereas O atom by C atom driving (ASM) method. **Figure 12** depicts the different point defects models, where: O vacancy (O_v), Zn vacancy (Zn_v), O interstitial (O_i) and Zn interstitial (Zn_i) respectively. Quite interestingly, there is another important defect points not noticed in our study like: anti-site defects (O replaces Zn or contrary), O octahedral and Zn octahedral, that is back to the little influencing of O octahedral and Zn octahedral to the calculation results [19].



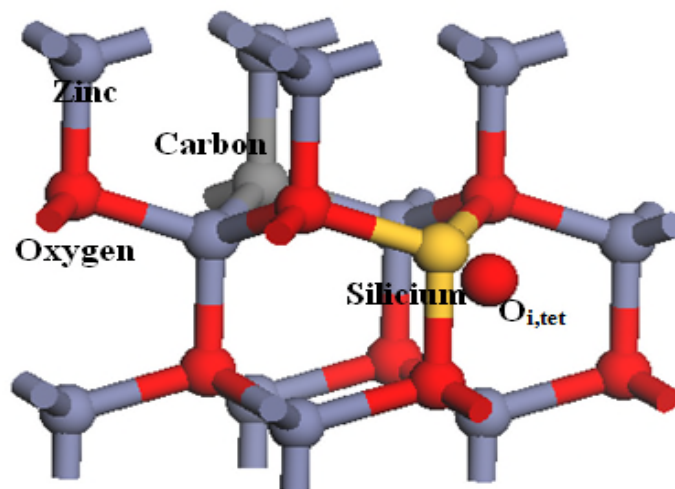
(a)



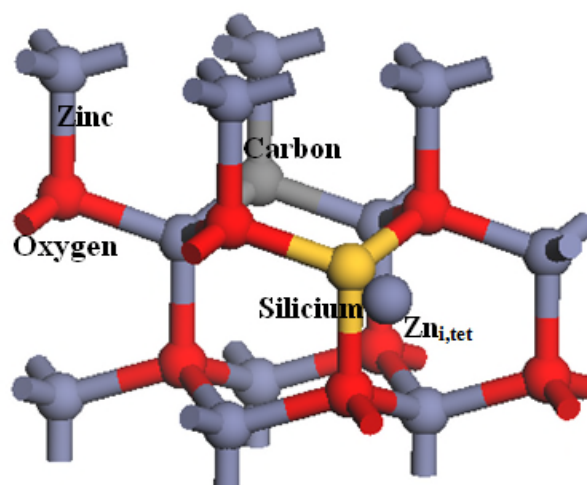
(b)



(c)



(d)



(e)

Fig.12: Defects model: (a) ZnO-C: Si, (b) (ZnO-C: Si)- O_v , (c) (ZnO-C: Si)- Zn_v , (d) (ZnO-C: Si)- O_i and (e) (ZnO-C: Si)- Zn_i .

2.5.1 Structural properties

After structural minimization, we obtained the perfect equilibrium crystallographic lattice, final energy; optimize volume and final bulk modulus of four defects points models compared to C-Si co-doped ZnO. These final stable configurations are shown in **Table 6**. By adjusting the energy-volume results using the Birch-Murnaghan equation state [81]; we found that the lattice parameters and volume of O_V and Zn_V decrease than O_i and Zn_i , which are expanded and their energies increased, and Zn^+ , O^- ions become more exciting. This clearly indicates that interstitial site defects are the most stable and easiest to form than vacancies defects, which is consistent with the total energy of undoped ZnO and C:Si:ZnO. We have been described the last geometric structures of these systems above. This finding may be due to the close distance length between C, Si, and O_i , Zn_i .

Models	a (Å)	c (Å)	V (Å ³)	E (eV)	B (GPa)
C:Si:ZnO	3.371	5.2443	51.17	-15293.1209	157.8
(C:Si:ZnO)O_v	3.3737	5.2471	51.235	-15293.1210	179.87
(C:Si:ZnO)Zn_v	3.3717	5.2453	51.201	-15293.118	218.17
(C:Si:ZnO)O_i	3.407	5.457	54.109	-15728.6996	146.695
(C:Si:ZnO)Zn_i	3.67	5.271	53.464	-17001.9937	160.82

Tab.6: Calculated lattice parameters a , c , the volume V , final energy E and bulk modulus B of ZnO-C: Si, (ZnO-C: Si)- O_V , (ZnO-C: Si)- Zn_V , (ZnO-C: Si)- O_i and (ZnO-C: Si)- Zn_i .

Similarly, this significant increase on lattice parameter and volume of (C:Si:ZnO) O_i (C:Si:ZnO) Zn_i can be explained by the repulsive effect of Si on the surrounding Zn and Zn vacancy has a repulsive effect on the surrounding O [82-83]. These two types of repulsive effects were more important than the impact of the ion radius of C^- and Si^+ . *Lin et al* [84], indicate that the system with Zn_i achieves the largest lattice extension after relaxation due to a strong electrostatic capacity. This result is on the same trend with the experimental results [85]. Depending on the band gap energy and state density, the electronic properties of a semiconductor can be explained.

2.6 Electronic properties

2.6.1 Band structure

Table 7 displays the band gap of various defects models compared to C-Si co-doped ZnO ($E_g = 2.1\text{eV}$), in Brillouin zone integration.

At first sight, we can say that the introducing of O and Zn vacancy (O_V , Zn_V) make the band gap of C:Si:ZnO smaller and help the quick transition of the charges (e^- , h^+) from valence band to conduction band. It has the lowest energy defects, but largely up-shifts when oxygen atoms become rich (O_i), and are thought to act as acceptors on C: Si doped ZnO with a new states of energy valence of the bands inwards for the C:Si doped ZnO, mainly come from the bond between interstitial oxygen and its first neighbors oxygen and zinc [86]. Meanwhile, point defects induce occupied states in band gaps. These outcomes indicate that in this case, there are strong interactions between the C,Si and defects on ZnO. These findings agreed with a several calculations [87-88-89].

Defect models	(C: Si:ZnO) O_V	(C: Si:ZnO) Zn_V	(C: Si:ZnO) O_i	(C:Si:ZnO) Zn_i
Band gap(eV)	0.17	0.25	0.96	0.6

Tab.7: Band gap of C: Si:ZnO, (C: Si:ZnO) O_V , (C: Si:ZnO) Zn_V , (C: Si:ZnO) O_i and (C: Si:ZnO) Zn_i .

2.6.2 Density of state

Like sulfide dopants in ZnO [90], many dopants can change different ZnO properties, including electronic properties. It is noticed that there is no significant change in state density after incorporation of native defect points on C: Si doped ZnO, exactly for Zn-3d, O-2p, C-2s and Si-2s states. TDOS calculations are consistent with theoretical and experimental results [86-91]. The lowest valence bands have a strong Zn-3d contribution. For O interstitial and Zn interstitial, Si-2p disappears completely near the conduction band region. It indicates that is a weak interactions between Si and defects points, but very strong with C on the band gap region, when the localization of C-2p states is more stable on band gap region and has relatively highest energy, except for (ZnO-C: Si)- O_i and (ZnO-C: Si)- Zn_i . This may suggest that Carbon atoms and Zn_i have a major effect on the electronic properties [29]. (See **Figure 13**)

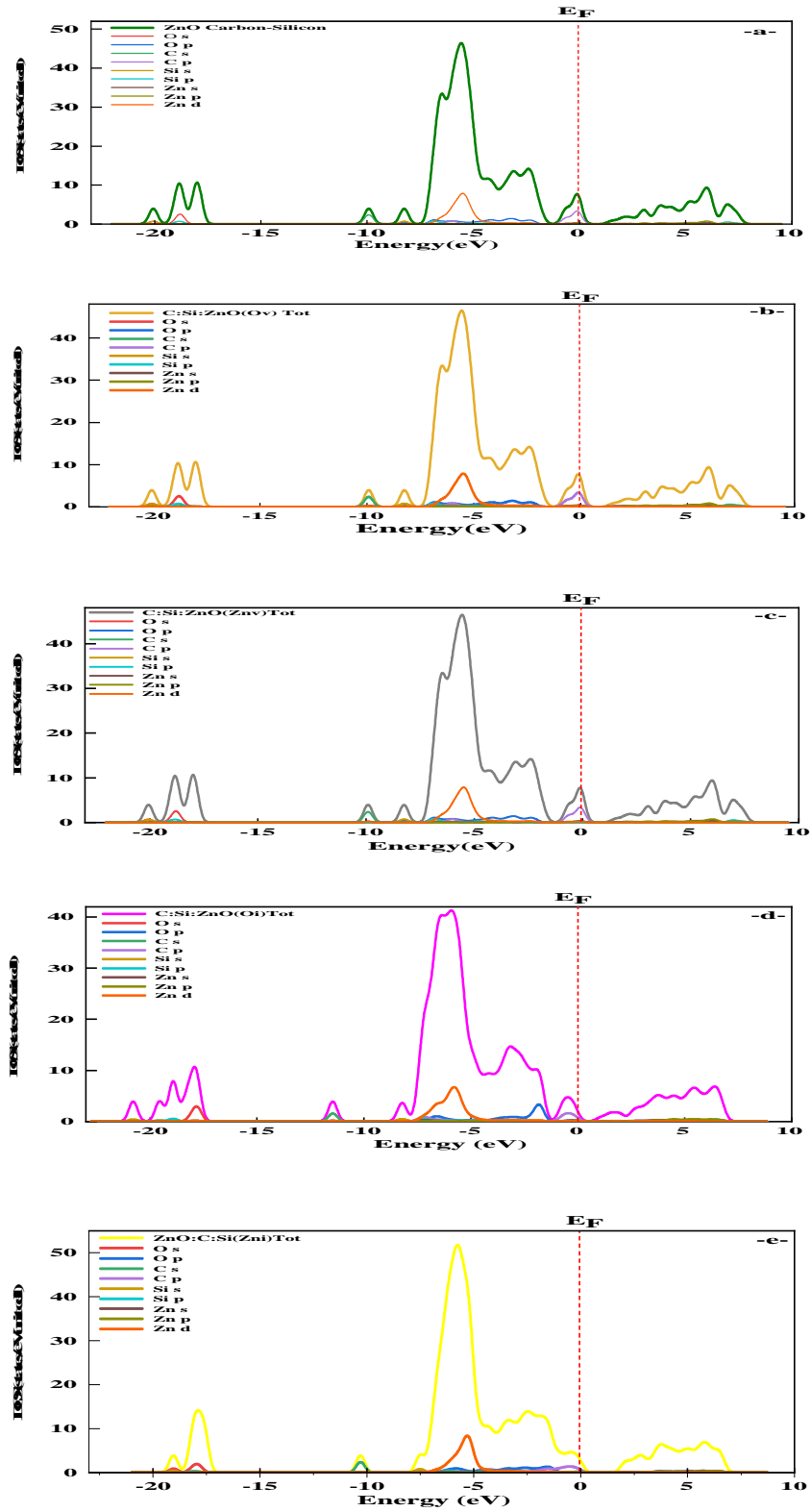


Fig.13: TDOS and PDOS of (a) C: Si:ZnO, (b) (C: Si:ZnO)_{O_v}, (c) (C: Si:ZnO)_{Zn_v}, (d) (C: Si:ZnO)_{O_i} and (e) (C: Si:ZnO)_{Zn_i}.

2.6.3 Optical properties

2.6.3.1 Dielectric function

The dielectric function describe as $\varepsilon(\omega) = \varepsilon_1(\omega) + i\varepsilon_2(\omega)$. where $\varepsilon_1(\omega)$ represents the dielectric real part and $\varepsilon_2(\omega)$ is the dielectric imaginary part. The real part of dielectric function $\varepsilon_1(\omega)$, represents the dispersion of the incident photons by the materials, while the imaginary part $\varepsilon_2(\omega)$ results from the inter band transition between occupied states below Fermi level and unoccupied state on top Fermi level due the photon absorption. In fact, the absorption coefficient, reflectivity, and transmittance are also calculated from the dielectric function.

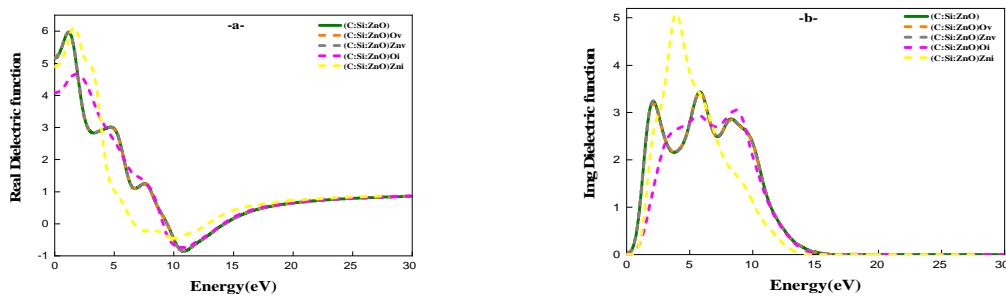


Fig.14: Dielectric Function of of C: Si:ZnO, (C: Si:ZnO) O_V , (C: Si:ZnO) Zn_V , (C: Si:ZnO) O_i and (C: Si:ZnO) Zn_i in the range (0 eV – 30 eV): (a) real parts and (b) imaginary parts.

The **Figure 14** displays the dielectric function of C: Si:ZnO, (C: Si:ZnO) O_V , (c) (C: Si:ZnO) Zn_V , (C: Si:ZnO) O_i and (C: Si:ZnO) Zn_i in the energy range (0 eV, –30 eV), (a) real parts and (b) imaginary parts. In the visible region and compared to C: Si:Zn, ε_1 of Zn_i and O_V have a reach maximum around $\varepsilon_1 = 6\text{eV}$, after, it decreases to the lower energy, Zn_i takes the different character than other defects. While the imaginary part $\varepsilon_2(\omega)$ of the dielectric function of C: Si:ZnO, (C: Si:ZnO) O_V , (C: Si:ZnO) Zn_V , (C: Si:ZnO) O_i and (C: Si:ZnO) Zn_i is important to determine the different transitions due to photons absorption.

In terms of impact, the same observation for ε_2 , there is a big difference between vacancies and interstitials models, for Zn_i , a new high peak is observed at low energy near 5eV. Therefore we expected that the calculated optical properties of different defects are more improved compared to other classical approximations (mBJ or LDA)

2.6.3.2 The absorption coefficient and reflectivity

The optical properties can be described by the dielectric function of the material (Equation 3). Absorption coefficient (α) is derived from the following equation as [92]:

$$\alpha(\omega) = \sqrt{2} \omega \sqrt{[\sqrt{\epsilon_1^2(\omega) - \epsilon_2^2(\omega)} - \epsilon_1(\omega)]} \quad (6)$$

Figure 15 display the optical absorption (a) and reflectivity (b) of C: Si:ZnO, (C: Si:ZnO) O_V , (C: Si:ZnO) Zn_V , (C: Si:ZnO) O_i and (C: Si:ZnO) Zn_i . versus energy within the range (0 eV-30 eV).

Generally, for α , three sharp peaks were shown after C and Si doped ZnO located approximately 3.38 eV, 6.28 eV and 10.52 eV, which are mainly due to transition processes. This indicates a poor interaction between the vacancy and its neighbor, but remain the same edges after the introduction of vacancy defects. Instead, interstitial defects have a great influence on the interacting direction, the peak of the treble disappears directly when the incorporation of interstitial defects.

Bellow 6.28 eV; there is a slight stability in the absorbance for all samples (co-doped and vacancy). In visible region, α increases until it arrives a maximum at 10.52 eV for vacancies and 9.88 eV for interstitials. After 10 eV, absorbance weakens and eventually decreases may be due to the weak interaction.

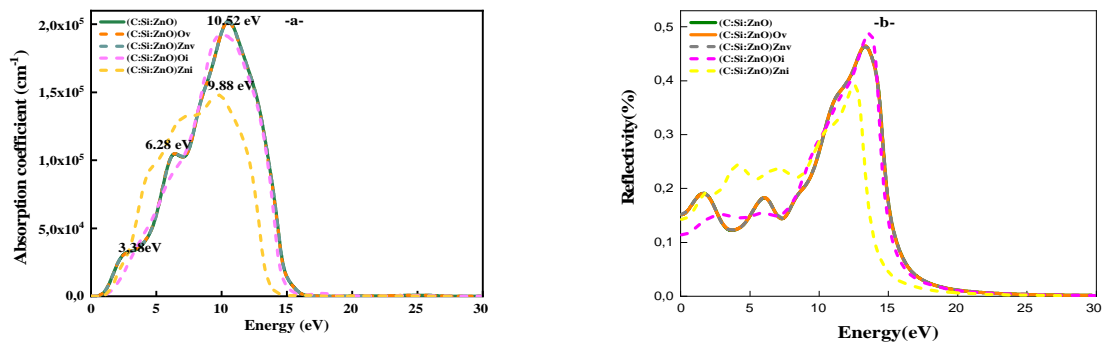


Fig.15: The absorption coefficient (a) and reflectivity (b) of C: Si:ZnO, (C: Si:ZnO) O_V , (C: Si:ZnO) Zn_V , (C: Si:ZnO) O_i and (C: Si:ZnO) Zn_i

The entire C: Si doped systems with incorporating of O_i with Zn_i present a better absorption property in the UV-Vis region than the donor type. The strong interactions can be seen between the C: Si atoms and the acceptor-type defects. This suggested that Zn_V defects upgrade the efficiency on optoelectronic properties and hasty interest.

The reflectivity spectra are shown in **Figure 15.b**. This Figure shows that the reflection in the infrared zone is strong; higher than 60%, is located in the range 4 eV-13 eV. As the vibrational modes are active in the infrared, the transmission property would be poor in

this range. The reflectivity reaches its maximum of 49% at 14 eV in ZnO-C: Si, (ZnO-C: Si) O_V , (ZnO-C: Si) Zn_V , (ZnO-C: Si) O_i and 41% in (ZnO-C: Si) Zn_i .

2.6.3.3 Loss function energy

Figure 16 illustrates the calculated loss function. The static was deduced from the figure 16 as 0.05 for all defects model. Similar values are observed for all model compared to those reported in part one. The presence of three maximum peaks, the smallest of them is $Zn_i=8$, with a slight deviation in the behavior of Zn. Increasing behavior can be found with O_i doping which consequently affects considerably the exciton energy (60 meV for ZnO).

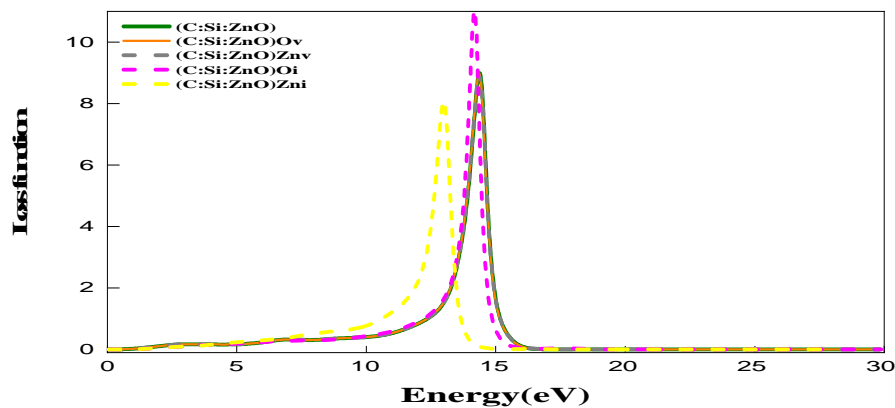


Fig.16: The loss function of C: Si:ZnO, (C: Si:ZnO) O_V , (C: Si:ZnO) Zn_V , (C: Si:ZnO) O_i and (C: Si:ZnO) Zn_i

2.6.3.4 Refractive index and extinction coefficient

The refractive index is an important factor influencing the phase matching for light in solid state lasers, while the extinction coefficient is related to the dielectric loss. From the dispersion of the dielectric function we can calculate the dispersion relations for the index of refractive index n the extinction coefficient k .

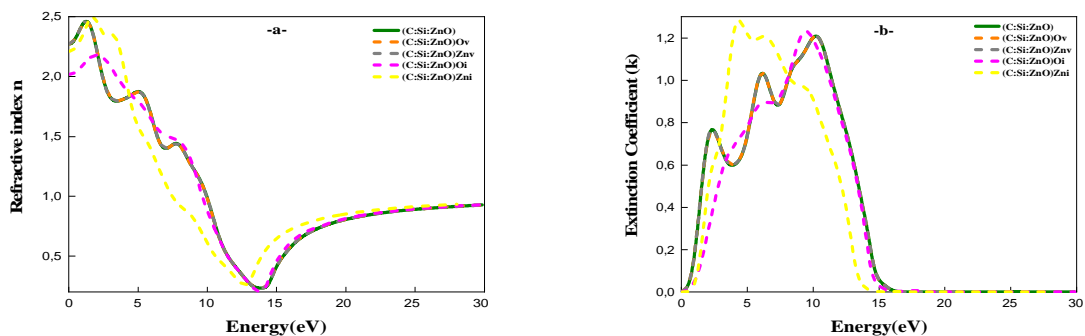


Fig.17: Refractive index (a) and extinction coefficient (b) of C: Si:ZnO, (C: Si:ZnO) O_V , (C: Si:ZnO) Zn_V , (C: Si:ZnO) O_i and (C: Si:ZnO) Zn_i

The refractive index spectra and extinction coefficient of ZnO-C: Si, (ZnO-C: Si) O_V , (ZnO-C: Si) Zn_V , (ZnO-C: Si) O_i and (ZnO-C: Si) Zn_i are shown in **Figure 17**. From this figure, we can see that the spectra of the refractive index n of ZnO-C: Si, (ZnO-C: Si) O_V , (ZnO-C: Si) Zn_V are very similar and the extinction coefficient of ZnO-C: Si, (ZnO-C: Si) O_V , (ZnO-C: Si) Zn_V are also very similar. The opposite of (ZnO-C: Si) O_i and (ZnO-C: Si) Zn_i , which take on different behavior. It should be noted that the maximum value of the refractive index is approximately equal to 2.4 at the visible region in ZnO-C: Si, (ZnO-C: Si) O_V , (ZnO-C: Si) Zn_V and (ZnO-C: Si) Zn_i , 2.2 at the in (ZnO-C: Si) O_i . The maximum of the extinction coefficient is 0.7 at the energy 3 eV in ZnO-C: Si, (ZnO-C: Si) O_V , (ZnO-C: Si) Zn_V , 1.2 at the energy 10 eV in (ZnO-C: Si) O_i and 1.3 at the energy 5 eV in (ZnO-C: Si) Zn_i .

2.6.3.5 Optical conductivity

The real and imaginary parts of the conductivity of ZnO-C: Si, (ZnO-C: Si) O_V , (ZnO-C: Si) Zn_V , (ZnO-C: Si) O_i and (ZnO-C: Si) Zn_i calculated in the range 0 eV-30eV are shown in **Figure 18**. From this Figure, we can note that the real part of the conductivity reaches a maximum at the energy 11 eV in ZnO-C: Si, (ZnO-C: Si) O_V , (ZnO-C: Si) Zn_V , at the energy 10eV in (ZnO-C: Si) O_i , 5eV in (ZnO-C: Si) Zn_i , while the maximum of the imaginary part is reached at the 12.5 eV in ZnO-C: Si, (ZnO-C: Si) O_V , (ZnO-C: Si) Zn_V , (ZnO-C: Si) O_i and 10.5eV in (ZnO-C: Si) Zn_i .

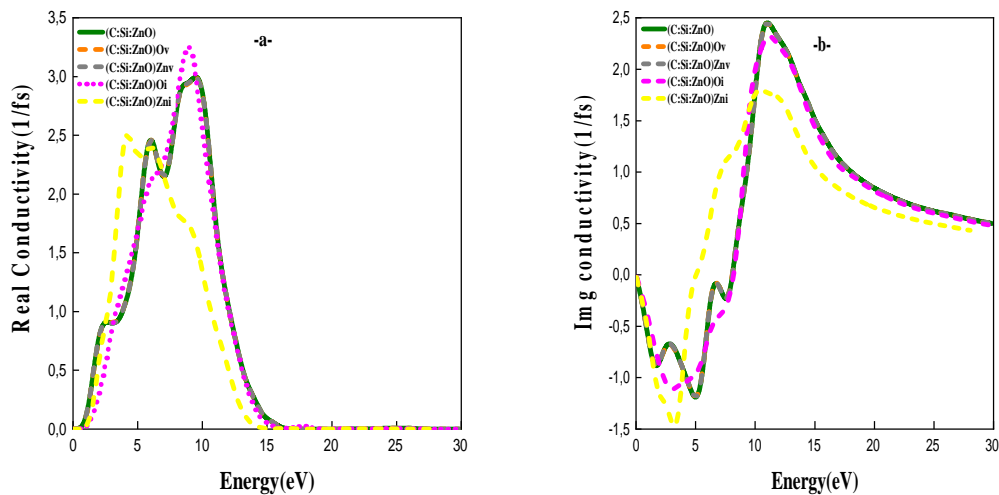


Fig.18: Optical conductivity of C: Si:ZnO, (C: Si:ZnO) O_V , (C: Si:ZnO) Zn_V , (C: Si:ZnO) O_i and (C: Si:ZnO) Zn_i in the range (0 eV – 30 eV): (a) real parts and (b) imaginary parts.

Bibliography

- [1]M.Rahman, M.Rahaman, E.Chowdhury, M.Motalab, A.Hossain, M.Roknuzzaman, Understanding the role of rare-earth metal doping on the electronic structure and optical characteristics of ZnO,J. Molecular Systems Design & Engineering,2022, <https://doi.org/10.1039/D2ME00093H>.
- [2]H.Hong, J.Shi, Y.Zhang, J.Engle, R.Nickles, X.Wang, W.Cai, Cancer-Targeted Optical Imaging with Fluorescent Zinc Oxide Nanowires,J. Nano Letter,2011, P 3744,<https://doi.org/10.1021/nl201782m>.
- [3]S.Chu, G.Wang, W.Zhou, Y.Lin, L.Chernyak, J.Zhao, J.Kong, L.Li, J.Ren, J.Liu, Electrically pumped waveguide lasing from ZnO nanowires,J Nature Nanotechnology,2011,P 506,<https://doi.org/10.1038/nnano.2011.97>.
- [4]Y.Zhang, M.Ram, E.Stefanakos, D.Goswami, Synthesis, Characterization, and Applications of ZnO Nanowires,J Nanomaterials,2012,P 2, <https://doi.org/10.1155/2012/624520>.
- [5]C.Bhakat, P.Singh, Zinc Oxide Nanorods: Synthesis and Its Applications in Solar Cell,J Modern Engineering Research,2012,P 2.
- [6]N.Aisah, D.Gustiono, V.Fauzia, I.Sugihartono, R.Nuryadi, Synthesis and Enhanced Photocatalytic Activity of Ce-Doped Zinc Oxide Nanorods by Hydrothermal Method,J Materials Science and Engineering,2017,<https://doi.org/10.1088/1757-899X/172/1/012037>.
- [7]X.Zhang, J.Qin, R.Hao, L.Wang, X.Shen, R.Yu, S.Limpanart, M.Ma, R.Liu, Carbon-Doped ZnO Nanostructures: Facile Synthesis and Visible Light Photocatalytic Applications,J Physical Chemistry C,2015,<https://doi.org/10.1021/acs.jpcc.5b07116>.
- [8]K.Badreddine, I.Kazah, M.Rekaby, R.Awad, Structural, Morphological, Optical, and Room Temperature Magnetic Characterization on Pure and Sm-Doped ZnO Nanoparticles,J Nanomaterials,2018,P 11,<https://doi.org/10.1155/2018/7096195>.
- [9]R.Swanepoel, Determination of the thickness and optical constants of amorphous silicon,J Physics E: Scientific Instruments,1983,<https://doi.org/10.1088/0022-3735/16/12/023>.
- [10]Y.Fang, J.Dilworth, M.Pepper ,P.Edwards, Investigations of the optical and electronic effects of silicon and indium co-doping on ZnO thin films deposited by spray Pyrolysis,J Zeitschrift fur Naturforschung,2020,P 25,<https://doi:10.1515/znb-2019-0196>.

- [11] R. Gharehbagh, S. Özen, H. Yudar, S. Pat, Ş. Korkmaz, The electrical, elemental, optical, and surface properties of Si-doped ZnO thin films prepared by thermionic vacuum arc, *J Materials Research Express*, 2017, V 4, <https://orcid.org/0000-0002-0333-487X>.
- [12] A. Das, P. Misra, L. Kukreja, Effect of Si doping on electrical and optical properties of ZnO thin films grown by sequential pulsed laser deposition, *J Physics D: Applied Physics*, 2009, V 42, <https://doi.org/10.1088/0022-3727/42/16/165405>.
- [13] W. Körner, C. Elsässer, Density functional theory study for polycrystalline ZnO doped with Si or Nb, *J Physical Review B*, 2011, <https://doi.org/10.1103/PhysRevB.83.205306>.
- [14] S. Clark, M. Segall, C. Pickard, P. Hasnip, First principles methods using CASTEP, *J Zeitschrift für Kristallographie, Crystalline Materials*, 2005, V 220, P 567–570, <https://doi.org/10.1524/zkri.220.5.567.65075>.
- [15] V. Anisimov, J. Zaanen, O. Andersen, Band theory and Mott insulators: Hubbard U instead of Stoner I, *J Physical Review B*, 1991, V 44, <https://doi.org/10.1103/PhysRevB.44.943>.
- [16] J. Perdew, K. Burke, M. Ernzerhof, Generalized Gradient Approximation Made Simple, *J Physical Review Letters*, 1996, V 77, <https://doi.org/10.1103/PhysRevLett.77.3865>.
- [17] J. Perdew, Y. Wang, Accurate and Simple Analytic Representation of the Electron-Gas Correlation Energy, *J Physical Review B*, 1992, V 45, <http://dx.doi.org/10.1103/PhysRevB.45.13244>.
- [18] S. Nayak, M. Ogura, A. Hucht, H. Akai, P. Entel, Monte Carlo simulations of diluted magnetic semiconductors using ab initio exchange parameters, *J Physics: Condensed Matter*, 2009, V 21, <https://doi.org/10.1088/0953-8984/21/6/064238>.
- [19] Z. Meng, X. Mo, X. Cheng, Y. Zhou, X. Tao, Y. Ouyang, Interactions between Er dopant and intrinsic point defects of ZnO: a first-principles study, *J Materials Research Express*, 2017, V 4, <https://doi.org/10.1088/2053-1591/aa6292>.
- [20] B. Amrani, R. Ahmed, F. Hassan, Structural, electronic and thermodynamic properties of wide band gap $Mg_xZn_{1-x}O$ alloy, *J Computational Materials Science*, 2007, V 40, P 66–72, <https://doi.org/10.1016/j.commatsci.2006.11.001>.
- [21] Z. Chun, Z. Yong, Z. Hu, Y. Feng, Y. Ni, First-principles study of the electronic and optical properties of ZnO nanowires, *J Chinese Physics B*, 2009, V 18, <https://doi.org/10.1088/1674-1056/18/6/065>.

- [22]G.Tse, The optical and elastic properties of strained ZnO by first principle calculations,J Computational Condensed Matter,2021,V 26,https://doi.org/10.1016/j.cocom.2020.e00525.
- [23]A.Schleife, F.Fuchs, J.Furthmüller,F.Bechstedt, First-principles study of ground- and excited-state properties of MgO, ZnO, and CdO polymorphs,J Physical Review B,2006,V 73,https://doi.org/10.1103/PhysRevB.73.245212.
- [24]A.Mohamad, M.Hassan, M.Yaakob, M.Taib, F.Badrudin, O.Hassan, M.Yahya, First-principles calculation on electronic properties of zinc oxide by zinc–air system,J King Saud University-Engineering Sciences,2017,V 29, P 278-283, https://doi.org/10.1016/j.jksues.2015.08.002.
- [25]W.Peng, Y.Zeng, C.Zhang, Y.Yan, W.Hu, First-principles study on La-doped ZnO used as transparent electrode for optoelectronic device,J International Journal of Physical Sciences,2012,V 7,P 2174-2180,https://doi.org/10.5897/IJPS11.1543.
- [26]R. Chowdhury, S.Adhikari, P.Rees, Optical properties of silicon doped ZnO,J Physica B: Condensed Matter,2010,V 405, P 4763-4767,https://doi.org/10.1016/j.physb.2010.08.072.
- [27]K. Klaa, S.Labidi, M.Bououdina, A.Amara, Temperature and pressure dependence on structural, electronic and thermal properties of ZnO wurtzite phase – first principle investigation,J phase transitions,2020,V 93,P 654-665, https://doi.org/10.1080/01411594.2020.1771562.
- [28]C.Fan, Q.Wang, L.Li, S.Zhang, Y.Zhu, X.Zhang, M.Ma, R.Liu, W. Wang, Bulk moduli of wurtzite, zinc-blende, and rocksalt phases of ZnO from chemical bond method and density functional theory,J Applied Physics Letters,2008,V 92,https://doi.org/10.1063/1.2895635.
- [29]W.Yu, Ji.Zhang , T.Peng, New insight into the enhanced photocatalytic activity of N-, C- and S-doped ZnO photocatalysts,J Applied Catalysis B: Environmental,2016,V 181,P 220-227,https://doi.org/10.1016/j.apcatb.2015.07.031.
- [30]L. Xiao, X. Li, Li Zeng, Theoretical Studies on the Geometrical and Electronic Structures of C-Doped ZnO under High Pressure,J Russian Journal of Physical Chemistry A,2019,V 93,P 2407-2413,https://doi.org 10.1134/S0036024419120173.
- [31]M.Farooq, X.Xu, H.Yang, C.Ran, Y.Wang, J.Miao, Y.Jiang, Intrinsic Room Temperature Ferromagnetism of Silicon Doped ZnO Thin Films,J Modern Physics Letters B,2013,V 27,https://doi.org/10.1142/S0217984913500929.
- [32]R.Reeber, Lattice parameters of ZnO from 4.2° to 296°K,J Applied Physics,1970,V 41,https://doi.org/10.1063/1.1658600.
- [33]F.Decremps, F.Datchi, A.Saitta, A.Polian, S.Pascarelli, A.Cicco, J.Itié, F. Baudelet, Local structure of condensed zinc oxide,J Physical Review B,2003,V

68,<https://doi.org/10.1103/PhysRevB.68.104101>.

[34]S.Akbar, S.Hasanain , M.Abbas, S.Ozcan, B.Ali , S.Shah, Defect induced ferromagnetism in carbon-doped ZnO thin films,J Solid State Communications,2011,V 151,P 17-20,<https://doi.org/10.1016/j.ssc.2010.10.035>

[35]J.J.Beltrán, C.A.Barrero, Alex Punnoose, Relationship between ferromagnetism and formation of complex carbon bonds in carbon doped ZnO powders,J Physical Chemistry Chemical Physics,2019,V 21,P 8808-8819,<https://doi.org/10.1039/C9CP01277J>.

[36]D.Mishra, J.Mohapatra, M.Sharma, R.Chattarjee, S.Singh, S.Varma, S.Behera, S.Nayak, P.Entel, Carbon doped ZnO: Synthesis, characterization and interpretation,J Magnetism and Magnetic Materials,2013,V 329,P 146-152,<https://doi.org/10.1016/j.jmmm.2012.09.058>.

[37]H.Karzel, W.Potzel, M.Köfferlein, W.Schiessl, M.Steiner, U.Hiller, G.Kalvius, D.Mitchell, T.Das, P.Blaha, K.Schwarz, M.Pasternak, Lattice dynamics and hyperfine interactions in ZnO and ZnSe at high external pressures,J Physical Review B ,1996,V 53,<https://doi.org/10.1103/PhysRevB.53.11425>.

[38]J.Clatot , G.Campet , A.Zeinert, C.Labrugère , M.Nistor , A.Rougier, Low temperature Si doped ZnO thin films for transparent conducting oxides,J Solar Energy Materials & Solar Cells,2011,V 95,P 2357-2362,<https://doi.org/10.1016/j.solmat.2011.04.006>.

[39]H.Wu, X.Cheng, C.Hu, P.Zhou, The structure and thermodynamic properties of zinc oxide with wurtzite and rocksalt structure under high pressures,J Physica B: Condensed Matter,2010,V 405,P 606-612,<https://doi.org/10.1016/j.physb.2009.09.074>.

[40]L.B.Shi, C.Y.Xu, H.K.Yuan, A CASTEP study on magnetic properties of C-doped ZnO crystal,J Physica B,2011,V 406,P 3187-3191,<https://doi:10.1016/j.physb.2011.05.022>.

[41]B.Nagare, S.Chacko, D.Kanhere, Ferromagnetism in Carbon-Doped Zinc Oxide Systems ,J Physical Chemistry A , 2010,V 114,P 2689-2696,<https://doi.org/10.1021/jp910594m>.

[42]Z.Wang, S.Li, Y.Lu, D.Zhao, Y.Lu, D.Zhao, J.Liu, L.Wang, J.Zhang, Y.Gao, Z.Wang, Preparation, characterization, and optical properties of carbon doped ZnO nanocrystal,j ICO20: Materials and Nanostructures,2006,V 6029,<https://doi.org/10.1117/12.667707>.

[43]P.Dufek, P.Blaha, K.Schwarz, Applications of Engel and Vosko's generalized gradient approximation in solids,J Physical Review B,1994,V 50,P 7279-7238, <https://doi.org/10.1103/PhysRevB.50.7279>.

[44]S.Fahy, K.Chang, S.Louis, M.Cohen, Ab initio calculation of pressure coefficients of band gaps of silicon: Comparison of the local-density approximation and quasiparticle results,J Physical Review B,1989,V 39, P 7840-7847, <https://doi.org/10.1103/PhysRevB.39.7840>.

- [45] A. Mahmood, F. Tezcan, G. Kardaş, F. Karadağ, Effect of Sr doping on the electronic band structure and optical properties of ZnO: A first principle calculation, *J Applied Physics*, 2017, V 122, <https://doi.org/10.1063/1.5002075>.
- [46] H.I. Berrezoug, A.E. Merad, A. Zerga, Z.S. Hassoun, Simulation and modeling of structural stability, electronic structure and optical properties of ZnO, *J ScienceDirect*, 2015, V 74, P 1517-1524, doi: 10.1016/j.egypro.2015.07.711.
- [47] S. Karimi, A. esmaeili, The performance of various GGA and LDA based mixed and improved exchange-correlation functionals for ZnO and ZnO:Mn: A first principles study, *J. Computational Condensed Matter*, 2020, P 2-9, <https://doi.org/10.1016/j.cocom.2020.e00501>.
- [48] M. Khuili, N. Fazouan, S.M. Slimane, H.A. El Makarim, E. Atmani, Study of properties of (Mg, Al)-codoped ZnO with GGA and mBJ approximations, *Physics Letters A*, 2016, P 1-17, <http://dx.doi.org/10.1016/j.physleta.2016.06.034>.
- [49] R. Baghdad, N. Lemée, G. Lamura, A. Zeinert, N. Hadj-Zoubir, M. Bousmaha, M. Bezzerrouk, H. Bouyanfif, B. Allouche, K. Zellama, Structural and magnetic properties of Co-doped ZnO thin films grown by ultrasonic spray pyrolysis method, *J Superlattices and Microstructures*, 2017, V 104, P 553-569, <https://doi.org/10.1016/j.spmi.2016.11.069>.
- [50] V. Srikant, D. Clarke, On the optical band gap of zinc oxide, *J Applied Physics*, 1998, V 83, P 5447-5451, <https://doi.org/10.1063/1.367375>.
- [51] A. Alsaad, Q. Al-Bataineh, A. Ahmad, Z. Albatineh, A. Telfah, Optical band gap and refractive index dispersion parameters of boron-doped ZnO thin films: A novel derived mathematical model from the experimental transmission spectra, *J Optik*, 2020, V 211, <https://doi.org/10.1016/j.ijleo.2020.164641>.
- [52] S.A. Ansari, S.G. Ansari, H. Foad, M. Cho, Facile and sustainable synthesis of carbon-doped ZnO nanostructures towards the superior visible light photocatalytic performance, *J New Journal of Chemistry*, 2017, V 41, P 9314-9320, <https://doi.org/10.1039/C6NJ04070E>.
- [53] A. Alshammari, L. Chi, X. Chen, A. Bagabas, D. Kramer, A. Alromaeh, Z. Jiang, Visible-light photocatalysis on C-doped ZnO derived from polymer-assisted Pyrolysis, *J RSC Advances*, 2015, V 5, P 1-8, <https://doi.org/10.1039/C4RA17227B>.
- [54] V. Kuznetsov, A. Vai, M. Al-Mamouri, J. Abell, M. Pepper, P. Edwards, Electronic transport in highly conducting Si-doped ZnO thin films prepared by pulsed laser deposition, *J Applied Physics Letters*, 2015, V 107, P 232103, <https://doi.org/10.1063/1.4936613>.

- [55] A. Jilani, M. Abdel-wahab, H. Zahran, I. Yahia, A. Al-Ghamdi, Linear and nonlinear optical investigations of nano-scale Si-doped ZnO thin films: spectroscopic approach, *J Applied Physics A*, 2016, V 122, P 1-11, <https://doi.org/10.1007/s00339-016-0392-1>.
- [56] S. Wakhare, M. Deshpande, Structural, electronic and optical properties of metalloid element (B, Si, Ge, As, Sb, and Te) doped g-ZnO monolayer: A DFT study, *J Molecular Graphics and Modelling*, 2020, V 101, <https://doi.org/10.1016/j.jmglm.2020.107753>.
- [57] J. Luo, X. Zhu, G. Chen, F. Zeng, F. Pan, The electrical, optical and magnetic properties of Si-doped ZnO films, *J Applied Surface Science*, 2012, V 258, P 2177–2181, <https://doi.org/10.1016/j.apsusc.2011.02.093>.
- [58] S. Panpan, S. Xiyu, H. Qinying, L. Yadong, C. Wei, First-principles calculation of the electronic band of ZnO doped with C, *J. Semiconductors*, 2009, V 30, <https://doi.org/10.1088/1674-4926/30/5/052001>.
- [59] D. Das, L. Karmakar, Optimization of Si doping in ZnO thin films and fabrication of *n*-ZnO:Si/*p*-Si heterojunction solar cells, *J Alloys and Compounds*, 2020, V 824, <https://doi.org/10.1016/j.jallcom.2020.153902>.
- [60] A. Abbassi, A. El Amrani, H. Ez-Zahraouy, A. Benyoussef, Y. El Amraoui, First-principles study on the electronic and optical properties of Si and Al co-doped zinc oxide for solar cell devices, *J Applied Physics A*, 2016, V 122, P 1-7, <https://doi.org/10.1007/s00339-016-0111-y>.
- [61] M. Khan, W. Cao, J. Li, M. Zaman, A. Manan, Density functional theory calculations for the investigation of (Ag, N) codoping effect on the electronic and optical properties of anatase TiO₂, *J International Journal of Modern Physics B*, 2014, V 28, <https://doi.org/10.1142/S0217979214501124>.
- [62] X. Si, Y. Liu, W. Lei, J. Xu, W. Du, J. Lin, T. Zhou, L. Zheng, First-principles investigation on the optoelectronic performance of Mg doped and Mg–Al co-doped ZnO, *J Materials & Design*, 2016, V 93, P 128-132, <https://doi.org/10.1016/j.matdes.2015.12.033>.
- [63] M. Xu, H. Zhao, K. Ostrikov, M. Y. Duan, and L. X. Xu, Effect of doping with Co and/or Cu on electronic structure and optical properties of ZnO, *J Applied Physics*, 2009, V 105, <https://doi.org/10.1063/1.3082023>.
- [64] L. Chen, Y. Tu, Y. Wang, R. Kan, C. Huang, Characterization and photoreactivity of N-, S-, and C-doped ZnO under UV and visible light illumination, *J Photochemistry & Photobiology, A: Chemistry*, 2008, V 199, P 170-178, <https://doi.org/10.1016/j.jphotochem.2008.05.022>.
- [65] J. S. Jang, J. K. U. Ghorpade, H. H. Shin, M. G. Gang, S. D. Park, H. J. Kim, D. S. Lee, J. H. Kim, Comparison study of ZnO-based quaternary TCO materials for photovoltaic application, *J Alloys and Compounds*, 2019, V 793, P 499-504, <https://doi.org/10.1016/j.jallcom.2019.04.042>

- [66] A.Klein, C.Korber, A.Wachau, F.Sauberlich, Y.Gassenbauer, S.Harvey, D.Proffit, T.Mason, Transparent Conducting Oxides for Photovoltaics: Manipulation of Fermi Level, Work Function and Energy Band Alignment, *J Materials*, 2010, V 3, P 4892–4914, <https://doi.org/10.3390/ma3114892>.
- [67] P.Samarasekara, Udumbara Wijesinghe, Optical Properties Of Spin Coated Cu Doped ZnO Nanocomposite Films, *J Georgian Electronic Scientific Journals : Physics*, 2015, P 41-50.
- [68] E.M. Bachari, G.Baud, S.Ben Amor, M.Jacquet, Structural and optical properties of sputtered ZnO film, *J Thin Solid Films*, 1999, V 348, P 165-172, [https://doi.org/10.1016/S0040-6090\(99\)00060-7](https://doi.org/10.1016/S0040-6090(99)00060-7).
- [69] B.Swain, Investigation of fractal behavior, optical properties and electronic environments of carbon-doped ZnO Thin Films, *J Applied Physics A*, 2021, V 127, <https://doi.org/10.1007/s00339-021-04516-7>.
- [70] A.Lawal, A.Shaari, R.Ahmed, N.Jarkoni, First-principles investigations of electron-hole inclusion effects on optoelectronic properties of Bi₂Te₃, a topological insulator for broadband photodetector, *J Physica B: Condensed Matter*, 2017, V 520, P 69-75, <https://doi.org/10.1016/j.physb.2017.05.048>.
- [71] R.John, S.Padmavathi, Ab Initio Calculations on Structural, Electronic and Optical Properties of ZnO in Wurtzite Phase, *J Crystal Structure Theory and Applications*, 2016, V 5, P 24-41, <http://doi.org/10.4236/csta.2016.52003>.
- [72] Y.Sun, H.Xu, B.Da, S.Mao, Z.Ding, Calculations of Energy-Loss Function for 26 Materials, *J Chinese Journal of Chemical Physics*, 2016, V 29, <https://doi.org/10.1063/1674-0068/29/cjcp1605110>.
- [73] J.Sun, H.Wang, J.He, Y.Tian, Ab initio investigations of optical properties of the high-pressure phases of ZnO, *J Physical Review B*, 2005, V 71, <https://doi.org/10.1103/PhysRevB.71.125132>.
- [74] N.Rasheed, N.Al-Sahib, A.Khalifa, Optical Properties of Carbon Doped by Nano Particle Titanium Dioxide to Enhance Solar Energy Absorption, *J Nanomedicine & Nanotechnology*, 2020, V 5, <https://doi.org/10.23880/nnoa-16000182>.
- [75] A.S.Gadallah, M.El-Nahass, Structural, Optical Constants and Photoluminescence of ZnO Thin Films Grown by Sol-Gel Spin Coating, *J Advances in Condensed Matter Physics*, 2013, V 2013, P 1-11, <https://doi.org/10.1155/2013/234546>.
- [76] B.Mehmood, M.Khan, M.Iqbal, A.Mahmood, W. Al-Masry, Structural and optical properties of Ti and Cu co-doped ZnO thin films for photovoltaic applications of dye

sensitized solar cells, *J International Journal of Energy Research*, 2021, V 45, P 2445-2459, <https://doi.org/10.1002/er.5939>.

[77] Y. Hwang, H. Kim, Y. Um, H. Park, Optical properties of post-annealed ZnO:Al thin films studied by spectroscopic ellipsometry, *J Materials Research Bulletin*, 2012, V 47, P 2898-2901, <https://doi.org/10.1016/j.materresbull.2012.04.111>.

[78] S. Xue, X. T. Zu, W. G. Zheng, H. X. Deng, X. Xiang, Effects of Al doping concentration on optical parameters of ZnO:Al thin films by sol-gel technique, *J Physica B: Condens Matter*, 2006, V 381, P 209-213, <https://doi.org/10.1016/j.physb.2006.01.342>.

[79] C. Aydin, Synthesis of Pd:ZnO nanofibers and their optical characterization dependent on modified morphological properties, *J Alloys and Compounds*, 2019, V 777, P 145-151, <https://doi.org/10.1016/j.jallcom.2018.10.325>.

[80] S. Bhat, K. Sandeep, P. Kumar, M. Venu, S. Dharmaprasanth, J. Bhat, Effect of Al doping on the carrier transport characteristics of TiO₂ thin films anchored on glass substrates, *J Applied Physics A*, 2019, V 125, <https://doi.org/10.1007/s00339-019-2464-5>.

[81] C. Loschen, C. Carrasco, K. Neyman, F. Illas, First-principles LDA+U and GGA+U study of cerium oxides: Dependence on the effective U parameter, *J Physical Review B*, 2007, V 75, <https://doi.org/10.1103/PhysRevB.75.035115>.

[82] F. Birch, Finite strain isotherm and velocities for single-crystal and polycrystalline NaCl at high pressures and 300°K, *J Geophysical Research: Solid Earth*, 1978, V 83, P 1257-1268, <https://doi.org/10.1029/JB083iB03p01257>.

[83] Q. Hou, C. Zhao, X. Jia, L. Qu, Effect of Ga doping and point defect on magnetism of ZnO, *J Physica B: Condensed Matter*, 2017, V 506, P 109-114, <https://doi.org/10.1016/j.physb.2016.11.006>.

[84] C. Park, S. Zhang, S. Wei, Origin of p-type doping difficulty in ZnO: The impurity perspective, *J Physical Review B*, 2002, V 66, <https://doi.org/10.1103/PhysRevB.66.073202>.

[85] Q. Lin, G. Li, N. Xu, H. Liu, D. J. E, C. L. Wang, A first-principles study on magnetic properties of the intrinsic defects in wurtzite ZnO, *J Journal of Chemical Physics*, 2019, V 150, <https://doi.org/10.1063/1.5063953>.

[86] J. Lu, Y. Zhang, Z. Ye, Y. Zeng, H. He, L. Zhu, J. Huang, L. Wang, J. Yuan, B. Zhao, X. Li, Control of p- and n-type conductivities in Li-doped ZnO thin films, *J Applied Physics Letters*, 2006, V 89, <https://doi.org/10.1063/1.2354034>.

- [87]Y.Sun, H.Wang, The electronic properties of native interstitials in ZnO,J Physica B: Condensed Matter,2003,V 325,P 157-163,[https://doi.org/10.1016/S0921-4526\(02\)01517-X](https://doi.org/10.1016/S0921-4526(02)01517-X).
- [88]A.Janotti, C.de Walle, Fundamentals of zinc oxide as a semiconductor,J Reports on Progress in Physics,2009,V 72,<https://doi.org/10.1088/0034-4885/72/12/126501>.
- [89]F.Oba, S.R. Nishitani, S.Isotani, H.Adachi, Energetics of native defects in ZnO,J Applied Physics,2001,V 90,<https://doi.org/10.1063/1.1380994>.
- [90]P.Erhart, K.Albe, A.Klein, First-principles study of intrinsic point defects in ZnO: Role of band structure, volume relaxation, and finite-size effects,J Physical Review B,2006,V 73,<https://doi.org/10.1103/PhysRevB.73.205203>.
- [91]B.Y.Geng, G.Z.Wang, Z.Jiang, T.Xie, S.H.Sun, G.W.Meng, L.D.Zhang, Synthesis and optical properties of S-doped ZnO nanowires,J Applied Physics Letters,2003,V 82,P 4791-4793,<https://doi.org/10.1063/1.1588735>.
- [92]R. R.Gay, M.H.Nodine, V.E.Henrich, H.J.Zeiger, E.I.Solomon, Photoelectron study of the interaction of carbon monoxide with zinc oxide,J American Chemical Society,1980,V 102,P 6752–6761,<https://doi.org/10.1021/ja00542a014>.
- [93]S.Saha, T. P.Sinha, A.Mookerjee, Electronic structure, chemical bonding, and optical properties of paraelectric BaTiO₃,J Physical Review B ,2000,V 62, <https://doi.org/10.1103/PhysRevB.62.8828>

General Conclusion

General Conclusion

In the present study, we have performed first-principles calculations of the optoelectronic properties of C, Si doped ZnO as well as C-Si co-doped ZnO and the influence of native defect points, on this kind of co-doping. The ZnO lattice parameters are greatly affected by the nature of the dopants. This variation is mainly attributed to the change in doping of Zn^{2+} ions with those of Si^{4+} and O^{2-} with those of C^{4-} . By introducing carbon atoms, the optoelectronic properties of ZnO change and we show a best visible light absorption as compared to other dopants. The introduction of C and Si into the ZnO matrix leads to a smaller refractive index and an increased absorption coefficient. Furthermore, C and Si co-doping change the band gap, the dielectric function and the loss energy.

It is found that the lattices parameters of interstitials defects increase, highest stable and easiest to form than the vacancies sites. Beside this, we also obtained that the energy gap of $O_{i,tet}$ increases more than other defects and creating of new levels defects bands inward C: Si doping ZnO, involve transitions between different charge and $Zn-3d$ states are motivated. Furthermore, the absorption properties peak of C: Si doped ZnO with vacancies defects stay stable and biggest than interstitials defects, but this dopant causes the decrease of average absorbance in UV region, that is , there is stronger interaction in vacancies defects than in interstitials . These features may come to make acceptor type defects doped C: Si: ZnO as a good p-type conducting semiconductor, which will upgrade the industrial optoelectronic and photovoltaic applications of ZnO-based devices.

ملخص:

الدراسة الحالية هي عمل نظري لتأثير التكعيم بالكربون والسيليكون على الخصائص الإلكترونية الضوئية لأكسيد الزنك، باستعمال التقريب التدرجي العام (GGA) وباستخدام تبادل الارتباطات الوظيفي (Perdew Burke Ernzerhof) (PBE). أكدت النتائج أن ذرات O تعمل كموقع تفضيلي للمطعمات في الشبكة البلورية. من خلال إدخال ذرات الكربون، تتغير الخصائص الإلكترونية الضوئية لأكسيد الزنك ونظهر امتصاصاً أفضل للضوء المرئي مقارنة بالمطعمات الأخرى. يؤدي الإدخال المشترك لذرات الكربون و السيليكون في أكسيد الزنك إلى معامل انكسار أصغر وزيادة معامل الامتصاص. علاوة على ذلك، فإن ادخال الشوائب (كربون و سيليكون) يغير فجوة النطاق والوظيفة العازلة وطاقة الخسارة. نبلغ أيضاً في هذه الورقة عن النتائج المحققة في تأثير التطعيم مع نقاط العيوب الأصلية على الخصائص الإلكترونية لأكسيد الزنك .

Abstract

The present study is a theoretical work of the effect of carbon and silicon co-doping on the optoelectronic properties of ZnO, by generalized gradient approximation (GGA) using the Perdew Burke Ernzerhof functional correlations (PBE) exchange. The results confirmed that O atoms act as a preferential doping site in the crystal lattice. By introducing carbon atoms, the optoelectronic properties of ZnO change and we show a better absorption of visible light compared to other dopants. The co-insertion of C and Si atoms in ZnO matrix, leads to a smaller refractive index and the absorption coefficient increases. Furthermore, C and Si co-doping changes the band gap, the dielectric function and the loss energy. We also report in this paper the achieved results in the effect of co-doping with native defects points on electronic properties of ZnO.

Résumé:

La présente étude est un travail théorique de l'effet du carbone et du silicium co-doping sur les propriétés optoélectroniques de ZnO, par approximation de gradient généralisée (GGA) en utilisant l'échange de corrélations fonctionnelles (PBE) Perdew Burke Ernzerhof. Les résultats ont confirmé que les atomes d'O agissent comme un site de dopage préférentiel dans le réseau cristallin. En introduisant des atomes de carbone, les propriétés optoélectroniques de ZnO changent et nous montrons une meilleure absorption de la lumière visible par rapport aux autres dopants. La co-insertion des atomes C et Si dans la matrice ZnO, conduit à un indice de réfraction plus petit et le coefficient d'absorption augmente. De plus, le co-couplage C et Si modifie l'écart de bande, la fonction diélectrique et la perte d'énergie. Nous rapportons également dans ce document les résultats obtenus dans l'effet de co-doping avec les points de défauts natifs sur les propriétés électroniques de ZnO.